THE INTEGRATED BARIUM CARBONATE PROCESS FOR SULPHATE REMOVAL FROM ACID MINE WATER

PS HLABELA
Student Number: 13219375

A thesis submitted for the degree Doctor of Philosophy in Chemical Engineering at the Potchefstroom campus of North-West University

Promoter: Prof. FB Waanders
Co-promoter: Prof. OSL Bruinsma

May 2009

DECLARATION

I, the undersigned, declare that the work contained in this thesis is my own original study and has not previously been submitted at any university for a degree.

PS. Hlabela **Date**

ACKNOWLEDGEMENTS

There are people and institutions without whom this work would have not been a success and I extend my gratitude to them.

Prof. FB Waanders, my overseer promoter who took over forom Prof. OSL Bruinsma, who emigrated back to the Netherlands, is thanked for his supervision, understanding and unending motivation.
Prof. OSL Bruinsma and Prof. HWJP Neomagus, my technical advisors, your professional and uncompromised technical guidance have taught me a lot about the subject matter of my work.
Prof. JP Maree, is thanked for introducing me to this field of research and helping me choose the topic.

THRIP is thanked for its generous financial support.
CSIR is being acknowledged for its provision of research facilities.
The School of Chemical and Minerals Engineering at the North-West University, Potchefstroom Campus, is acknowledged for making all the instrumentation used in this research available for my work.
The technical staff of the School of Chemical and Minerals Engineering are thanked for their cooperation and patience every time I needed their help.

I owe a debt of gratitude to my beloved mother, Meiggy Tlhabela, my two sisters, Grace and Margaret Tlhabela and my brother, Peter Tlhabela for their continued moral support and for believing in me at all times and whose love and prayers have kept me going.
A special thank you goes to Miss Lebogang Mekgwe for her moral support.

Finally praise and honour be to God Almighty for helping me against all odds of life.

“Dedicated to my late brother, Nicholas Tlhabela, and late sister, Annah Khoele (RIP)”

SUMMARY OF THESIS

The mining industry in South Africa is one of the primary sources of water pollution. Mines leave a legacy of chemically polluted water, after closure, and currently operating mines are continously discharging polluted water into the environment, and polluting water resources. The chemical pollutants found in this mine waste water include high concentrations of sulphate (up 5 000 mg/L), dissolved heavy metals principally iron (II). This water can have pH levels as low as 2.5 and is therefore termed Acid Mine Drainage (AMD). AMD is formed as a result of the oxidation of pyritic material, which becomes exposed to oxygen and water during minig activities. While neutralization of the AMD and metal removal has been acheived using alkaline compounds, sulphate removal to environmentally acceptable levels still has shortcomings in meeting effluent standards. Environmental, health and water governing bodies are exerting pressure on mines to treat water for sulphate removal.

A number of processes aimed at sulphate removal, to acceptable levels, are currently in use, and the scope of this thesis concentrates on their development and optimization. Previous research has shown that while limestone ($CaCO_3$) and lime (CaO) are used for neutralization and metal removal from AMD, these two chemicals also have potential for partial sulphate removal from sulphate rich water, via gypsum ($CaSO_4$) crystallization. However, a number of drawbacks such as the inability to remove sulphate to low levels without addition of excess chemicals has led to the exploration of other chemicals for potential sulphate removal from AMD. Barium salts such as $Ba(OH)_2$, BaS and $BaCO_3$, can also be employed for stoichiometric sulphate removal from sulphate-rich water, via $BaSO_4$ precipitation. The use of these chemicals offers an added advantage of recyclability, via thermal reduction of the precipitated $BaSO_4$ to BaS, in the presence of a reducing reagent.

In this thesis, the integrated barium carbonate process for sulphate and metal removal from AMD is presented and consists of the pre-treatment with lime, removal of sulphate as barium sulphate by dosing barium carbonate, the thermal reduction of $BaSO_4$ to BaS for sulphur production and possible $BaCO_3$ recycling, and finally H_2S stripping from a concentrated solution of recovered BaS, leading to sulphur recovery.

From beaker studies it became evident that sulphate can be removed by dosing a stoichiometric amount of $BaCO_3$ into sulphate-rich water. The rate of sulphate removal is dependent on the $BaCO_3$ concentration and sulphate removal is not directly inhibited by the presence of magnesium in the treated water, as was previously assumed to be the case. The sulphate removal rate is only retarded by an alkalinity ≥ 200 mg/L as $CaCO_3$.

An online particle size measuring experimental set-up was developed to study the precipitation process of $BaSO_4$ from the reaction of $Ba^{+2+}{}_{(aq)}$ and $SO_4^{-2-}{}_{(aq)}$), with the aim of enhancing particle growth over nucleation, in order to produce $BaSO_4$ crystals with improved settling properties. The studies demonstrated that by changing the reactant concentration, the number of feeding points into the precipitator, and the stirrer speed, one can affect the extent of the feeding zone and the level of supersaturation in this zone and control the size of the precipitated particles. The Crystal Size Distribution (CSD) analysis of the precipitation process has shown that growth takes place in all the crystal size ranges, but faster in larger crystals, suggesting a size dependent type of particle growth rate. By lowering the concentrations of the fed Ba^{+2+} the local supersaturation was reduced thus lowering the nucleation rate and as a result increased particle growth rate. Increasing the number of feed points into the precipitator tube enhanced particle growth. Improved mixing due to increased stirrer speed led to increased particle growth rate, in all particle size ranges and reduced nucleation rates. However, an excessively high stirrer speed led to attrition type nucleation, the result of which was reduced/stunted growth of particles.

The results from the studies, carried out using activated carbon as a reducing agent, in a furnace, have shown that the optimum temperature for the reduction of $BaSO_4$ to BaS is 950 – 1050^0C, within 15 minutes, for a complete reduction in a tube furnace. More than 1 hour was required for more than 60% yield to be obtained in a muffle furnace. The presence of $CaCO_3$ in the reaction mixture lowers the BaS% yield by about ±50% and the BaS% yield in the tube furnace was higher compared to the muffle furnace.

The TGA isothermal studies revealed that the reduction rate of $BaSO_4$ using CO is dependent on the partial pressure of CO in the system and is also dependent on the

temperature. A first order reaction rate with the average activation energy of 149 (±10) kJ/mol and constant value (k) of 0.59 were found to best describe the reaction.

An effective H_2S stripping depends on the balance between the CO_2 concentration and the sulphide concentration in the BaS solution. The molar proportionality between CO_2 fed and the sulphide stripped was almost equal to 1 only when the pH of the BaS solution was > 12.

The results from these studies were used in a pilot-scale implementation of the integrated barium carbonate process at Harmony Gold Mine in Randfontein, which were recently completed.

SUMMARY OF THESIS

The mining industry in South Africa is one of the primary sources of water pollution. Closed down mines leave a legacy of chemically polluted water after closure, and current operating mines are continuously discharging polluted water into the environment, consequently polluting water resources. The chemical pollutants found in this mine waste water include high concentrations of sulphate (up 5 000 mg/L), dissolved heavy metals and iron (II). This water can have pH levels as low as 2.5 and it is therefore named Acid Mine Drainage (AMD). AMD is formed as a result of the oxidation of pyritical material, which becomes exposed to oxygen and water during mining activities. While neutralization of the AMD and metal removal has been achieved by using alkaline compounds, sulphate removal to environmentally acceptable levels is still a source of controversy. Environmental, health and water governing bodies are exerting pressure on mines to treat water for sulphate content.

A number of processes aimed at sulphate removal, to acceptable levels, are currently in use, and the scope of this thesis concentrates on their development and optimization. Previous research has shown that while limestone ($CaCO_3$) and lime (CaO) were conventionally used for neutralization and metal removal from AMD, these two chemicals also have a potential for partial sulphate removal from sulphate rich water, via gypsum ($CaSO_4$) crystallization. However, a number of drawbacks such the inability to remove sulphate to low levels without addition of excess chemicals has led to the exploration of other chemicals for potential sulphate removal from AMD. Barium salts ($Ba(OH)_2$, BaS and $BaCO_3$) can also remove sulphate from sulphate rich water, stoichiometrically, via $BaSO_4$ precipitation. The use of these chemicals offers an added advantage of recyclability, via thermal reduction of the precipitated $BaSO_4$ to BaS, in the presence of a reducing reagent

In this thesis, the integrated barium carbonate process for sulphate and metal removal from AMD is presented and consists of the pre-treatment with lime,

removal of sulphate as barium sulphate by dosing barium carbonate, the thermal reduction of $BaSO_4$ to BaS for sulphur production and possible $BaCO_3$ recycling, and finally H_2S stripping from the concentrated solution of the recovered BaS is done, leading to sulphur production.

From the beaker studies it became evident that sulphate can be removed by dosing the stoichiometrical amount of $BaCO_3$ into the sulphate rich water. The rate of sulphate removal is dependent on the $BaCO_3$ concentration and the sulphate removal is not directly inhibited by the presence of magnesium in the treated water, as was previously assumed to be the case. The sulphate removal rate is only retarded by an alkalinity ≥ 200 mg/L (as $CaCO_3$.)

An online particle size measuring experimental set-up was developed to study the precipitation process of $BaSO_4$ from the reaction of $Ba^{+2}_{(aq)}$ and $SO_4^{-2}{}_{(aq)}$), with the aim of enhancing particle growth over nucleation, in order to produce $BaSO_4$ crystals with improved settling properties. The studies have demonstrated that by changing the reactant concentration, number of feeding points into the precipitator and the stirrer speed, one can affect the extent of the feeding zone and the level of supersaturation in this zone and control the size of the precipitated particles. The Crystal Size Distribution (CSD) analysis of the precipitation process has shown that growth takes place in all the crystal size ranges, but faster in larger crystals, suggesting a size dependent type of particle growth rate. By lowering the concentrations of the fed Ba^{+2} the local supersaturation was reduced thus lowering the nucleation rate and as a result increasing particle growth rate. Increasing the number of feed points into the precipitator tube enhanced particle growth. Improved mixing due to increased stirrer speed led to increased particle growth rate, in all particle size ranges and reduced nucleation rate. However, an excessive high stirrer speed led to attrition type nucleation, the result of which is reduced/stunted growth of particles.

The results from the studies, carried out using activated carbon as a reducing agent, in a furnace, have shown that the optimum temperature for the reduction of $BaSO_4$ to BaS is 950 – 1050^0C, within 15 minutes for a complete

reduction in a tube furnace. More than 1 hour was required for more than 60% yield to be obtained in a muffle furnace. The presence of $CaCO_3$ in the reaction mixture does not have a significant effect on the BaS% yield and the BaS% yield in the tube furnace is higher compared to the muffle furnace.

The TGA isothermal studies have revealed that the reduction rate of $BaSO_4$ using CO is dependent on the partial pressure of CO in the system and is also dependent on the temperature. A first order reaction rate with the average activation energy of 149 ($\pm$10) kJ/mol and constant value (k) of 0.59 were found to best describe the reaction.

An effective H_2S stripping depends on the balance between the CO_2 concentration and the sulphide concentration in the BaS solution. The molar proportionality between CO_2 fed and the sulphide stripped was almost equal to 1 only when the pH of the BaS solution was > 12.

The results from these studies will be used in the pilot scale implementation of the integrated barium carbonate process which is currently underway at Harmony mine in Randfontein.

OPSOMMING VAN PROEFSKRIF

Die mynbou-industrie is in Suid-Afrika een van die hoofbronne van waterbesoedeling. Uitgewerkte myne sorg vir 'n nalatenskap van chemies-besoedelde water na sluiting, en myne wat huidig in bedryf is, laat voordurend besoedelde water in die omgewing vry en besoedel gevolglik waterbronne. Die chemiese besoedelingstowwe wat in dié myn-afvalwater aangetref word, sluit in hoë konsentrasies van sulfaat (tot 5 000 mg/L), opgeloste swaarmetale en yster (II). Hierdie water kan pH-vlakke van so laag as 2.5 hê en dit word gevolglik Suur Myn Afloop (SMA) genoem. SMA word gevorm as gevolg van die oksidasie van piritiese materiaal wat gedurende mynbedrywighede aan suurstof en water blootgestel word. Terwyl neutralisering van die SMA en metaalverwydering bereik word deur die gebruik van alkaliese verbindings, is sulfaatverwydering tot die vlak van omgewings-aanvaarbare vlakke steeds 'n bron van twis. Omgewings-, gesondheids- en waterbeheer-liggame oefen druk op myne uit om die water ten opsigte van die sulfaat-inhoud te behandel.

'n Aantal prosesse, gemik op sulfaatverwydering tot aanvaarbare vlakke, is huidiglik in gebruik, en die bestek van hierdie proefskrif konsentreer op hulle ontwikkeling en optimering. Vorige navorsing het getoon dat, terwyl kalksteen ($CaCO_3$) en kalk (CaO) gewoonlik gebruik word vir neutralisasie en metaalverwydering uit SMA, hierdie twee chemikalieë ook potensiaal het vir gedeeltelike sulfaatverwydering uit sulfaatryke water, *via* gips ($CaSO_4$)-kristallisasie. 'n Aantal nadele, egter, soos die onvermoë om sulfaat tot lae vlakke te verwyder sonder byvoeging van 'n oormaat chemikalieë, het gelei tot die ondersoek van ander chemikalieë met potensiële sulfaat-verwyderingsvermoë uit SMA. Die bariumsoute ($Ba(OH)_2$, BaS en $BaCO_3$) kan ook sulfaat uit sulfaatryke water stoichiometries verwyder, *via* die neerslaan van $BaSO_4$. Die gebruik van hierdie chemikalieë bied die verdere voordeel van herwinbaarheid van die neergeslane $BaSO_4$, *via* termiese reduksie tot BaS, in die teenwoordigheid van 'n reduseermiddel.

In hierdie proefskrif word die geïntegreerde bariumkarbonaat-proses vir sulfaat- en metaalverwydering uit SMA aangebied, wat bestaan uit die

voorbehandeling met kalk, verwydering van sulfaat as bariumsulfaat deur dosering met bariumkarbonaat, die termiese reduksie van $BaSO_4$ tot BaS vir swawelproduksie en moontlike $BaCO_3$-hersiklisering, en uiteindelik H_2S-stroping vanuit die gekonsentreerde oplossing van die herwonne BaS, wat lei tot swawelproduksie.

Uit die glasbekerstudies het dit duidelik geword dat sulfaat verwyder kan word deur dosering van die sulfaatryke water met die stoichiometriese hoeveelheid $BaCO_3$. Die tempo van sulfaatverwydering is afhanklik van die $BaCO_3$-konsentrasie en die sulfaatverwydering word nie direk gestrem, soos wat voorheen verwag is nie. Die sulfaatverwyderingstempo word slegs vertraag deur 'n alkaliniteit ≥ 200 mg/L (as $CaCO_3$.)

'n Eksperimentele opstelling vir die aanlyn-partikelgroottemeting is ontwikkel om die presipitasieproses van $BaSO_4$ in die reaksie van $Ba^{2+}{}_{(aq)}$ en $SO_4^{2-}{}_{(aq)}$ te bestudeer, met die doel om partikelgroei te bevorder, eerder as kernvorming, ten einde $BaSO_4$-kristalle te produseer met verbeterde besinkingseienskappe. Die studies het getoon dat deur die reaktantkonsentrasie, die aantal toevoerpunte tot die presipiteerder en die roersnelheid te verander, die omvang van die toevoersone en die vlak van oorversadiging in hierdie sone beïnvloed en die grootte van die neergeslane partikels beheer kan word. Die kristalgrootte-verspreidingsanalise van die neerslaanproses het getoon dat groei van kristalle in alle grootte-bereike plaasvind, maar dat groter kristalle vinnger groei, wat 'n grootte-afhanklikheid-tipe van partikelgroeitempo suggereer. Deur die konsentrasie van die toegevoerde Ba^{2+} te verlaag, is die lokale oorversadiging verminder en die kernvormingtempo is dus verlaag, met 'n verhoging in die partikelgroeitempo. Vermeerdering van die aantal toevoerpunte na die presipiteerderbuis bevorder partikelgroei. Verbeterde menging as gevolg van hoër roersnelheid het gelei tot 'n hoër partikelgroeitempo in alle partikelgroottebereike en 'n verminderde kernvormingtempo. 'n Uitermate hoë roersnelheid het egter gelei tot 'n vryf-tipe kernvorming, wat aanleiding gegee het tot verminderde/belemmerde partikelgroei.

Die bevindinge van die studies, uitgevoer met geaktiveerde koolstof as reduseermiddel in 'n oond, het getoon dat die optimum-temperatuur vir die reduksie van $BaSO_4$ na BaS vir volledige reduksie binne 15 minute in 'n buisoond 950 – 1050°C is. Meer as 1 uur was nodig vir die bereiking van 'n groter as 60% opbrengs in 'n moffeloond. Die teenwoordigheid van $CaCO_3$ in die reaksiemengsel het nie 'n noemenswaardige invloed op die BaS%-opbrengs nie en die BaS%-opbrengs in die buisoond is hoog in vergelyking met dié in 'n moffeloond.

Die TGA-isotermiese studies het openbaar dat die reduksietempo van $BaSO_4$, met die gebruikmaking van CO, afhanklik is van die parsiële druk van CO in die sisteem en ook afhanklik is van die temperatuur. 'n Eerste-orde reaksietempo met 'n gemiddelde aktiverinsenergie van 149 ($\pm$10) kJ/mol en 'n waarde van die konstante (k) van 0.59 het die reaksie die beste te beskryf.

Effektiewe H_2S-stroping hang af van die balans tussen die CO_2-konsentrasie en die sulfiedkonsentrasie in die BaS-oplossing. Die molare proporsionaliteit tussen CO_2-toevoer en die sulfied gestroop, was amper gelyk aan 1, slegs as die pH van die BaS-oplossing >12 was.

Die bevindinge van hierdie studie sal gebruik word in die loodsskaal-implementasie van die geïntegreerde bariumkarbonaatproses wat tans onderweg is by die Harmony-myn in Randfontein.

CONTENTS

GLOSSARY

Acidity The measure of how acidic the water is, measured in mg/L $CaCO_3$

Acid Mine Drainage Acidic water, rich in iron, produced from the oxidation of pyrites (FeS_2) in a reaction catalyzed by iron oxidizing bacteria during mining activities.

Alimentary Canal The system of organs within multicellular animals that takes in food, digests it to extract energy and nutrients, and expels the remaining waste.

Alkalinity The measure of how alkaline the water is, measured in mg/L $CaCO_3$.

Catchment Area The area from which any rainfall will drain into the watercourse or part of a watercourse, through surface flow to a common point or common points.

Coagulant A chemical that reduces net repulsion between particles

Ground Water Water that occurs in the voids of saturated rock and soil material beneath the ground surface.

Fluidised bed A column type reactor, packed with solids, e.g limestone, through which a fluid is oved, at a rate high enough to expand the volume in the reactor occupied by the.

Flocculant A chemical that aggregates or combines particles by bridging the spaces between particles surfaces, thereby forming bridges of polymer chains and creating larger particles.

Laxative effects The ability to cause a running stomach.

Lime CaO.

Limestone Sedimentary rock containing mainly $CaCO_3$ solid.

Mine Closure The processes by which all the the primary mine operations are terminated.

Pipco Process An American patented process by which SO_2 is converted to liquid elemental sulphur when contacted with H_2S in potassium citrate solution.

Pyrites	FeS_2.
Reclamation	Return of disturbed land to a stable, productive and self-sustaining condition after taking into account beneficial uses of the site and surrounding land. surfaces, thereby promoting consolidation of smaller particles into larger particles.
Reynolds number	A dimensionless number that gives a measure of the ratio of inertial forces ($V\rho$) to viscous forces (μ/*L*) and, consequently, it quantifies the relative importance of these two types of forces for given flow conditions in a fluid.
Salination	Increasing levels of salt in topsoil caused by irrigation and land clearing.
Seepage	The act or process involving the slow movement of water or another fluid through porous material like soil, slimes or discard.
Slaked lime	$Ca(OH)_2$.
Surface Water	All water naturally open to the atmosphere (rivers, lakes, rsevoirs, streams, inpoundments, seas, estuaries, etc.
Water Resource	Includes a water course, surface water, estuary or acquifer.
Wet Thiogen	The process by which elemental sulphur is recovered from contacting BaS with SO_2 from smelter smoke.

Abbreviations and Acronyms

APHA	American Public Health Association
ARD	Acid Rock Drainage
AMD	Acid Mine Drainage
BPGs	Best Practice Guidlines
CESR	Cost Effective Sulphate Removal
CFD	Computational Fluid Dynamics
CMRO	Chamber of Mines Research Organization
CRTA	Constant Rate Thermal Analysis
CSD	Crystal Size Distribution

CSIR	Council for Scientific and Industrial Research
CSTK	Continous Stirred Tank Reactor
DTA	Differential Thermal Analyzer
DSC	Differential Scanning Calorimetry
DWAF	Department of Water Affairs and Forestry
FT	Flocculant Tank
HDS	High Density Sludge
IKP	Inverse Kinetic Problem
INAP	International Network for Acid Prevention
IWWMP	Integrated Water and Waste Management Plan
LR	Line Reactor
LOAEL	Lowest Observed Adverse Effect Level
NAS	National Academy of Science
NWA	National Water Act.
NWA GN	National Water Act. Government Notice
PSD	Particle Size Distribution
RMT	Rapid Mix Tank
RO	Reverse Osmosis
SAMI	South African Mining Industry
SAVMIN	SAVannah mining and MINtek project.
SEM	Scanning Electron Microscopy
SMCRA	Surface Mine Control Reclamation Act.
SRB	Sulphate Reducing Bacteria
TDS	Total Dissolved Soids
TG	Thermogravimetry
TGA	Thermogravimetric Analyzer or Analysis
WHO	World Health Organization
WQA	Water Quality Association
USEPA	United States Environmental Protection Agency
XRD	X-ray Diffraction

List of notations and symbols

a	=	activity coefficient
a_{eq}	=	equilibrium activity coefficient
A	=	specific area of a crystal
A	=	frequency factor
B	=	nucleation rate, birth rate (#/s)
C	=	concentration (mol/dm^3)
c*	=	equilibrium concentration(mol/dm^3)
$\mathbf{c}_f$	=	concentration of the added reagent
$\mathbf{c}_F$	=	concentration of the added reagent
E_a	=	activation energy
g	=	9.81 - gravitation constant (m/s^2)
G	=	linear crystal growth rate (m/s)
G_{av}	=	average crystal growth rate (m/s)
G(L)	=	growth rate as a function of length
G/G_0	=	relative crystal growth
IP	=	Ionic Product (mol/dm^3)^2
J/J_0	=	relative nucleation growth
k_g	=	rate factor
k_v	=	particle size-shape factor
K_{sp}	=	solubility product (mol/dm^3)^2
n	=	amount of particle (#/m)
N		number of dosing oints
$\mathbf{M}_T$	=	total mass of the crystals in the vessel
$\mathbf{N}_T$	=	total number of the crystals in the vessel
P	=	product rate
Re	=	Reynolds number (-)
rpm	=	revolutions per minute
R	=	8.314 – gas constant (J/mol.K)
S	=	supersaturation (-)
S_a	=	affinity based supersatiration
S_{crit}	=	the critical supersaturation
S_{crit}	=	the critical supersaturation

S_{critF} = the feed-based supersaturation

T = temperature (K)

Greek Letters

ρ = density (kg/m^3)

ρ_f = fluid density (kg/m^3)

ρ_p = particle density (kg/m^3)

ρ_{avg} = average fluid density (kg/m^3)

σ = relative supersaturation

γ = activity coefficient for solution

$\Delta\mu$ = chemical potential difference

μ = viscosity of fluid (Pa.m/s)

U_T = Terminal velocity of falling particle (m/s)

U_{rel} = relative velocity of falling particle (m/s)

Φ = affinity based supersaturation

x = particle size/length (micrometer)

Δx = particle size/length interval (micrometer)

List of Tables

List of Figures

CHAPTER 1

INTRODUCTION

1.1. Acid Mine Drainage formation and its impact.

South Africa has extensive mineral resources such as coal, iron ore, diamonds, mineral sands, copper, gold and, oil and gas which have given rise to extensive mining activities in many regions of the country. Many of these mineral resources are mined through surface mining operations. There are, currently, ongoing prospective programmes in many areas of South Africa and these programmes will give rise to further mining activities (DWAF BPGs A5, 2008).

In 2003, the mining sector contributed R78.5 billion (7.1%) to the gross value added in South Africa, and 11.9% to the Total Fixed Capital Formation (DWAF BPGs A5, 2008). In the same year, sales of primary mineral products accounted for 29.85% of South Africa's total export revenue. The mining industry employs about 2.7% of South Africa's economically active population.

On the other hand, mining activities have a negative impact on the environment. Water is typically the prime environmental medium, besides air, that is affected by mining activities. Mining adversely affects water quality by polluting water resources and this poses a significant risk to South Africa's water resources (DWAF BPGs G3, 2006). While it is well known that South Africa is a water-stressed country, with a predominantly semi-arid climate, varying from desert and semi-desert in the west to sub-humid along the eastern coastal region, pollution of water resources by mining activities aggravates the situation. Large volumes of polluted water exist both underground and on the land surface in South Africa due to existing and closed mining activities (Heynike, 1981).

Of all the mining sectors coal mining is by far the largest contributor to water pollution in South Africa. The process of coal mining, which is common in South Africa, produces large amounts of waste rock referred to as overburden or mine tailings. The mine tailings are normally deposited in piles around the mining sites. Upon exposure to atmospheric oxygen and water, this material begins to undergo a process of natural weathering, which starts almost immediately after deposition (Mead, 2005).

The weathering of coal mine tailings, containing iron pyrite (FeS_2) or other sulphide minerals (Table 1.1), produces an acidic runoff which has an adverse impact on the environment (Skousen *et al.,* 2002). This acidic runoff is commonly referred to as Acid Mine Drainage (AMD) or Acid Rock Drainage (ARD). For the purpose of this thesis this mine acidic runoff will be referred to as AMD. Due to its acidic nature, AMD can leach metals such as iron, manganese, aluminium, lead, arsenic, and zinc from the waste rock. In areas with a history of coal mining, AMD can detrimentally impact ground water and/or surface water quality (Mead, 2005).

As has already been mentioned, AMD is commonly associated with coal mining, but it is also formed where geological strata containing sulphides are exposed, such as in road construction, metal mining, or other deep excavations (Skousen *et al.,* 2002). Therefore, the formation of AMD is a general consequence of the exposure of pyrite containing rock to oxygen and water, leading to the oxidation of pyrite. The chemistry of pyrite oxidation, the production of ferrous ions (Fe^{2+}) and subsequently ferric ions (Fe^{3+}), is very complex, and this complexity has hampered the design of effective water treatment options considerably (INAP, 2005).

Table 1.1. The metal sulphides responsible for AMD formation, during mining activities (INAP, 2005).

FeS_2	Pyrite
FeS_2	Marcasite
Fe_xS_x	Pyrrhotite
Cu_2S	Chalcosite
CuS	Covellite
$CuFeS_2$	Chalcopyrite
MoS_2	Molybdenite
NiS	Millerite
PbS	Galena
ZnS	Sphalerite

Although numerous chemical processes contribute to the formation of AMD, pyrite oxidation is by far the greatest contributor. The general reaction equations for the formation of AMD during mining activities are as follows:

$$2FeS_2 + 8O_2 + 2H_2 \longrightarrow 2Fe^{2+} + 4SO_4^{2-} + 4H^+ \quad (1)$$

$$4Fe^{2+} + O_2 + 4H^+ \longrightarrow 4Fe^{3+} + 2H_2O \quad (2)$$

$$4Fe^{3+} + 12H_2O \longrightarrow 4Fe(OH)_3 + 12H^+ \quad (3)$$

$$FeS_2 + 14Fe^{3+} + 8H_2O \longrightarrow 15Fe^{2+} + 2SO_4^{2-} + 16H^+ \quad (4)$$

These reactions reveal the quantity of acid (H^+ ions) produced during the oxidation of pyrite. Oxidation of sulphide to sulphate solubilizes the ferrous iron which leads to the oxidation to ferric iron. While this reaction is faster at higher pH, bacteria (*Acidothiobacillus ferro-oxidans*), which are widespread in the environment, greatly accelerate this reaction under low pH conditions (Barnes & Romberger, 1968).

Not all coal mines produce AMD. The potential for AMD to be produced from a coal mine is related to its geological history i.e. how the coal was formed (Skousen *et al.,*

2002). Therefore, the drainage quality emanating from underground mines or backfills of surface mines is dependent on the acid-producing (sulphides) and alkaline (carbonate) minerals contained in the rock being mined. Generally, sulphide-rich and carbonate poor rock is responsible for the production of acidic drainage. On the other hand, alkali-rich strata, even with significant sulphide content, produce alkaline conditions in water (Skousen *et.al.,* 1993). Acidic drainage is high in acidity while alkaline drainage is high in alkalinity. The acidity and the alkalinity of the waste-water are both measured in terms of mg/L $CaCO_3$.

The acidity in AMD is comprised of mineral acidity (iron, aluminium, manganese, and other metals depending on the specific geological setting and metal sulphide) and hydrogen-ion acidity (Skousen *et.al.,* 1993). The high sulphate concentration in AMD is a result of the sulphur in pyrite minerals being oxidised to sulphate (Equations 1 & 4, above). The sulphate concentrations in AMD can be as high as thousands of mg/L. Figure 1.1 shows AMD in a storage dam, where the red-brown colour is due to the Fe^{3+} present in the water.

Figure 1.1. A typical occurrence of AMD in a storage dam.

Thomas, (1970*)* described AMD as one of South Africa's major pollution problems as the run-off water from such storage dams can enter nearby water-courses. Maree et

al., (1989), confirmed this, through analysis of water samples taken from various streams. This showed that the sulphate content in run-off water from areas with high mining activities varied between 200-2000 mg/L (Maree *et al.,* 1989) and furthermore, this water was found to be rich in heavy metals. This run-off water has a negative impact on both industry and on the environment.

1.2. The impacts of AMD.

Industrially, AMD has a corrosive effect on mining equipment due to its low pH and high Fe^{3+}-concentration. This leads to a requirement for regular replacement or maintenance of equipment which has a severe impact on the capital cost of mining.

As mentioned previously, contact of untreated AMD with water courses has a negative impact on the environment and on water users. Mine closure leaves a legacy of sulphate-rich water both on the surface and in underground workings. The high sulphate concentrations prohibit discharge of untreated AMD into streams and rivers owing to the detrimental effect on aquatic plant and fish life. However, seepage from sources of AMD from time to time, inevitably pollutes streams and rivers (Volman, 1984).

It is estimated that about 540 ML/d of acid mine water is produced in the Gauteng region alone (Volman, 1984). It was also estimated that 200 ML/d of mining effluents, saturated with calcium sulphate, are discarded into water courses of the Pretoria-Witwatersrand-Vereenig region, now known as Gauteng (Maree, 1988). Mine water in the Upper Olifants River catchment in Mpumalanga (upstream of Loskop Dam) is at times discharged into local streams, resulting in local acidification and regional salination of surface water resources such as rivers, dams and ponds (Maree, 1988).

Salination is one of the most important water quality problems in South Africa (Heynike, 1981). Reports on the accelerated increase of 100 mg/L to 500 mg/L in the average total dissolved solids (TDS) in some of the areas around South Africa, since 1965, are attributable to the sulphate content of the wastewater discharge (Heynike, 1981; Heynike, 1987). Loewenthal *et al*., (1986), reported that it is

generally accepted that chloride and sulphate ions stimulate the rate of corrosion and inhibit passivation in, for example, metal pipes (Loewenthal *et al.,* 1986).
For the purpose of mine water re-use, sulphate concentration (SO_4^{2-} > 2500 mg/L) needs to be reduced to levels below gypsum oversaturation levels (SO_4^{2-} = 1500 - 2500 mg/L), in order to avoid salinity-associated corrosion to equipment, scaling of pipes, boilers and heat exchangers (Maree *et al.,* 1990*).*

Environmentally, the damage caused by sulphate emissions is not direct, since sulphate is a chemically inert, non-volatile, and relatively non-toxic compound. As reported, a lethal dosage for humans is 4 500 mg/kg as K_2SO_4 or $ZnSO_4$ and the minimum lethal dosage of magnesium sulphate in mammals is 200 mg/kg (WHO, 1984a). The major health effect observed following sulphate ingestion is laxative action (Daniels, 1988; NAS, 1977), and the cation associated with the sulphate anion appears to have some effect on the laxative potency (Daniels, 1988). Calcium sulphate, for example, is much less potent than magnesium sulphate or sodium sulphate. This may be due to the laxative properties of the cations themselves or from differences in solubility (Daniels, 1988).

Infants appear to be more sensitive to the laxative action of sulphate than adults. Infants, 5 to 12 months old, that were given formulas prepared with water containing 630 to 1 150 mg/L sulphate developed diarrhoea shortly after ingestion of the formula (Chien *et. al.,* 1968). The effect was reversible after the use of high sulphate water was discontinued. Similar effects have been observed in adults; however, adults are able to adapt to high sulphate levels in a short period of time (USEPA, 1990*).* Results of a questionnaire sent to North Dakota residents indicate that laxative effects increased at sulphate levels above 500 mg/L. At sulphate concentrations exceeding 1000 mg/L, the majority of respondents indicated a laxative effect (Peterson, 1990; Moore, 1952).

Sulphates can also contribute to an undesirable taste in water. The taste threshold for the sulphate ion in water is 300 - 400 mg/L (NAS, 1977), and a guideline value of 400 mg/L based on aesthetic quality has been suggested

(WHO, 1984a). The current USEPA Secondary Maximum Contaminant Level (SMCL) for sulphate, based on organoleptic effects, is 250 mg/L (USEPA, 1990).

Pursuant to the Safe Drinking Water Act, the USEPA has proposed Maximum Contaminant Level Goals of either 400 or 500 mg/L to protect infants (based on and has identified a LOAEL (Lowest-Observed-Adverse-Effect-Level) of 630 mg/L based (Chien *et. a*l., 1968; Peterson, 1990; Moore, 1990), on diarrhoea in infants receiving formula made with high-sulphate water (USEPA, 1990).

The Drinking Water Standards of the U.S. Public Health Service recommend that sulphate in water should not exceed 250 mg/L, except when no more suitable supplies are or can be made available. The World Health Organization, in the European Standards for Drinking Water, also set a sulphate limit of 250 mg/L (NAS, 1977). The Canadian guideline for the maximum acceptable concentration of sulphate in drinking water is 500 mg/L (USEPA., 1990). The U.S. Army has set a standard of 100 mg sulphate/L for personnel in arid climates who consume up to 15 liters of water per day, and the Army standard for soldiers serving under less strenuous conditions, consuming 5 litres of water per day, is 100 mg/L (USEPA., 1990). In South Africa the generally acceptable highest concentration of sulphate in drinking water has been set to 200 mg/L (DWAF BPGs – H3, 2006; DWAF, 1996).

1.3. The AMD treatment regulations for environmental sustainability.

Increasingly, regulatory agencies are becoming concerned about elevated sulphate concentrations in effluents which lead to pollution of public streams (INAP, 2006). The principles of sustainable environmental management have developed rapidly over the past few years at an international level (INAP, 2006). Concern about environmental sustainability will result in more stringent standards for sulphate in effluents and this will lead to a requirement for sulphate treatment at many mining sites around the world. In response to such concerns, several sites in the United States, Australia, Canada and South Africa are currently investigating sulphate removal technologies or using some form of sulphate treatment system (INAP, 2006).

Since the passage of the Surface Mining Control and Reclamation Act (SMCRA) in 1977, coal mine operators in the U.S have been required to meet environmental land reclamation performance standards. Operators must also meet water quality standards established in the Clean Water Act of 1972 (CWA), which regulates discharges into waters of the U.S. If AMD problems develop during mining or after reclamation, a plan to treat the discharge must be developed (Skousen *et al*., 2002).

In South Africa the Department of Water Affairs and Forestry (DWAF) is currently exerting pressure on the mining industry to treat water effluents for sulphate and other chemical pollutants before discharge into water systems. DWAF has outlined best practice guidelines for water resource protection in the South African Mining Industry (SAMI) and in these guidelines mining industries are urged to develop water management systems effective enough to minimize environmental pollution by AMD. A pro-active management system of environmental impact is required from the outset of mining activities (DWAF, BPG – H3, 2006).

The rights and other requirements regarding the environment and water are legislated through the National Water Act (NWA, 1998). The use of water for mining and related activities is also regulated through regulations that were updated after the promulgation of the National Water Act (NWA GN704, 1998). Table 1.2 shows the general criteria for effluent discharge into public water courses.

Table1.2. The general criteria for the discharge of effluents into public water courses (NWA GN704, 1998).

Parameter	**General standard**	**Special standard**
pH	5.5 – 9.5	5.5 – 7.5
Sulphide (mg/L as S)	1.0	0.05
Sulphate (mg/L SO_4^{2-})	< 200	Not specified
Conductivity (µS)	≤ 75 above intake value ≤ 250/25^{0}C	≤ 15 above intake value ≤ 250/25^{0}C

The source directed measures aim to control the impacts at source through the identification and implementation of pollution prevention, water reuse and water treatment mechanisms (DWAF BPG - H3, 2006). This is depicted in Figure 1.2 by

the hierarchy of decision-taking which is aimed at protecting the water resource from waste impacts

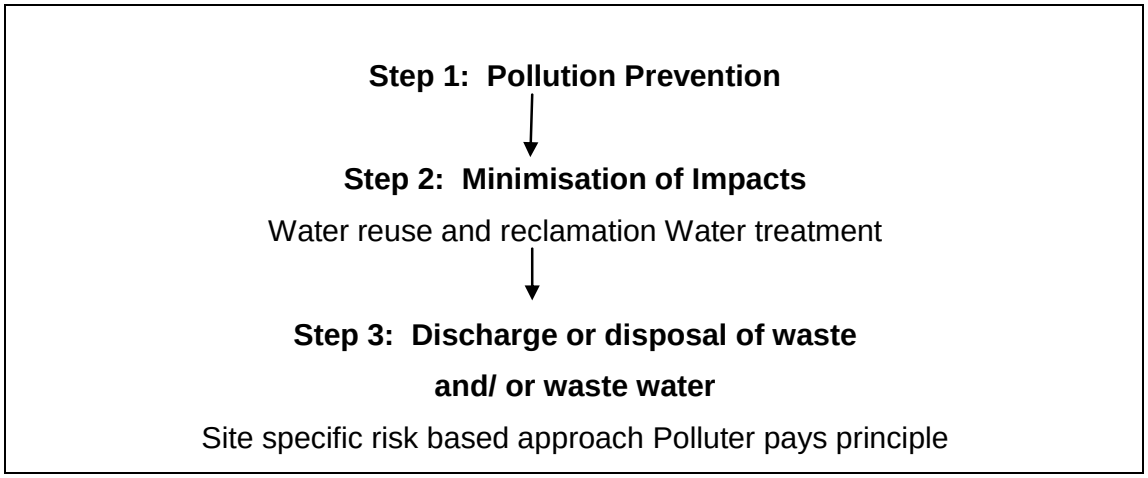

Figure 1.2. The resource protection and waste management hierarchy (DWAF BPGs - H3, 2006).

While measures to prevent the production of AMD (Step 1) are virtually impossible, the mining industry has control over Steps 2 and 3. Minimisation of impacts alleviates the financial burden of the "polluter pays" principle on the mine operator. An effective and viable water treatment technology will lead to safe discharge of mine waste water at a low cost. Figure 1.3 depicts the concepts of water re-use, recycle and reclamation as part of the Integrated Water and Waste Management Plan (IWWMP) (Aubé & Zinck, 2003).

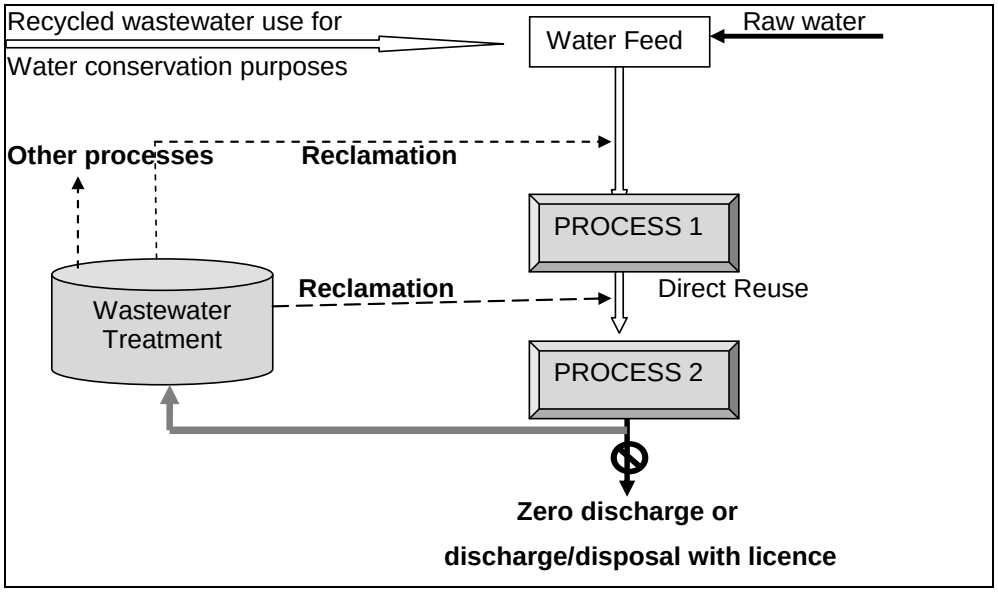

Figure 1.3. The schematic representation of the concepts of water re-use, recycle and reclamation *(*Aubé & Zinck, 2003).

1.4. AMD treatment technology development.

Treatment of AMD includes neutralization of the acidity, removal of metals and most importantly removal of the sulphate to meet the relevant effluent standards. The treatment processes should aim at the recovery of re-usable or environmentally safe dischargeable water from acidic and sulphate-rich effluents. In most cases, a variety of treatment methods can be employed to attain the specified water quality.

1.4.1. Neutralization and metal precipitation.

The neutralization of acid mine water and removal of metals can easily be achieved by use of alkali chemicals (Skousen *et al.,* 1993). Table 1.3 shows the eight primary chemicals that have been used to treat AMD for acidity and metal removal. Each chemical has characteristics that make it more or less appropriate for specific conditions. The best choice among alternatives depends on both technical and economic factors. The technical factors include acidity levels, flow, the types and concentrations of metals in the water, the rate and the degree of chemical treatment needed, and the desired final water quality. The economic factors include prices of

reagents, labour, machinery and equipment, the number of years that the treatment will be needed, interest rates and risk factors.

Table1.3. The typical alkali chemical compounds used in AMD treatment (Skousen *et al.,*1990; Skousen *et al.,*1993*)*.

Common Name	**Chemical Name**	**Formula**	**[1]Conversion Factor**	**[2]Neutralization Efficiency**
Limestone	Calcium carbonate	$CaCO_3$	1	30%
Hydrated Lime	Calcium hydroxide	$Ca(OH)_2$	0.74	90%
Pebble Quicklime	Calcium oxide	CaO	0.56	90%
Soda ash	Sodium carbonate	Na_2CO_3	1.06	60%
Caustic soda (solid)	Sodium hydroxide	NaOH	0.8	100%
20% Liquid caustic	Sodium hydroxide	NaOH	784	100%
50% Liquid caustic	Sodium hydroxide	NaOH	256	100%
Ammonia	Anhydrous ammonia	NH_3	0.34	100%

[1] The conversion factor may be multiplied by the estimated 10^6 mg acid/yr to get mg of chemical needed for neutralization per year. For liquid caustic, the conversion factor gives ML needed for neutralization.
[2] Neutralization Efficiency estimates the relative effectiveness of the chemical in neutralizing AMD acidity. For example, if 10^8 mg of acid/yr was the amount of acid to be neutralized, then it can be estimated that 8.2×10^9 mg of hydrated lime would be needed to neutralize acidity in the water ($10^8(0.74)/0.90$). The price of the chemical to be used depends on the quantity being delivered.

The principle of AMD neutralization and metal removal lies in the addition of sufficient alkali to the AMD to raise the pH, and the insolubility of the heavy metal hydroxides under the alkaline conditions created by the addition of such alkali. Enough alkali must raise the pH and supply hydroxyl ions (OH^-) so that dissolved metals will form insoluble metal hydroxide precipitates (Reaction Equations 5 – 11) . The following equations show the precipitation of different metals under alkaline conditions (Aubé & Zinck, 2003).

$$Co^{2+} + 2OH^- \longrightarrow Co(OH)_2 \quad (5)$$

$$Cu^{2+} + 2OH^- \longrightarrow Cu(OH)_2 \quad (6)$$

$$Fe^{2+} + 2OH^- \longrightarrow Fe(OH)_2 \quad (7)$$

$$Fe^{3+} + 3OH^- \longrightarrow Fe(OH)_3 \quad (8)$$

$$Ni^{2+} + 2OH^- \longrightarrow Ni(OH)_2 \quad (9)$$

$$Pb^{2+} + 2OH^- \longrightarrow Pb(OH)_2 \quad (10)$$

$$Zn^{2+} + 2OH^- \longrightarrow Zn(OH)_2 \quad (11)$$

The precipitates can be formed individually as miniscule particles smaller than a micron (1 µm). By controlling the pH to set-point of 9.5, metals such as iron, zinc and copper are precipitated (Aubé & Zinck, 2003). Figure 1.4 shows the metal precipitation out of solution as a function of pH. Other metals such as cadmium require a higher pH, in the range of 10.5 to 11, in order to effectively form the corresponding hydroxides.

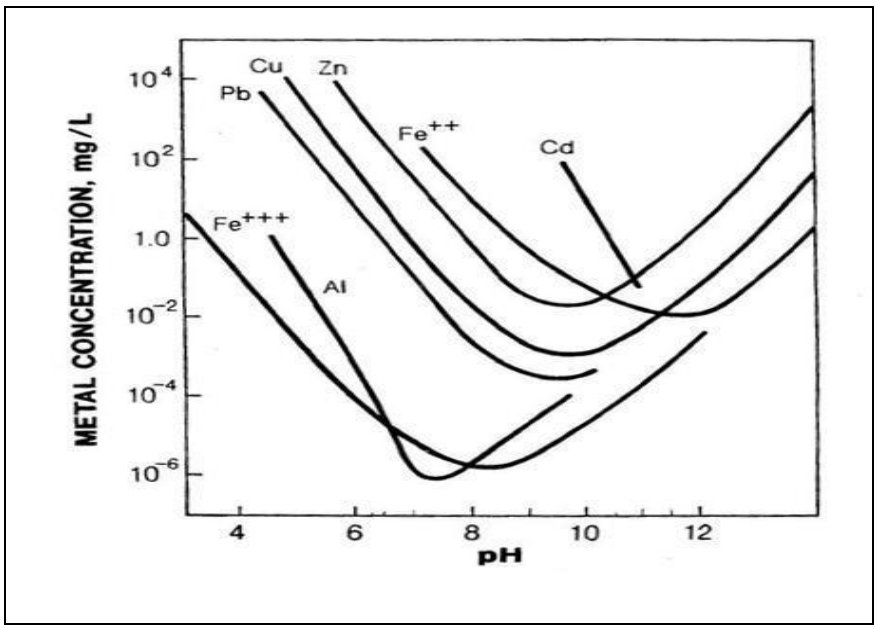

Figure 1.4. The metal hydroxide precipitation curves with pH variation (Aubé & Zinck, 2003). .

Although many different chemicals can be used for neutralization of AMD, lime and limestone have so far been extensively exploited (Aubé & Zinck, 2003; Faulker, 199; Skousen & Ziemkiewicz, 1995). The wide use of these two chemicals is based on

their cost effectiveness, in large volume flow treatment, and their ability to easily raise the pH of the AMD. A brief discussion of these two technologies follows.

1.4.1.1. Lime treatment.

The large AMD treatment systems use a method called Quicklime. The Quicklime method involves a direct dosing of lime into the AMD storage pond or dam. In this method the AMD does not have to be pumped into a treatment plant and there is no control system for lime dosage. A number of quicklime treatment systems have been in use and differ according to the type of AMD to be treated but the resulting effluent chemistry is similar for all treatment processes (Aubé & Zinck, 2003). The lime must first be hydrated (slaked as shown in reaction equation 12) and is normally fed to the process as slurry. The lime dissolution is the first step in the neutralization process (Equation 13). This step is responsible for raising the pH of the AMD and provides hydroxide ions for metal precipitation.

$$CaO + H_2O \longrightarrow Ca(OH)_2 \quad (12)$$

$$Ca(OH)_2 \longrightarrow Ca^{2+} + 2OH^- \quad (13)$$

The older methods for lime handling, though simple, use lime less efficiently and do not allow for good control of the treatment system. The more recent processes require a greater capital investment but are considerably more efficient for lime usage and waste production. The scope of this thesis encompasses discussion of selected and recent processes only.

1.4.1.1 (a). The conventional lime treatment plant.

A basic requirement for all lime treatment systems is the dissolution and mixing of the lime. A conventional treatment plant is one where the AMD is neutralized in a mixing tank with controlled addition of lime to attain a desired pH set-point as demonstrated by Figure 1.5 (Aubé & Zinck, 2003). The slurry is then contacted with a flocculant and finally fed to a clarifier for solid/liquid separation. The sludge is collected from the bottom of the clarifier and can either be pumped into a storage area or pressure-filtered to increase its density prior to transport.

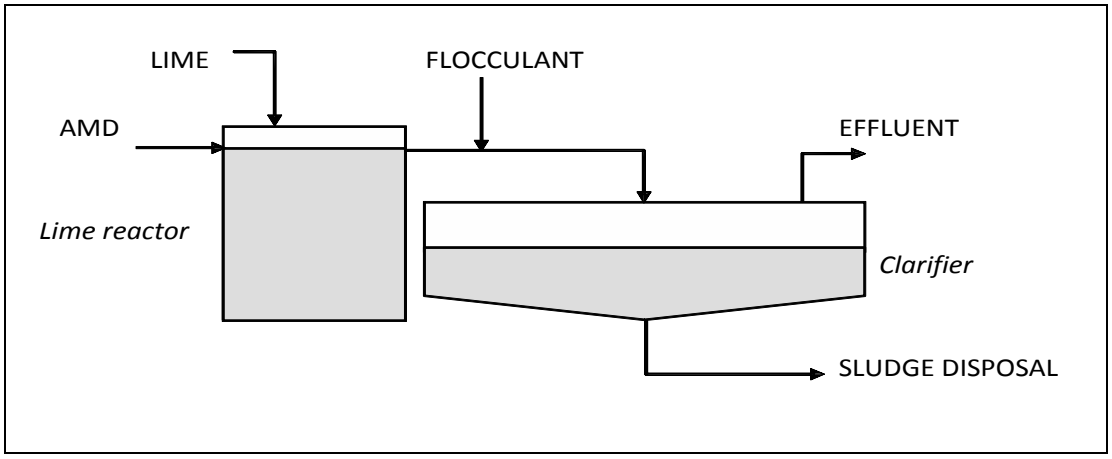

Figure 1.5. Schematic diagram of a lime treatment plant (Aubé & Zinck, 2003).

The fact that the feed is pumped to the plant and that the processes can be well automated, means that this type of treatment is well controlled. This process has a better lime efficiency compared to the old pond and pit treatment processes, however it would have been more efficient if the sludge from the process was to be recycled.

The search for increased lime-use efficiency has led to the modification of the conventional treatment plant into the high density sludge (HDS) process, which is the standard process in the AMD treatment industry today (Aubé & Zinck, 2003). In this system the recycled sludge is contacted with the lime slurry for neutralization instead of contacting lime directly with the AMD (Figure 1.6). This is done by pumping the sludge from the bottom of the clarifier to a "Lime/Sludge Mix Tank" where sufficient lime is fed to neutralize the AMD to the desired set-point.

The pH is controlled in the Rapid Mix Tank (RMT) and the precipitation reactions are completed in the Lime Reactor (LR). The precipitated particles agglomerate as they come into contact with the flocculant in the Flocculant Tank (FT). This process promotes particle settling in the clarifier due to increased particle size and density. The key to the HDS process lies in the mixing of lime and sludge prior to neutralization.

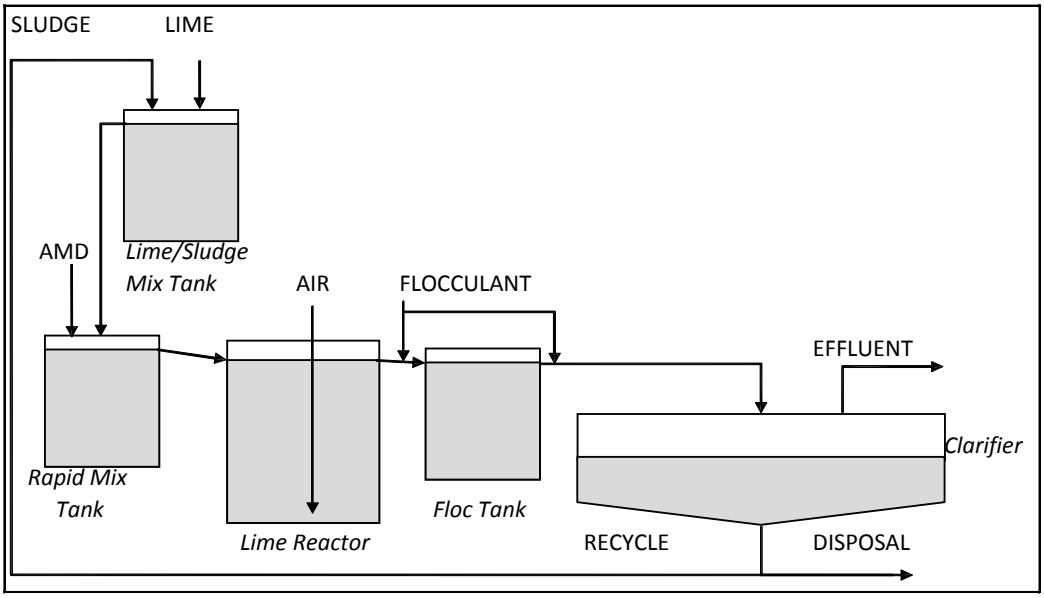

Figure 1.6. The schematic diagram showing a typical HDS process (Osuchowski, 1992).

The precipitates from this process are different from those of the conventional process on a microphysical scale. Osuchowski (1992) reported that sludge 10-times denser than that of the conventional sludge used in the plant, was produced when AMD was treated in an HDS plant. A DEGREMONT TURBOCIRCULATOR, modified to act as thickener, was used in the solid/liquid separation stage. The same degree of solid/liquid separation would require a larger clarifier in a conventional plant.

Since the development of the HDS Process, further modifications of this generic concept have been developed (Aubé, 1999). While the original HDS Process in Figure 1.6 contains a Rapid Mix Tank and a Flocculation Tank, its variant, the Heath Steele Process, is identical in concept and provides the same physical and chemical advantages but without these two reactors (Aubé & Zinck, 2003).

Aubé, (2004), carried out tests on a pilot scale to demonstrate, that there is no advantage to using a Rapid Mix Tank for pH control. The Flocculation Tank was removed, as it is possible to ensure proper flocculant contact by providing turbulence in the conduit leading from the Lime Reactor to the Clarifier. Other lime based

processes such as the Geco and Staged Neutralization Processes have been developed from the modification of the HDS Process (Aubé & Zinck, 2003).

1.4.1.1 (b). The limestone treatment process.

Although lime has proved to be the best alkali for AMD neutralization, it has its own drawbacks, requiring accurate dosing to prevent under or over dosage, and pH controlled dosing systems have proved to be unreliable due to fluctuations in the water flow-rate and poor maintenance (Osuchowski, 1992).

Under-dosage of lime leads to flow of low pH water in the pipelines which results in corrosion of equipment. To counteract this effect, larger amounts of lime are dosed into the system which then readily leads to over-dosage. This results in gypsum crystallization due to the high calcium concentration (above super-saturation of $CaSO_4$). Gypsum crystallization during neutralization of AMD with lime leads to the formation of scale in the pipelines, which reduces the effective diameter of the pipes (Figure 1.7).

Figure 1.7. Partially blocked pipelines, caused by gypsum crystallization due to lime over-dosage into AMD.

The worst case scenario is a complete blockage of pipes and valves which requires extensive maintenance or replacement on a regular basis. The high cost associated

with the need for high dosage of lime is, therefore, exacerbated by the high cost of regular maintenance of the equipment.

Maree and Clayton, (1992), succeeded in demonstrating that replacing lime with limestone yields various advantages and benefits, as listed below:

- Limestone is cheaper than lime which results in a cost saving.
- It dissolves at pH values below 7 hence no pH control is required.
- It is not readily soluble in neutral water, therefore can be stored in the open.
- Limestone is safe and easy to handle.
- It is possible to utilize the equipment on an existing lime plant, for limestone

In spite of all these advantages, limestone neutralization has had limited application due to its low neutralization rates compared to lime and other alkalis. In their studies, Maree and Du Plessis, (1993) discovered that this is due to a phenomenon of surface scaling of the limestone particles, which in turn inhibits its reaction rate. This drawback can be overcome by using a fluidized-bed process (Maree & Clayton, 1992). A fluidized-bed process ensures a high effective limestone presence in the reactor and counteracts scale formation through attrition.

Another drawback associated with limestone neutralization is its inability to dissolve at pH values higher than 7. This means that Fe(II), which can only precipitate as Fe(III) at pH values higher than 7, cannot be removed by limestone neutralization alone. A two-staged limestone-lime neutralization process, in which limestone is dosed first, followed by lime, has the ability to remove iron as $Fe(OH)_3$ while remaining cost effective compared to the lime process but has proved to be too complex for adoption by most mines (Wilmoth, 1974).

Following research conducted at the CSIR, a pilot-scale, fluidized-bed neutralization process, which operates at pH values lower than 7 using limestone, was developed (Maree & Du Plessis, 1994; Maree *et al.,* 1996a; Maree *et al.,* 1996b). In order to overcome the problem of the inability of limestone to remove iron(II), this process was integrated into a three-stage process which consisted of:

1. A biological iron(II) oxidation stage
2. A limestone neutralization stage, and
3. A gypsum crystallization stage

A three year, on-site evaluation study of this process at Navigation, Landau Colliery, (Maree, 1994) showed that:

- Discard leachate containing only 10 g/L acid (as $CaCO_3$) and 4000 mg/L iron(II) could be achieved in a limestone neutralization, fluidized-bed reactor, provided iron(II) was oxidized beforehand.
- Iron(II) could be oxidized biologically to iron(III) at low pH values, requiring a residence time of 18 hours.
- Sulphate concentration could be lowered from 18 000 mg/L to less than 2 500 mg/L via gypsum crystallization in a fluidized-bed contactor with a residence time of 2 h.

This three-stage process showed a number of advantages but its main drawback was its high cost, owing to the long residence time of 18 hours, required for the biological iron(II) oxidation.

1.4.2. The sulphate removal processes.

The current literature has shown that while neutralization and removal of metals from effluents can be easily achieved with the use of a number of chemicals, the sulphate content is often the cause of contravention of effluent standards. Unlike in other countries such as the United States where emphasis is placed on removal of acidity and heavy metals, in South Africa the emphasis is placed on the removal of sulphate from effluents. The reason for this is because South Africa has small rivers, compared to the United States where dilution is more significant when effluents are discharged into rivers (Mudder, 1995). It is, therefore, vitally important to develop effective techniques and approaches for sulphate removal from mine water in South Africa in order to prevent the salination of surface water.

The drivers for research into sulphate removal processes are:

- Efficiency, controllability, and sustainability.
- Up-scalability and easy handling.
- Economic viability.

Efficiency refers to the ability of the process to remove sulphate effectively and the ability of the process to handle high volume flows of effluents. The process should be versatile in order to adapt to different qualities of effluents. While the basic principle of the process remains the same, the system should be able to allow for minor variations/adjustments but retain the sulphate removal capability. The monitoring and maintenance required to sustain the performance of the sulphate treatment process should be practical with few potential complications.

The development of a sulphate removal process starts with conception of the sulphate removal idea, which is based on a certain principle, after which laboratory experiments are planned and carried out in order to evaluate the feasibility of the idea. The laboratory results are treated as the primary application of the principle and are used to plan for pilot scale studies. Scaling up from the laboratory studies to pilot studies may require some readjustment or even a complete change of the initial idea. It is normally at this stage of research where potential problems associated with the process are encountered and dealt with.

Previous experience has shown that it is common for problems to arise, with regard to the practicability of the process, at full scale operation, hence a process should allow for adjustments at this stage as well. The process should be relatively uncomplicated and should be easy to operate with minimum manpower and maximum safety for operators.

The implementation of the process should be cost-effective and produce as little waste as possible. Where concomitant production of further waste during the process is inevitable, a further downstream process for the treatment of the resultant waste should be developed concurrently. The downstream process should be cost effective or even financially viable for the user, if possible.

1.4.3. Conventional sulphate removal methods.

Several sulphate removal processes have been studied and extensively exploited. These processes are broadly categorized as those using:

- Biological mechanisms
- Semi-permeable membranes
- Ion-exchange processes
- Chemicals

In biological sulphate removal processes sulphate is converted to sulphide by sulphate reducing bacteria (SRB) when an energy source such as sugar, ethanol or hydrogen is provided. The sulphide produced is then removed as elemental sulphur in a downstream process (Mudder, 1995).

Semi-permeable membrane processes include Reverse Osmosis (RO) and Electro dialysis (CMRO, 1988). In these processes sulphate rich water is forced through a semi-permeable membrane. Sulphate is retained on one side while water permeates to the other. Because solids are retained on the membrane surfaces, these systems are highly susceptible to fouling and resultant loss of production capacity.

Ion-exchange processes use ion-exchange resins where sulphate from the sulphate rich water is exchanged for an easily collectable ion. A well established example of such a process is the SAVMIN process which is an ion exchange process in which sulphate is removed through gypsum and ettringite precipitation. The regeneration of cation and anion resins is achieved using sulphuric acid, lime and alum. This process combines two techniques i.e ion exchange and chemical mineral precipitation and will be discussed again in the next section (1.4.3.1). The use of chemicals in sulphate removal involves the precipitation of sulphate by adding a chemical that will react with dissolved sulphate in the AMD to form a sulphate compound that can be easily separated from the water.

The scope of this thesis is to focus specifically on chemical sulphate removal processes and it is for this reason that fairly detailed discussions of some of the previously successful chemical processes are given in the following section.

1.4.3.1. Chemical treatment of AMD for sulphate and metal removal.

Chemicals with the ability to precipitate sulphate from aqueous solutions are available and some of them have already been extensively exploited in the treatment of AMD.

1.4.3.1 (a). Lime and limestone treatment processes.

As mentioned earlier, lime and limestone are traditionally used for neutralization of AMD, but can also be used in the processes for sulphate removal from AMD through precipitation of gypsum ($CaSO_4 \cdot 2H_2O$):

$$Ca(OH)_{2\,(s)} + H_2SO_4 \longrightarrow (CaSO_4 \cdot 2H_2O)_{(s)} \quad (14)$$

$$CaCO_{3\,(s)} + H_2O + H_2SO_4 \longrightarrow (CaSO_4 \cdot 2H_2O)_{(s)} + CO_2 \quad (15)$$

In these processes the levels to which sulphate concentrations are lowered are controlled by the solubility of gypsum, which, depending on the composition and ionic strength of the solution, ranges from 1500 - 2000 mg/L. Maree, (1994) demonstrated the ability of limestone to partially remove sulphate during AMD neutralization. However the sulphate concentration could not be lowered to the required level. Lime neutralization followed by nano-filtration has also been used to lower sulphate concentrations from 3 500 mg/L - 500 mg/L (Mead, 2005). This latter process is expensive and cannot be adopted by most mines in South Africa.

More recently, an integrated limestone/lime process, capable of lowering the sulphate concentration in AMD to less than 1200 mg/L (Geldenhuys *et al*., 2003), has been developed. A schematic representation of this process is shown in Figure 1.8 and consists of the following three steps:

1. Limestone neutralization to raise the pH to near-neutrality, resulting in CO_2 production and gypsum precipitation.
2. Lime treatment to raise the pH to 12 for $Mg(OH)_2$ precipitation and enhanced gypsum precipitation.
3. pH adjustment with CO_2 (recovered from Step 1) with concurrent $CaCO_3$ precipitation.

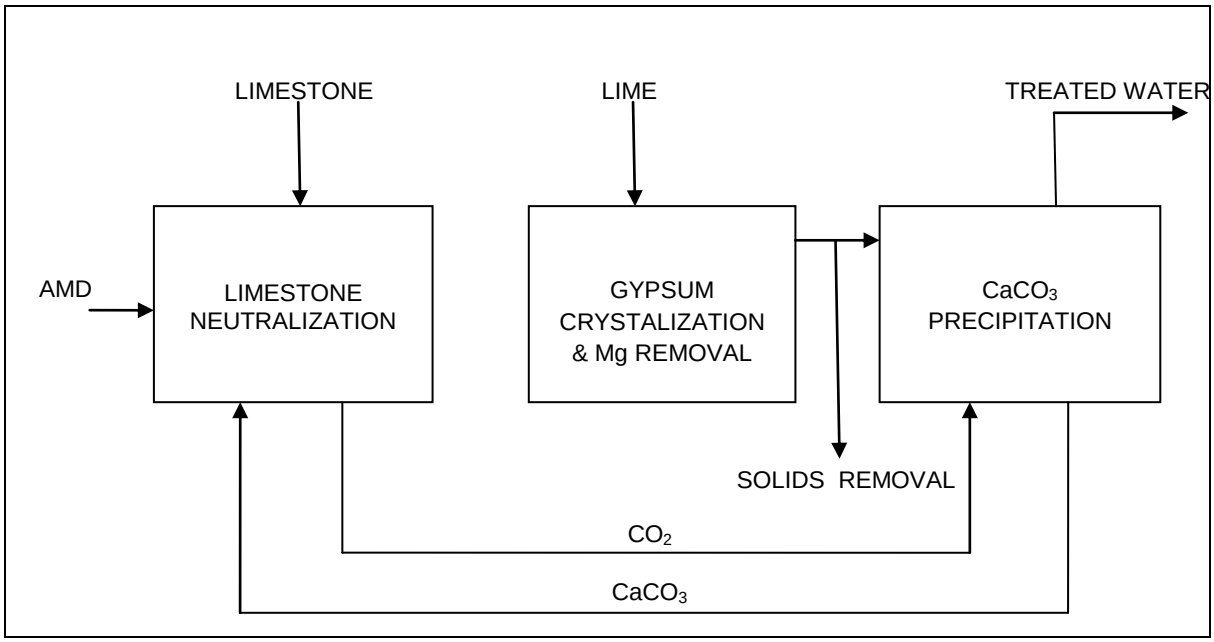

Figure 1.8 Schematic diagram of the Integrated Lime/Limestone Process used for AMD neutralization with concomitant metal and partial sulphate removal (Geldenhuys *et al.,* 2003), .

In work on this process it was discovered that the key processes responsible for the improved sulphate removal are the prior precipitation of $Mg(OH)_2$ and the presence of gypsum seed in the second phase. These two processes both lead to enhanced gypsum precipitation. The sulphate concentration was lowered to 1 200 mg/L when AMD with a sulphate concentration of 3000 mg/L was treated. The lime dosing step has an added benefit of removing trace metals as a result of a raised pH.

1.4.3.1 (b). The SAVMIN treatment process.

The SAVMIN process involves precipitation reactions, in successive stages, to remove dissolved sulphates from AMD (Smit, 1993). The different stages are illustrated in Figure 1.9.

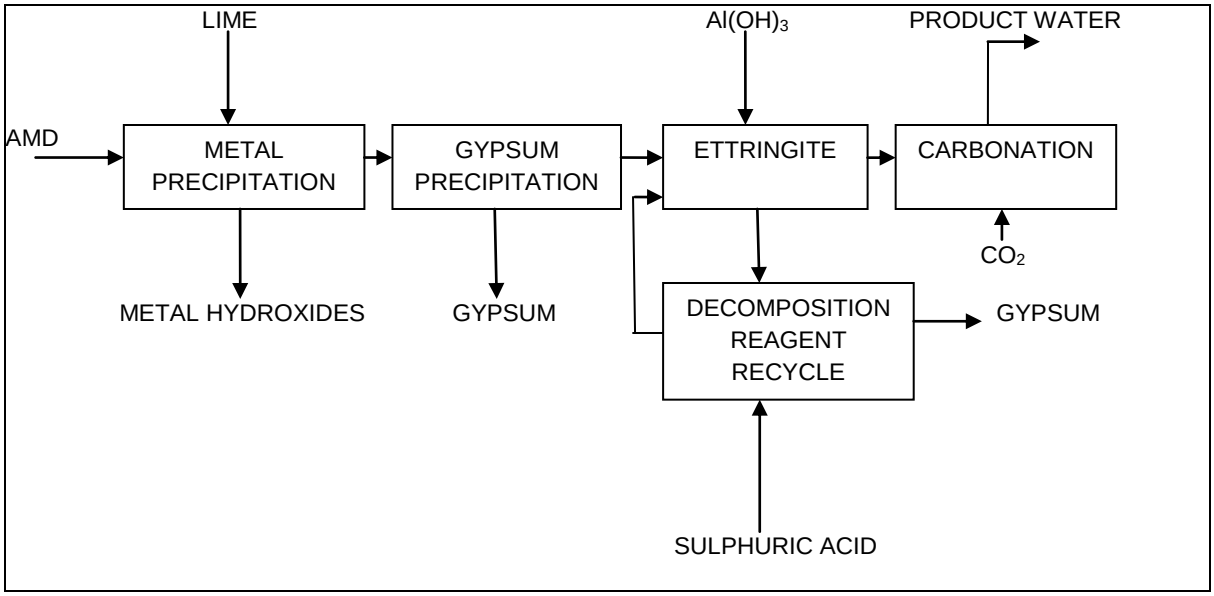

Figure 1.9 Schematic illustration of the different stages in the SAVMIN process (Smit, 1993).

Lime is added in the first stage, to raise the pH of the AMD to approximately 12 during which dissolved metals and magnesium are precipitated as hydroxides according to the general reaction equation (16):

$$Me^{2+} + Ca(OH)_{2\,(s)} \longrightarrow Me(OH)_{2\,(s)} + Ca^{2+} \qquad (16)$$

After the removal of metals and magnesium, the water is seeded with gypsum crystals to catalyze gypsum precipitation from the saturated solution. A portion of the precipitated gypsum is returned as seed crystals to the feed water while the rest is removed from the process. In the third stage, aluminium hydroxide is added to the water, which is still supersaturated with respect to gypsum. The addition of aluminium hydroxide results in the precipitation of ettringite ($3CaO{\cdot}3CaSO_4{\cdot}Al_2O_3{\cdot}31H_2O$) as indicated by reaction equation 17.

$$6Ca^{2+} + 3SO_4^{2-} + 2Al(OH)_3\,(s) + 37H_2O \longrightarrow 3CaO{\cdot}3CaSO_4{\cdot}Al_2O_3{\cdot}31H_2O + 6CH_3O^{+} \qquad (17)$$

Precipitation of ettringite occurs between pH 11.6 - 12.0, removing both dissolved calcium and sulphate. This elevated pH is maintained through the addition of lime. The ettringite slurry is removed from the feed water by filtration and thickening.

In the fourth stage, the waste-water stream, with pH 11.7 and dissolved SO_4^{2-} < 200 mg/L, is treated with CO_2 to lower the pH (to about pH 7). A relatively pure $CaCO_3$ of commercial value is precipitated and collected by filtration from this process. The ettringite slurry is then decomposed with sulphuric acid to regenerate aluminium hydroxide (reaction equation 18) for reuse in the third stage of the treatment process.

$$3CaO{\cdot}3CaSO_4{\cdot}Al_2O_3{\cdot}31H_2O + 6CH_3O^+ \longrightarrow 6Ca^{2+} + 3SO_4^{2-} + 2Al(OH)_3\,(s) + 37H_2O \quad (18)$$

The aluminium hydroxide is recovered by thickening and filtration methods. The remaining solution is seeded with gypsum crystals to precipitate gypsum. The removal of gypsum, by filtration and thickening, is followed by the return of the solution to the ettringite decomposition stage.

In a demonstration plant at the Stilfontein Gold Mine, in South Africa, 500 ML of sulphate rich water (600 – 800 mg/L SO_4^{2-}) was treated with the SAVMIN process at a throughput of 1 100 L/hr. The results showed that the dissolved sulphate concentration was lowered to below 200 mg/L and metals were removed to very low levels.

Another process that is very much similar to the ettringite process is the Cost Effective Sulphate Removal (CESR), also known as the 'Walhalla' process. This process uses the same principles as the SAVMIN but the pH is maintained at a level that prevents precipitation of metals during the first stage thus minimizing the volume of metal-laden sludge. This non-hazardous gypsum sludge is removed from the process by dewatering and filtration. Further lime is then added to raise the pH of the AMD to 10.5, the level at which precipitation of metals as metal hydroxides takes place. The metal-bearing sludge is removed from the process by settling, dewatering and filtration. This process, therefore, produces two gypsum sludges, differing in metal content. The removal of the dissolved sulphate is completed in the third stage of the process.

The primary distinction between the SAVMIN and CESR processes is that the proprietary reagent (derived from the cement industry instead of aluminium

hydroxide) is added in the CESR process, after raising the pH to 11.5 with lime. Another difference between these two processes is that unlike in the SAVMIN process, the ettringite is not recycled in the CESR process.

The CESR is used in treatment plants, at flow-rates as high as 1.32 ML/min, and can lower sulphate concentrations in most industrial waste water to less than 100 mg/L.

1.4.4. The Integrated Barium Carbonate process.

Chemical removal of sulphate by means of barium salts is a potentially promising process which has not received enough attention. This was a conclusion drawn from previous work carried out on the $Ba(OH)_2$, BaS, and $BaCO_3$ processes (Volman, 1984, Maree, 1988, Maree *et al*., 1989;). In general, all barium processes for sulphate removal use the same principle of sulphate removal, which is based on the precipitation of $BaSO_4$ when Ba^{2+} is contacted with SO_4^{2-} in water. The barium compound provides Ba^{2+} ions that precipitate sulphate from the AMD. The general chemical reaction representing this process is given in reaction equation 19.

$$Ba^{2+}{}_{(aq)} + SO_4{}^{2-}{}_{(aq)} \longrightarrow BaSO_4{}_{(s)} \qquad (19)$$

$BaSO_4$ is highly insoluble in water hence the reverse reaction (dissolution of $BaSO_4$) will not take place. The precipitation of $BaSO_4$ is fast hence the rate of this reaction will depend on the solubility of the Ba^{2+} source during the treatment process.

The use of barium salts in sulphate removal processes has a number of advantages that make it commercially viable and an attractive technology to explore:

- The fast precipitation of $BaSO_4$ when Ba^{2+} and SO_4^{2-} are contacted, in solution, makes it possible for the barium process to be stoichiometrically controlled. The correct amount of Ba^{2+} ions can be added in order to remove the desired amount of sulphate from sulphate-rich effluent. There is, therefore, no need for addition of excess amounts of the treatment chemical in this process, which is a financial incentive to employ this process.

- The resultant $BaSO_4$ precipitate can be thermally reduced to BaS in the presence of a carbon containing reducing according to reaction equation 20.

$$BaSO_4 + 2C \xrightarrow{\Delta} BaS + 2CO_2 \qquad (20)$$

- The BaS can be used in the sulphate removal stage or, as it is the starting material for production of most of the barium salts, it can be used to regenerate the barium compound used in the sulphate removal stage thus rendering this process financially viable.

The biggest disadvantage associated with the use of barium compounds for sulphate removal is the introduction of dissolved barium into the treated water. The presence of dissolved barium in water may cause harmful health effects in humans (WQA, 2005). However, barium becomes a harmless precipitate if it is associated with sulphate in water. The stoichiometric controllability of the barium process for sulphate removal makes it possible to leave enough residual sulphate to associate with barium in water, thus eliminating its harmful effect by precipitation.

Barium salts have different chemical and physical properties requiring different handling techniques, which lead to different processes for sulphate removal. These have different pros and cons which have opened research avenues into these processes.

1.4.4.1. The barium hydroxide process for sulphate and metal removal.

Initially the $Ba(OH)_2$ process was a promising treatment option for sulphate-rich effluents as it exhibited the following advantages over the other two barium salts:

- No lime pre-treatment was required to provide OH^- ions for metal precipitation
- H_2S stripping from the total effluent (as required in the BaS process) was completely eliminated.

By-products such as elemental sulphur, NaHS and $CaCO_3$ were recovered more economically as the H_2S stream was concentrated (from BaS lye) and $CaCO_3$ was precipitated from a weak $Ca(OH)_2$ solution (CMRO, 1988*;* Bosman *et al.,* 1990)

The one major disadvantage associated with this process is that crystallization of $Ba(OH)_2$ from BaS lye, to recycle $Ba(OH)_2$, was not successful. Attempts to crystallize this compound from BaS by adding alkaline solutions such as NaOH and Na_2CO_3 resulted in the formation of a complex between $Ba(HS)_2$ and $Ba(OH)_2$ (Bosman *et al.,* 1990).

For this reason this process was rejected as a practical sulphate removal process.

1.4.4.2. The barium sulphide process for sulphate and metal removal.

The studies by Maree *et al,* (1990), elucidated the ability of BaS to directly remove sulphate from acid waters. BaS is highly soluble in water and can therefore readily provide Ba^{2+} for fast interaction with SO_4^{2-} in sulphate rich water. Grayson (1979) noted that the maximum dissolution of BaS is 30 g/100 L and ten percent of the dissolved BaS dissociates into hydroxide and hydrosulphide. The ability of BaS to provide high pH and hydroxides is an advantage as it leads to its capability to remove ammonia, magnesium, manganese and other heavy metals as metal hydroxides (Adlem *et al.,* 1991). Another advantage of BaS is that by-products like sulphur and NaHS can be potentially derived from the H_2S produced during the H_2S stripping stage, and $CaCO_3$ from the softening stage (Adlem*, 1991;* Bosman *et al.,* 1990*;* Du Preez & Maree, 1994*;* Maree *et al.,* 1989).

Maree *et al.* (2004), presented a study where the purpose was to demonstrate the performance of the integrated barium sulphide process (Figure 1.10), consisting of the following stages:

- Removal of sulphate as barium sulphate to below 200 mg/L by means of barium sulphide treatment.
- H_2S-stripping with CO_2-gas.
- Stripping of CO_2 and crystallization of $CaCO_3$.
- Reduction of barium sulphate to barium sulphide in a kiln.

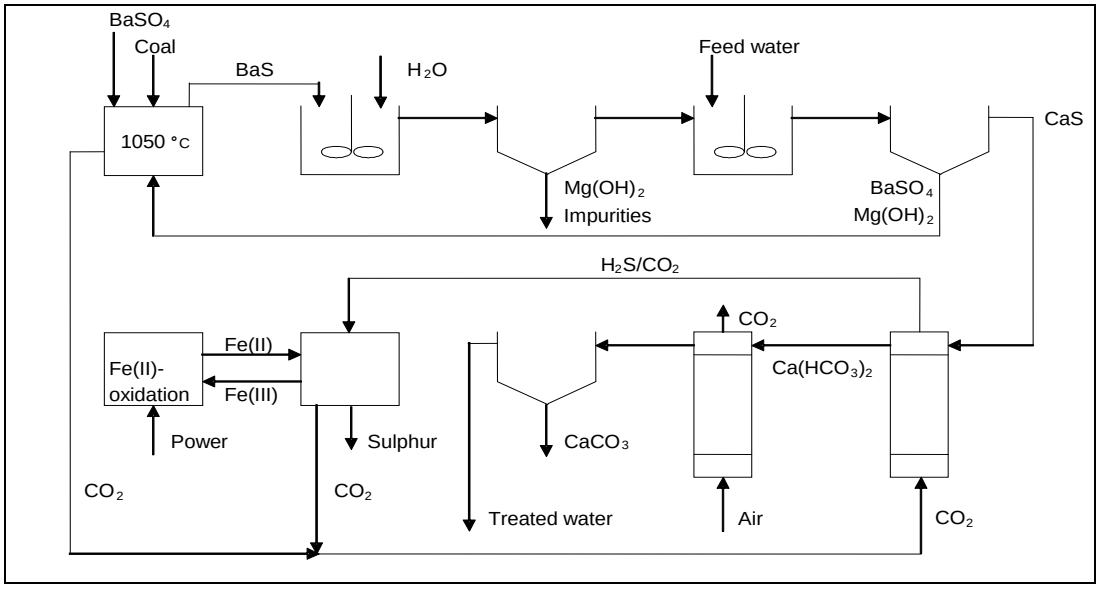

Figure 1.10 Schematic flow-diagram of the integrated barium sulphide process, for sulphate and metal removal (Maree *et al.,* 2004).

In general, the results from studies carried out for the individual steps showed that:

1. The sulphate concentration was lowered to less than 200 mg/L through $BaSO_4$ precipitation and metals were precipitated as hydroxides.
2. Calcium was introduced into the system via calcium-rich feed water and through the association of calcium and sulphide (reaction equation 21), CaS was formed in solution, from which H_2S was stripped.

$$Ca^{2+} + S^{2-} \longrightarrow CaS_{(aq)} \qquad (21)$$

The sulphide concentration was decreased from 333 mg/L to less than 10 mg/L (as S) in the stripping stage using CO_2 gas, with a concomitant crystallization of high quality $CaCO_3$ according to the overall reaction equation 22.

$$CaS + CO_2 + H_2O \longrightarrow H_2S + CaCO_3 \qquad (22)$$

3. Elemental sulphur was quantitatively produced when the stripped H_2S-gas was contacted with a Fe^{3+} solution via the overall reduction-oxidation reaction equation 23.

$$2Fe^{3+} + 3S^{2-} \longrightarrow 3S^{0} + 2Fe^{2+} + 4e^{-} \quad (23)$$

4. The resultant $BaSO_4$ was quantitatively reduced to BaS in a kiln at 1100^0C

The main disadvantage of this system is that sulphide is introduced into the treated water. Sulphide in water is accompanied by a bad odour due to the formation of H_2S. The minimum acceptable concentration of sulphide in water is 1 mg/L, therefore large volumes of water need to be treated further for sulphide removal. Therefore, besides the $BaSO_4$ reduction to BaS, as a downstream step of this process, the H_2S stripping step, the function of which is primarily the removal of sulphide from the treated water, is needed. The H_2S stripping in this process is not economical for production of elemental sulphur as the H_2S is not concentrated enough for the quantitative production of sulphur.

Disadvantages associated with the use of the barium hydroxide- and barium sulphide processes for sulphate and metal removal have led to the reviewing of the use of barium carbonate which was initially not given enough attention. The integrated barium carbonate process forms the basis of this thesis and is presented in detail in the following section. In this thesis the setbacks associated with this process are outlined and discussed and more attention is given to the advantages and the possibility of improving it.

1.4.4.3. The integrated barium carbonate process for sulphate and metal removal.

Since its conception, the barium carbonate process has shown a promising capability to be used for sulphate removal (Kun, 1972). However, associated with this capability are challenges that have been identified by other investigators (Kun,1972; Maree, 1989).
Initially, Kun (1972) studied the removal of sulphate with barium carbonate and obtained good results. However, three problems were identified:

- A long retention time was required for effective sulphate removal when this process was compared to its barium sulphide counterpart, due to the slow dissolution of barium carbonate in water.

- A high concentration of soluble barium remained in the treated water when more barium carbonate was dosed than stoichiometrically required in an attempt to increase the sulphate removal rate.
- The high cost of the barium carbonate was emphasised by the need for higher dosages than required by the stoichiometry of the reaction.

Further research into the barium carbonate process, aimed at finding solutions to these problems, has led to possible improvements. In order to overcome the long retention-time problem and the high barium concentration in the treated water, Trusler *et al.,* (1988) developed a barium carbonate method using a two-stage fluidised-bed reactor system. This allows fast removal of sulphate with $BaCO_3$ due to the fact that excess $BaCO_3$ is in contact with the sulphate-rich water (Maree *et al.,*1989). However, this resulted in barium carbonate becoming inactive when coated with metal hydroxide precipitates (mainly magnesium hydroxide), which rendered it unsuitable for most mine-water treatment processes *(*Trusler *et al.,* 1988*)*. This problem was overcome by pre-treatment of the AMD with lime during which metals and magnesium are removed prior to the barium carbonate dosage *(*Bosman *et al.,* 1990).

The lime pre-treatment stage, on the other hand, increases the calcium concentration in the AMD which then leads to $CaCO_3$ precipitation when $BaCO_3$ is dosed into the system (reaction equation 24).

$$Ca^{2+}(aq) + CO_3^{2-}{}_{(aq)} \longrightarrow CaCO_{3\,(s)} \qquad (24)$$

The $CaCO_3$ by-product produced in this process can be used in the limestone neutralization process or can be converted into lime (CaO) via thermal decomposition (reaction equation 25).

$$CaCO_3 \xrightarrow{\Delta} CaO + CO_2 \qquad (25)$$

However, Maree *et al.,* (1989) noted a problem in separating barium sulphate and calcium carbonate as there is co-precipitation of these two compounds during the

process. In laboratory studies, Adlem *et al.,* (1991) showed that separation of these two compounds can be achieved following the barium sulphate reduction stage (reaction equation 20). The BaS, produced from the reduction of barium carbonate was separated from the calcium carbonate decomposition product (CaO) using a controlled leaching method (Adlem *et al.,* 1991). This was based on the assumption that barium carbonate reduction and calcium carbonate decomposition can take place independently of each other.

Volman (1984) overcame the problem of the high cost of $BaSO_4$ by demonstrating that barium sulphate could be recovered and reduced, efficiently and economically with coal under thermal conditions, to barium sulphide. As mentioned earlier, barium sulphide by reaction with CO_2 can be converted to barium carbonate allowing recovery with consequent costs saving. Wilsenach (1986) calculated the cost of producing barium sulphide from barium sulphate thus demonstrating the economic viability of this process.

The main advantage associated of the use of barium carbonate as compared to barium sulphide, is that there is no introduction of sulphide into the treated water which would require removal in a downstream process. This advantage together with the recoveries of high quality elemental sulphur and calcium carbonate were the motivators for investigating and optimizing this process further.

In the current work, studies to optimize the integrated barium carbonate process for sulphate and metal removal were investigated. The following major stages were as follows:

1. Pre-treatment with lime for magnesium removal and partial sulphate removal.
2. Removal of sulphate as barium sulphate by dosing barium carbonate
3 Thermal reduction of $BaSO_4$ to BaS for sulphur production and $BaCO_3$ recycling.
4 Sulphide stripping from the concentrated solution of the recovered BaS, leading to sulphur production.

The integrated barium carbonate process flow diagram is shown in Figure 1.11.

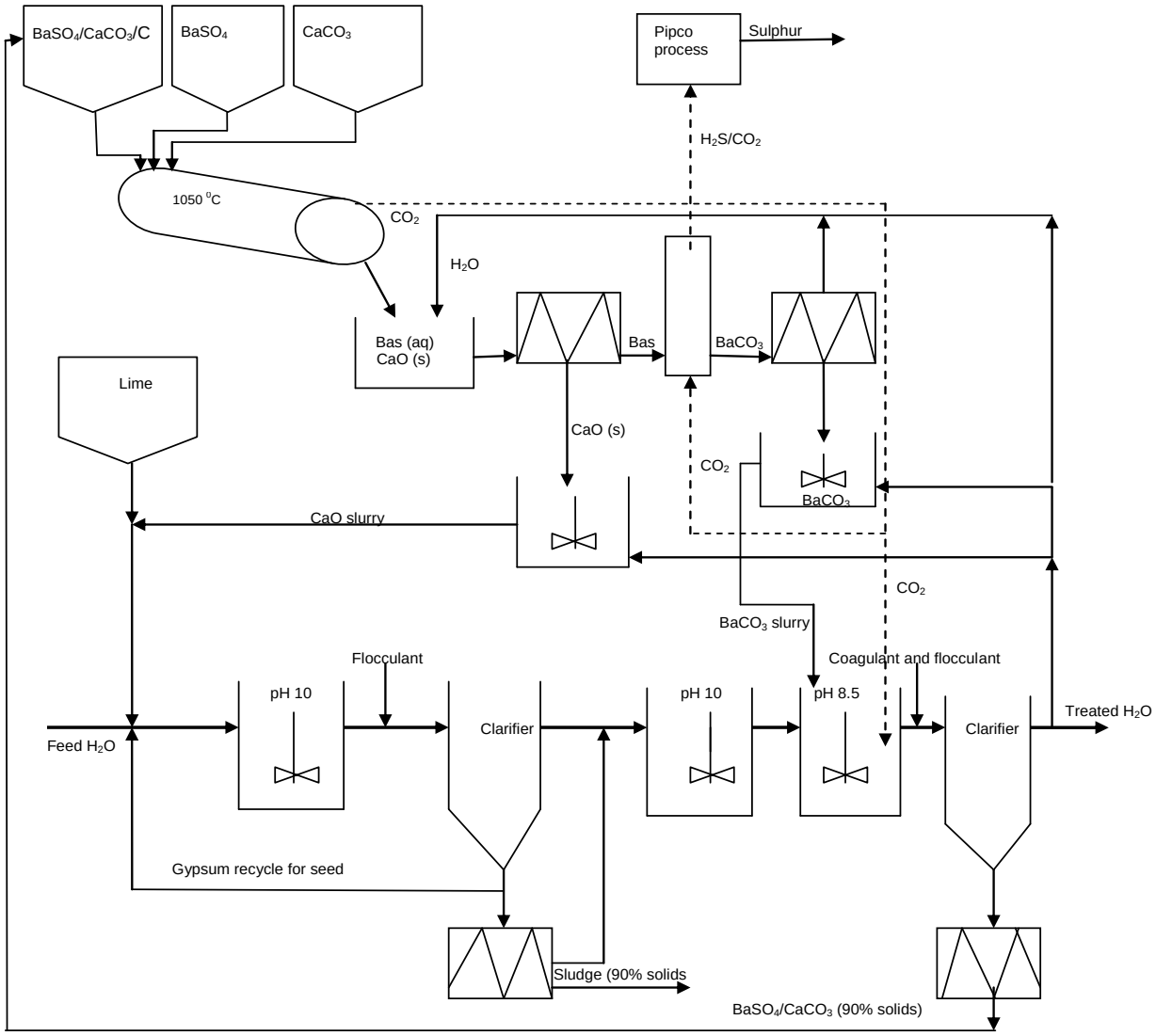

Figure 1.11. Schematic flow-diagram, of the integrated barium carbonate process, for sulphate and metal removal (Hlabela *et al.,* 2007).

In the first stage the feed water is pre-treated with lime slurry during which the pH of the feed is raised to 10. The lime pre-treatment results in partial gypsum precipitation and metal hydroxide precipitation. The sludge from this stage is collected through gravitational settling, which is enhanced by addition of a flocculant, in a clarifier tank. Of this sludge, 10% is recycled where it is used as seed for gypsum precipitation. The remaining 90% is dewatered.

In the second stage the metal-free water is treated with $BaCO_3$ for sulphate removal. In this stage co-precipitation of barium sulphate and calcium carbonate takes place, as mentioned earlier. The sludge is collected by gravitational settling in a clarifier tank, dewatered and subjected to thermal treatment in the third stage of the process.

The two products, BaS and CaO, from the thermal reaction in the kiln are then dissolved in water from which they can be separated according to their different solubilities. Due to its high solubility, BaS readily dissolves in water and CaO is collected, dewatered, slaked and used in the lime pre-treatment stage. The CO_2 that is produced from the thermal reaction is used to lower the pH of the treated water in the second stage of the process and for H_2S stripping in the fourth stage.

The sulphide stripping process in the barium carbonate process differs from that of the barium sulphide process. For the latter, the H_2S is stripped quantitatively from a concentrated small volume of BaS lye (reaction equation 26) as compared to a large volume of a less concentrated CaS solution (22) in the former.

$$BaS + CO_2 + H_2O \longrightarrow H_2S + BaCO_3 \qquad (26)$$

The H_2S produced is used in the Pipco process for elemental sulphur production, (Ray *et al*., 1990), which has been shown to produce elemental sulphur of high quality, making it of commercial value. The important step in the Pipco process is the absorption of sulphide into a sodium acetate solution, which is the first step in the sulphur production. The barium carbonate by-product from this step is collected via gravitational settling, dewatered and used in the second stage of the integrated barium carbonate process.

The ability to recycle barium carbonate is what constitutes the self-sustainability of the barium carbonate process and makes it financially viable. In order for the barium carbonate to be quantitatively regenerated, the two key stages of this process need to be thoroughly studied and optimized. These are as follows:

1. The separation of $BaSO_4$ from the treated water, which depends on the settling properties of the precipitated particles requires a closer investigation of the barium precipitation process, the information from which can be used to design a

crystallization plant that will favour formation of larger particles with improved settling properties.

2. The effective reduction of $BaSO_4$ to quality BaS which can be used in the re-generation of $BaCO_3$ and elemental sulphur production in the Pipco process. A kinetic study of the solid state reactions is necessary for the designing of a kiln in which the effective reduction of $BaSO_4$ to BaS can be achieved.

1.4.5. Separation of $BaSO_4$ from the treated water.

Due to the amorphous nature of barium sulphate, the particles settle slowly (Volman 1984). This makes the separation of the $BaSO_4$ precipitate from the treated water difficult and time consuming when gravitational settling techniques are employed. Generally, the gravitational settling rate of particles is determined by a number of factors such particle size, density and precipitate concentration.

Volman (1984) succeeded in showing the relationship between the settling rate of barium sulphate and its particle concentration to be as follows:

$$V = 2.56\, e^{-0.0185C} \qquad (27)$$

Where C = concentration of barium sulphate particles.

Using this relationship, Volman (1984) was able to prepare a flux curve which can be used in the design of settling tanks for barium sulphate, considering only the fine barium sulphate particles. Studies have shown that solid densities of about 16% for barium sulphate sludge leads to a settling rate of only 0.004 m/min (Volman 1984). For this reason, gravity settling coupled with filtration of the sludge was considered to be the most cost-effective way of collecting the barium precipitate (Volman 1984).

Rhodes (1998) described the settling rate of a particle as being proportional to the square of the particle diameter. This is shown by the relationship between the terminal velocity of the particle (U_T) and the particle diameter (x)

$$U_T = \frac{x^2 (\rho_p - \rho_f) g}{18\mu} \qquad (28)$$

where ρ_p is the particle density, ρ_f the fluid density, g the gravity acceleration constant and μ is the viscosity of the fluid. From this equation it is suggested that larger particles with densities significantly higher than that of the fluid will lead to a high terminal velocity, hence a high gravitational settling rate.

In their studies, Adlem *et al.* (1989), indicated that gravitational settling of barium sulphate particles can be enhanced by addition of coagulants or flocculants. The coagulants act by reducing the net electrical repulsive forces at the particle surfaces, thereby promoting consolidation of small particles into larger particles. The flocculants aggregates or combines particles by bridging the space between particles with chemicals (Skousen*, et al.,* 1993). The bridging process occurs when segments of a polymer chain absorb suspended particles, creating larger particles. The net effect of both coagulation and flocculation is the formation of particles with increased size and density, leading to faster gravitational settling.

While coagulants and flocculants have shown the ability to improve the settling rate of the $BaSO_4$ precipitation particles this can also be achieved by controlling the precipitation process to yield particles with properties that can lead to improved settling rates. In this way the cost implication due to addition of coagulants/flocculants can be alleviated from the barium carbonate process. The controlled precipitation can be achieved in a number of ways, all of which require knowledge about the fundamentals and dynamics of the precipitation process.

1.5. The precipitation process.

Precipitation or reactive crystallization, is a chemical process that has been applied for a very long time. The application of precipitation has, generally, found use in two different fields *(*Bramforth, 1965*)* namely:

- Production of solids (chemicals) with certain particulate properties and economic value.
- Removal of unwanted species from processes and waste water streams.

This summation includes the wide variety of precipitation processes and the importance of this technique as an industrial unit. The reasons for the application of precipitation reactions can be very different: ranging from the small particle sizes, the purity of the product, specific particle morphology, the selectivity of the process, or simply the easy use in large industrial equipment (van Leeuwen *et al.,* 1998).

This process is based on a simple principle whereby two reactants are brought together, either by mixing two solutions or by introducing one reactant from the gas phase into a solution of the other reactant (van Leeuwen *et al.,* 1998). Figure 1.12 shows a schematic representation of a precipitation reaction and the processes involved.

The primary processes, nucleation and crystal growth, will always take place during the precipitation process. Depending on the process conditions and nature of the precipitating compound, a number of secondary processes might occur after the primary processes have taken place. Often encountered secondary processes are agglomeration and ripening of the crystals (*Söhnel and Garside, 1992).*

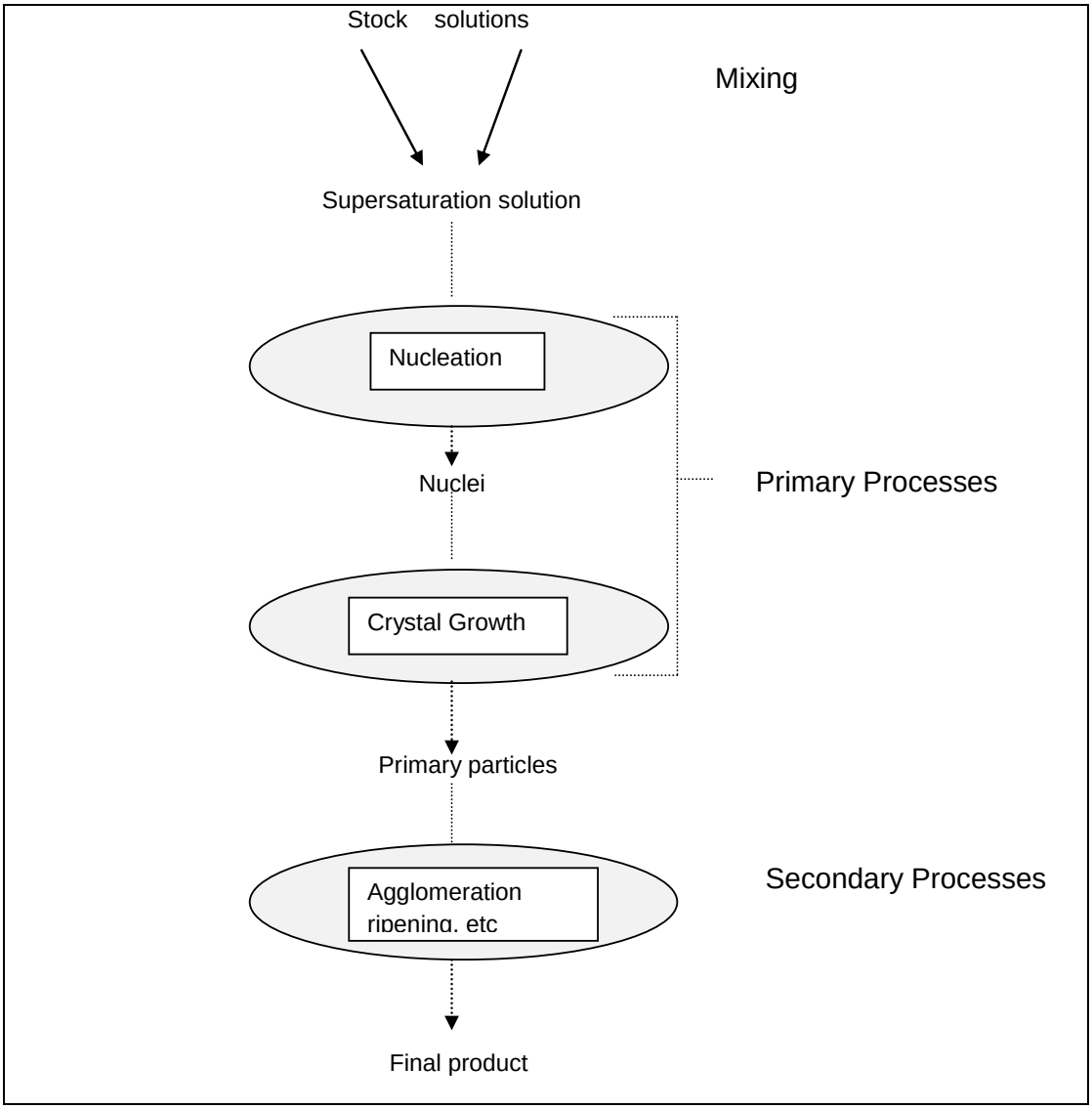

Figure 1.12 Schematic representation of a precipitation process (van Leeuwen, 1998).

1.5.1. The supersaturation ratio and precipitation.

Addition of reagents to the solution increases the ion concentration of the solution, thus leading to higher solution activities and chemical potential. As reagents are continuously added and well mixed, a saturation level (**S**) with reference to ion concentration is reached in the solution. The saturation ratio is based on the activities and interaction of the species in solution due to chemical potential.

The saturation ratio for low concentration binary solutions, as adapted from van Leeuwen *et al.* (1998) can be written as follows:

$$S = \sqrt{\frac{IP}{K_{sp}}} \tag{29}$$

where **IP** is the ionic product of the concentration of ions in solution and $\mathbf{K}_{sp}$ is defined as the solubility product of the salt being precipitated.

In a well mixed precipitation reaction, phase equilibrium between liquid and solid occurs at any given time (van Rosmalen *et al,* 2000). Addition of excess ions in the solution creates a supersaturation level in solution which is a result of the equilibrium shift to favour a solid phase. It is the difference in chemical potential of the species of interest in solution and in the solid state that leads to precipitation.

The chemical potential of the i^{th} species, composed of v_+ cations and v_- anions, in a mixture is defined as:

$$\mu_i = \mu_i^0 + RT \ln a_{\pm,i}^{\nu} \tag{30}$$

where μ^0 is the chemical potential of the i^{th} species in the standard state, $v = v_+ + v_-$, and $a_{\pm,i,eq}$ is the activity of species *i.* The difference in chemical potential between a supersaturated solution and the solid state can be defined as:

$$\frac{\phi}{RT} = \frac{\mu_{aq} - \mu_s}{RT} = \nu \ln \frac{a_{\pm,i}}{a_{\pm,i,eq}} = \nu \ln S_a \tag{31}$$

where $\phi(= -\Delta\mu)$ is called the affinity and $\mathbf{S_a}$ is the activity based supersaturation ratio (Davies, 1962).

The supersaturation ratio is a measurable entity and it is defined as a measure for the difference in chemical potential between the solute state and the crystal lattice of the species of interest (van Leewen, 1998). The relative supersaturation (**σ**) for a solution is described as:

$$\sigma = \frac{c - c^*}{c^*} \tag{32}$$

where **c** is the actual concentration of solids in the solution and **c*** is the equilibrium concentration of the solution. The values of **σ** are commonly in the order of 10^0 to 10^2 (van Rosmalen *et al,* 2000). The supersaturation ratio is the thermodynamic driving force for precipitation and induces nucleation and crystal growth. It is due to high supersaturation levels that nucleation and crystal growth proceed very fast and simultaneously. The resulting particles are in the order of few microns down to less than 100 nm (Kucher *et al,* 2005).

1.5.2. Mixing and precipitation.

Crystallization systems frequently exhibit high levels of supersaturation around the points where it is generated, such as evaporation interfaces and where two or more liquid reactants are brought into contact (Jones *et al*., 2005). Attainment of the uniform conditions throughout the reactor volume, therefore, becomes difficult and this mixing problem becomes magnified as the scale of operation increases, and can be particularly pronounced in fast precipitation systems.

The reaction time of precipitation is very short hence it is believed that precipitation is greatly affected by mixing conditions. Mixing is, therefore, directly tied to supersaturation and precipitation in the solution and it is responsible for bringing reagents into contact with each other so that the reaction can take place. It does this by regulating three processes in precipitation (Baldyga *et al*., 2007):

- It controls the local supersaturation in the fluid by dispersing the local concentrations of reagents at the feed inlets throughout the whole solution.
- It controls the agglomeration rate by contacting the particles and/or disrupting the aggregates.
- It keeps the slurry/particles in suspension.

Two types of mixing exist in precipitation *viz* macro- and micro-mixing. Macro-mixing is the mixing of reagent solutions by stirring the solution with propellers/stirrers. The micro-mixing process is mixing at molecular level, which happens through turbulent eddies in the solution. Micro-mixing coupled with ion diffusion in the solution lead to local differences in supersaturation.

Fitchett and Tarbell (1990) and van Leeuwen (1998) investigated the effect of mixing on barium sulfate precipitation. Fitchett and Tarbell (1990) concluded that the growth rate, nucleation rate and average particle length were sensitive to the mixing conditions in the reactor. Their experimental results showed that the mean particle length increased up to a factor of eight, whilst the nucleation rate dropped by an order of 2 with an increase of power input from 0 to 0.73 m^2/s^3. In these studies the growth rate was less affected by the stirrer speed as compared to nucleation. This finding was attributed to the fact that the nucleation rate has a stronger dependence on supersaturation than the growth rate of the crystals.

Another factor which needs to be taken into consideration as far as mixing in the precipitation reactor is concerned, is the number of feed points going into the stream mixed solution. The number of feed points into the bulk of the solution influences the local supersaturation and diffusion of ions in the solution. Previous studies to model the in-homogeneities in species concentration and to find the local concentrations of the species in the solution were carried out using Computational Fluid Dynamics (CFD) (van Leeuwen *et al.,* 1996; Baldyga & Orciuch 2001).

1.5.3. Nucleation.

From a supersaturated solution the new formation of solid material can take place spontaneously. Two mechanisms by which this process can occur exist, and these are primary and secondary nucleation. The primary nucleation is responsible for new phase formation from a clear liquid (Nielsen & Söhnel, 1971; Mersmann, 1990). This type of nucleation can be further subdivided into homogeneous and heterogeneous nucleation (van Leeuwen, 1998). In the latter situation a foreign substrate is present in the solution on which nucleation starts, where in the homogeneous nucleation such a substrate is absent and nucleation has to proceed by statistical fluctuations of solute entities clustering together (van Leewen, 1998). The limit of homogenous nucleation is the limit where spontaneous nucleation can occur from clear solution without a solid phase present.

Another type of nucleation, surface nucleation, can occur when the corresponding metastable zone limit is exceeded, and new nuclei form onto existing crystals. Attrition and breakage of existing crystals refer to the fourth nucleation type, which unlike the other nucleation types is not concentration dependent. Attrition occurs due to collisions of crystals with each other as well as to the crystallizer walls or to the impeller (Mersmann, 1994). The impeller configuration, impeller speed, crystallizer configuration, as well as properties of the solid and liquid phase, influence strongly on the degree breakage of crystals and attrition nucleation. In order for these attrition fragments to grow to nuclei and crystals, the supersaturated stage is required. Attrition nucleation is often the dominating nucleation mode in crystallizations from solution (Mersmann, 1994). Surface nucleation and attrition nucleation are referred to as secondary nucleation processes since those are due to the existing crystals in the system. CSD and mean crystal size of the product crystals are strongly dependent on the degree of the secondary nucleation processes.

Theoretically, the level of surface nucleation during a crystallization process could be avoided by controlling the supersaturation level to the stage where no nucleation processes exist. Consequently, this should lead to a narrow CSD. In practice, defining the metastable limits unambiguously, is not possible and the avoidance of nucleation during ongoing crystallization is difficult to do. The secondary surface nucleation and heterogeneous nucleation can cause also variations in the polymorphic composition due to different solubilities of the polymorphs in different stages of crystallization.

The attrition nucleation is not dependent on the supersaturation level, but the fragments grow differently at different supersaturation levels: at relatively high supersaturations, larger fragments grow faster than smaller fragments and at low supersaturations, zero growth and fragments can dissolve partially or totally (Mersmann, 1994). In practice, different nucleation processes, especially, heterogeneous, surface and attrition nucleation can be present simultaneously. Unlike primary nucleation, secondary nucleation only happens because of the prior presence of the material being crystallized (seeds).

1.5.4. Seeding.

Seeding is the addition of crystal seeds of the material to be precipitated. The addition of seed crystals in the bulk solution gives advantages to the precipitation process in that the high supersaturation ratio values needed to generate primary nucleation is lowered. Seeding also influences the specific crystal area, A, onto which crystal growth takes place, thus influencing the growth rate of the crystals (van Rosmalen *et al.,* 2000).

There are three main aspects that govern the influence of seeding during precipitation:

- The amount and size distribution of the seeds – the amount of seeds fixes the final crystal size for a certain mass production.
- Premature addition of seeds – early addition of seeds may lead to seed dissolution resulting in too high supersaturation for the rest of the experiment.
- Late addition of seeds – if seeds are added too late an excess of nuclei are generated resulting in formation of too small crystals.

1.5.5. Crystal growth.

The growth of crystals in a supersaturated solution is a very complex process. In general, an increase in supersaturation increases the crystal growth rate, but at the same time the secondary nucleation processes are increased (Ulrich & Strege, 2002; Myerson, 1993). The balance between the growth and nucleation is a critical issue regarding the product quality (Myerson, 1993). In order to minimize the width of the CSD, growth should be the dominating process over secondary surface nucleation. This can, in principle, be obtained by maintaining a very low supersaturation level throughout the crystallization process. This can, however, lead to the uneconomical operation of the crystallizer. The crystal growth rate is particle size dependent (Myerson, 1993; Mersmann, 2001) and, in practice, the growth rate decreases as the crystal sizes increases. To obtain an economical operation of the crystallizer, the

optimization of the equal growth in the dynamic transient state process should be considered. Different growth rates can also lead to different crystal shapes (Ulrich & Strege, 2002).

In industrial mixed tank crystallizers, crystal breakage due to collisions with each other, with the walls of the crystallizer and to the impeller can be of great importance. Therefore, in practice the true product outcome in terms of size or habit cannot be evaluated simply by crystal growth rates or directions, or supersaturation level, but it can strongly be altered by mixing conditions.

Various growth models have been developed for crystal growth from solution. The general relationship between the linear growth rate, G, and the supersaturation ratio of the solution is of the form (van Leeuwen, 1998):

$$G = \frac{dl}{dt} = k_g f(S) \qquad (33)$$

where k_g is a supersaturation independent rate constant, and f(S) is a given function of S, the supersaturation. Table 1.4 shows an overview of the most important growth mechanisms with their resulting f(S) function (van Leeuwen, 1998; van der Leeden, 1991).

Table 1.4 The function f(S) for the various growth mechanisms (van der Leeden, 1991; van Leeuwen, 1998).

Mechanism	**f(S)**
Normal growth	(S-1)
Spiral growth	$(S-1)^2$
2D nucleation-mediated growth	$(S-1)^{2/3}\, S^{1/3} \exp(-B_{2D}/\ln S)$
Volume diffusion-controlled growth	(S-1)

As can be seen from Table 1.4, f(S) can in most cases be approximated by a power law relation, with a power between 1 and 2, which is the method that is often applied for modelling crystal growth. From the above different growth rate mechanisms, the resulting relation for crystal growth (33) can, therefore, be written as:

$$G = k_g(S_a - 1)^a \qquad (34)$$

where **a** is either 1 or 2.

1.5.6. Crystal agglomeration.

Agglomeration is the process where two or more crystals attach to each other as a result of malgrowth crystals or crystal crystal collisions in supersaturated solutions. Agglomeration is a dominating process for the very small particles in the submicron and micron range and negligible for large particles (Hostomskỳ & Jones, 1991). The agglomeration level depends on the movement of primary particles and liquid as well as the number of collisions in the supersaturated solution. As the very small particles tend to agglomerate, the rate of nucleation should be neglible in order for agglomeration to be prevented, thus the crystallization process should be run within the metastable zone. In a primary nucleation process the number of crystals is related to the supersaturation level, and at low supersaturation level agglomeration is less probable than at high supersaturation levels (Hostomskỳ & Jones, 1991).

1.5.7. Crystal Size Distribution.

It is virtually impossible to have a precipitate in which all crystals are of the same size. In a particular precipitation product, all particles will be distributed within a certain size range known as the crystal size distribution (CSD). The CSD is the fundamental characteristic of the product formed in any precipitation reaction. It is, basically, the continuity statement expressed in terms of the particle number density function with the size of a particle and it is alternatively known as the population balance.

In some literature CSD is referred to as particle size distribution (PSD), which really makes no significant difference. For example Öncül *et al.* (2008) referred to the size

distribution in production of nano-particles as particle size distribution. A detailed discussion on the CSD is given in the Malvern Mastersizes data handling sub-section under section 1.5.9.

1.5.8. Barium sulphate precipitation.

Extensive studies with different aims have been conducted on the barium precipitation process. Part of the reason for the exploitation of this research area is the high industrial relevance of barium sulphate (e.g. in oil and paper industries and waste water treatment). The general underlying motive behind all the studies was to elucidate different factors that influence the growth and morphology of particles during the barium sulphate precipitation process. The findings from these studies have made the primary kinetics of this process to be known quite well, and for this reason this process has been found to be ideal to develop models for further precipitation processes (Judat and Kind, 2004). The key advantage of the barium sulphate precipitation is that barium sulphate has no hydrated form, thus its precipitation process does not have complicated kinetics.

Early studies on the barium sulphate precipitation process were conducted using batch stirred reactors. The barium sulphate crystal shape in relation with nucleation, diffusion and surface reaction was developed by Gunn and Murthy, (1972) and Murthy, (1994) in a stirred tank reactor. Hostomskỳ & Jones, (1991), using a continuous stirred tank reactor (CSTR), studied the crystallization and the agglomeration of the barium sulphate.

Different studies have shown that barium sulphate crystals can exhibit many different habits in a given experiment. Fichett & Tarbell, (1990*)* studied the effect of mixing intensity on size of crystals and they noticed a strong change in the crystal habits depending upon the reagent feed concentration. Using a double feed semi-batch reactor, Baldyga *et al,* (2007). In these studies a model which describes interactions between mixing of various scales (micro-, meso-, and macro-mixing) coupled with the population balance for crystallization was developed.

The dependence of the barium sulphate crystal growth and morphology on mixing has led to barium precipitation studies in different reactor configurations. In the last two decades, modelling attempts have been made to simulate the precipitation process with the help of computational fluid dynamics (CFD) codes for simple precipitator geometries and for stirred tanks as well. The first report of a successful CFD simulation of precipitation in a stirred tank was perhaps by *Wei, (1997)*, followed by papers by Wei and Garside (Wei & Garside,1997; Wei & Garside, 1999). Since the beginning of this kind of research, studies in reactors of simpler geometry have been more successful. A jet mixing device, tubular reactors as well as rectangular flat reactor with jet mixing were modelled.

1.5.9. How to control the precipitation processes.

The product quality is usually the control objective in precipitation processes. Unfortunately, the supersaturation is not easily monitored for active control. Therefore a better CSD control strategy is by means of operating variables that can be controlled. In designing an effective settler, the CSD will influence the settling velocity and residence time of the particles, thus the physical dimensions of the settler. CSD is a measurable and controllable parameter of precipitation and can therefore be manipulated to yield precipitate particles with improved settling properties.

There are basically 4 types of control options, depending on the dominant mechanisms or phenomena in the process:

a. *Kinetic or temperature control*

   Some precipitation processes require a higher than ambient temperature in order to overcome the activation energy. These processes are usually operated close to the normal boiling point of the mother liquor. An example is precipitation of ammonium jarosite, $NH_3Fe_3(SO_4)_2(OH)_6$, around 100 ^{0}C, in order to remove Fe^{3+} in zinc production (Kershaw, 1995).

b. *Control by means of other chemical and physical equilibria*

The most well-known application of this control mechanism is the selective precipitation of metal sulfides in hydrometallurgy. Figure 1.13 is a precipitation diagram for a range of metal sulfides, containing two types of information: solubility lines for the metal sulfides, which for Me^{+2} is given by:

$$K_{sp,MeS} = \left[Me^{+2} \right]\left[S^{-2} \right] \Rightarrow \log\left[Me^{+2} \right] = \log K_{sp,MeS} - \log\left[S^{-2} \right] \qquad (35)$$

as well as the H_2S-water equilibria:

$$H_2S(g) \overset{K_1}{=} H_2S(aq) \overset{K_2}{=} H^+(aq) + HS^-(aq) \overset{K_3}{=} 2H^+(aq) + S^{-2}(aq) \Rightarrow$$

$$\left[S^{-2} \right] = \frac{K_1 K_2 K_3 \dfrac{P_{H_2S}}{bar}}{\left[H^+ \right]^2} \Rightarrow \log\left[S^{-2} \right] = 2\,pH + \log\frac{P_{H_2S}}{bar} + \log\left(K_1 K_2 K_3 \right)$$

$$at\ 20^0 C: K_1 = 0.08\ mol/L/bar;\ K_2 = 9.1x10^{-8}\ mol/L;\ K_3 = 1.2x10^{-15}\ mol/L$$

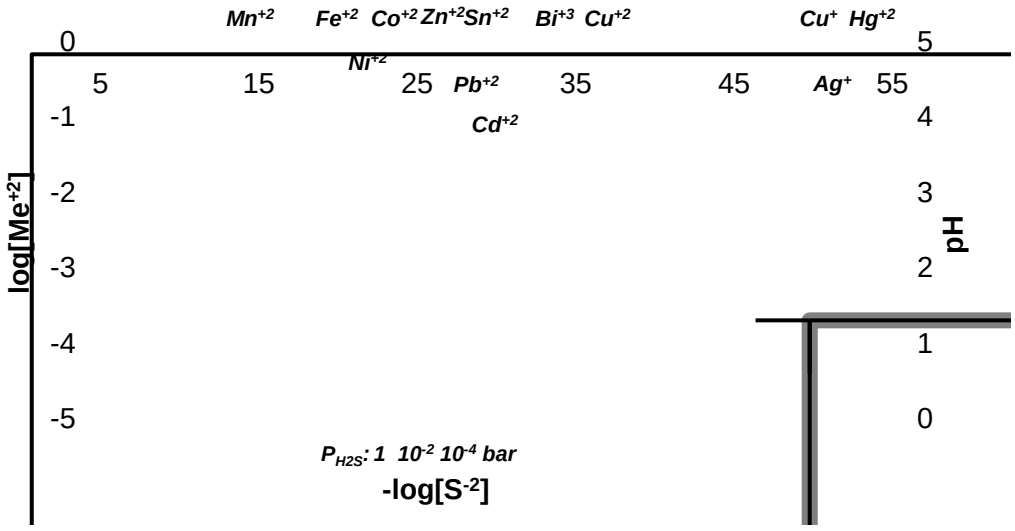

Figure 1.13 A precipitation diagram for a range of metal sulphides (Givan, 2001).

There are two external ways to control the S^{-2}-concentration in the solution, and that is by the partial H_2S pressure of the gas phase and by the pH of the solution. The challenge in selective MeS-precipitation is to find an operating window with respect to the H_2S partial pressure and the pH in order to recover specific metals from solution. From the graph it is clear that the partial pressure of the H_2S as a control tool is less effective than the pH.

Another way to control the supersaturation is by using a dissolving solid as one of the reagents, as in the $BaCO_3$-process. During this re-precipitation process the Ba^{+2}-concentration will be controlled somewhere between the levels dictated by the solubility products of $BaCO_3$ and $BaSO_4$. Although this is not necessarily the optimum level for $BaSO_4$ precipitation, $BaCO_3$ is an omni-present source of Ba^{2+} throughout the reactor which results in a constant Ba^{2+}-concentration. In this process the unreacted $BaCO_3$ should not leave the precipitator. This can be achieved by applying an efficient reactor configuration such as a fluidized bed or countercurrent reactors in series setup.

c. Pre-precipitation of metastable or amorphous compounds

In many industrial processes there is an automatic control of the supersaturation through the formation of a metastable or an amorphous intermediate, usually at the reagent feed inlet, where the highest supersaturation occurs. In a way this acts the same as in the $BaCO_3$-process and again measures have to be taken in order to avoid unwanted products in the reactor outlet. A typical industrial case where this happens is in the production of $CaCO_3$, where before one of the three possible stable polymorphs (calcite, vaterite or aragonite) is formed, amorphous $CaCO_3$ with a higher solubility is formed, which in turn dissolves and forms one of the crystalline phases

d. Mixing controlled precipitation

This type of control is probably the most complicated case and also the most difficult to scale up. As $BaSO_4$ precipitation from mine water using a BaS-solution as reagent falls in this category this will be discussed in more detail in the next paragraph. Studies conducted by Marchisio *et al.* (2002) on aggregation in barium sulphate precipitation have provided evidence that mixing is responsible for generating supersaturation and plays an important role in the competition between nucleation and crystal growth.

When precipitation is fast, relative to the mixing process the supersaturation profile in the precipitator is far from uniform. This has a major impact on the local growth and nucleation rates, which is qualitatively shown in Figure 1.14.

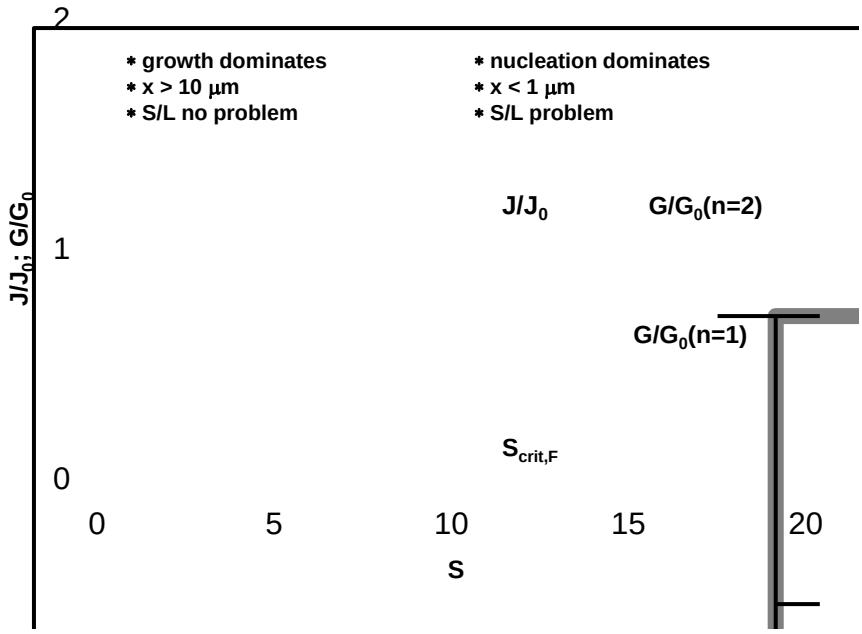

Figure 1.14 The qualitative effect of supersaturation on nucleation and growth rates in precipitators (Givan, 2001).

The nucleation and growth rate equations in figure 1.14 are of the general form:

$$\frac{J}{J_0} = \exp\left(-\frac{A}{(\ln S)^2}\right); \frac{G}{G_0} = (S-1)^n \text{ with } S = \frac{1}{\upsilon_{tot}} \ln\left(\frac{IP}{K_{sp}}\right) \qquad (36)$$

where, J/J_0 is the nucleation rate, **A** is the specific area of the crystal, **S** is the supersaturation, G/G_0 represents the growth rate, **n** is either 1 or 2, υ_{tot} is the total stoichiometric constant S_{crit} is the critical supersaturation, **IP** is the ionic product and K_{sp} is the solubility product of the formed salt.

Above the critical supersaturation, ratio based on the feed conditions, nucleation will be dominating and small crystals will be produced with a size smaller than 1 μm,

which are hard to recover in Solid-Liquid (**S/L**) separators. In Figure 1.14 the critical supersaturation is arbitrarily set at 10.

As mentioned before, the real supersaturation is not easily measured and in mixing controlled precipitation is varying so much that these measurements would be hardly relevant. Therefore, it is better to use a feed-based supersaturation, $\mathbf{S}_F$, defined as:

$$\mathbf{S_F} = \frac{1}{\upsilon_{\mathbf{tot}}} \mathbf{ln}\left(\frac{\mathbf{c_F c_f}}{\mathbf{K_{sp}}}\right) \tag{37}$$

where $\mathbf{c_F}$ is the concentration in the dominant feed, F, and $\mathbf{c_f}$ the concentration in the added reagent.

Although the feed rate, **f**, the concentration of the added reagent, $\mathbf{c}_f$, and the number of dosing points, **N**, are degrees of freedom, the molar balance over the precipitator gives a constraint over the $\mathbf{Nfc}_f$ product depicted as:

$$\upsilon_F F c_F = \alpha N \upsilon_f f c_f \tag{38}$$

where α is the required efficiency and υ_F and υ_f are the stoichiometric constants of the reaction, for $BaSO_4$ both equal to 1. In this case not all sulphate will be removed from the solution and α will be in the order of 0.8-0.9.

Combination of equations 37 and 38 gives:

$$S_F = \frac{1}{\upsilon_{tot}} \ln\left(\frac{\upsilon_f}{\upsilon_F} \frac{\alpha N f}{F} \frac{c_F^2}{K_{sp}}\right) \tag{39}$$

Because of the steep exponential dependence of the nucleation rate on **S**, the feed-based critical supersaturation, $\mathbf{S}_{crit,F}$, will be in the same range as the critical supersaturation, $\mathbf{S}_{crit}$. However, where the former is a more theoretical property, the

latter is more practical, because it contains only known physical properties and operational variables. It is logical to determine $\mathbf{S}_{crit,F}$ experimentally.

Furthermore, the production rate, **P** (mol/s), of the precipitator can be calculated in two ways. Assuming a type II precipitation:

$$P = fc_f \tag{40}$$

Assuming fast conversion in the direct confinement of the **N** dosing points, the precipitation "flames":

$$P = N\frac{3k_v\rho}{MW \cdot k_a} A \cdot \langle G \rangle_{flame} \cdot V_{flame} \tag{41}$$

where k_a and k_v are the surface and volume shape factors of the crystal, **A** is the crystal surface area per m^3 slurry, $\langle G \rangle_{flame}$ and V_{flame} are the averaged growth rate and the volume of the precipitation flames, respectively.

From this equation it can be seen that mixing in precipitation usually involves the contacting of three species: the two reagents to generate supersaturation as the driving force for growth and the crystal surface, A. For dilute feed streams like mine water it is thus essential to recycle a concentrated solution.

The real growth rate in the precipitator can therefore be written as follows:

$$G = \frac{N\langle G \rangle_{flame} V_{flame}}{F} \tag{42}$$

While the above information is only theoretical, the experimental determination of the precipitation parameters, using precipitation analysis instrumentation, requires some mathematical data manipulation. Following is the discussion on the precipitation data handling using the Malvern Mastersizer 2000.

The Malvern Mastersizer 2000 data handling

The data obtained from the Malvern Mastersizer 2000 can be handled first of all by considering trends in CSD-properties, such as the change of obscurity, average size and size width. These data are a measure of the consistency of the precipitation experiment and also provide data such as an average growth rate.

By using an initial seed size distribution that shows more than one maximum, more detailed information can be obtained regarding the growth rate of particles of different sizes by following the rate with which these maxima shift to larger sizes. This will reveal phenomena like size dependent growth and growth rate dispersion.

Even more detailed information is obtained by considering the dynamics of the complete CSD. This requires a closer look at the population balance for a fed-batch precipitator. The population balance for a continuous crystallizer or precipitator describing the population density, n, as a function of time, t, and size, x, is given by Randolph and Larson, (1988):

$$\frac{\partial n(x,t)}{\partial t} = -\frac{\partial (G(x,t)n(x,t))}{\partial x} + \Phi_{in}(t)n_{in}(x,t) - \Phi_{out}(t)n_{out}(x,t) + B(x,t) - D(x,t) \qquad (43)$$

For a batch reactor without feed (Φ_{in}-term) and product (Φ_{out}-term), streams and ignoring birth, B, and death, D, due to nucleation, agglomeration or breakage, this simplifies to:

$$\frac{\partial n(x,t)}{\partial t} = -\frac{\partial (G(x,t)n(x,t))}{\partial x} \qquad (44)$$

The experimental method using in-line measurements gives a large number of data at different size and time intervals. The analytical population balance is therefore rather given in a discrete form, as:

$$\frac{\langle n \rangle_{t+\Delta t} - \langle n \rangle_t}{\Delta t} = -\frac{\left(\overline{Gn}\right)_{x+\Delta x} - \left(\overline{Gn}\right)_x}{\Delta x} \qquad (45)$$

where $\langle \mathbf{n} \rangle$ is the size averaged and $\bar{\mathbf{n}}$ is the time averaged population density.

It is therefore possible to write the average growth rate over the time-size interval as:

$$\left\langle \bar{\mathbf{G}} \right\rangle = -\frac{\langle \mathbf{n} \rangle_{t+\Delta t} - \langle \mathbf{n} \rangle_{t}}{\bar{\mathbf{n}}_{x+\Delta x} - \bar{\mathbf{n}}_{x}} \frac{\Delta \mathbf{x}}{\Delta \mathbf{t}} \tag{46}$$

Or by considering the data-matrix as indicated in Figure 1.15, where the index i is used for size x and the index j for time t, the growth rate is calculated as:

$$\mathbf{G}_{i+\frac{1}{2},j+\frac{1}{2}} = -\frac{\Delta \bar{\mathbf{n}}}{\Delta \langle \mathbf{n} \rangle} \frac{\Delta \mathbf{x}}{\Delta \mathbf{t}} = -\frac{\mathbf{n}_{i,j+1} + \mathbf{n}_{i+1,j+1} - \mathbf{n}_{i,j} - \mathbf{n}_{i+1,j}}{\mathbf{n}_{i+1,j} + \mathbf{n}_{i+1,j+1} - \mathbf{n}_{i,j} - \mathbf{n}_{i,j+1}} \frac{\Delta \mathbf{x}}{\Delta \mathbf{t}} \tag{47}$$

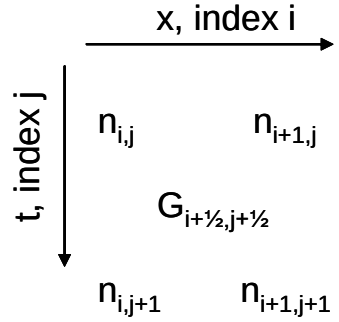

Figure 1.15. The Calculation scheme of time-size averaged growth rate, $G_{i+½,j+½}$

However, some additional data handling is required in order to be able to use the above matrix. First of all the population density will be considered as number of particles in a certain size class per unit of crystal size in the precipitator, rather than per m^3 in order to circumvent the problem of the slightly increasing volume by addition of reagent in the semi-batch experiment.

Since the data from the particle size analyzer are given as vol% rather than real population densities, the mass balance is used as follows:

The total crystal mass, M_T, in the precipitator is related to the population density as

$$\mathbf{M_T} = \mathbf{k_v} \rho_c \int_0^\infty \mathbf{n(x)} \mathbf{x}^3 \mathbf{dx} \tag{48}$$

where the volume shape factor of the crystals, k_v, and the crystal density, ρ_c, have been assumed to be constant.

The barium molar balance is given by:

$$\frac{1}{MW_{BaSO_4}}\frac{dM_T}{dt}+\frac{d(Vc)}{dt}=Fc_F \tag{49}$$

where the concentrations are expressed in mol/L and the molecular weight of $BaSO_4$, MW_{BaSO_4}, is used to transfer crystal mass into moles. By assuming that this a class II system, i.e. the Ba^{2+}-concentration in the solution, c, does not change relative to the other two terms, the mass balance for a seeded batch simplifies to:

$$\frac{dM_T}{dt}+\frac{d(Vc)}{dt}=Fc_F MW_{BaSO_4} \quad \text{with } M_T(0)=M_{seeds} \tag{50}$$

or for a constant feed rate to:

$$M_T(t)=M_{seeds}+Fc_F MW_{BaSO_4}\,t \tag{51}$$

The population density at a certain time, $n_i(t)$, at size interval Δx_i, is related to the vol% in that size interval, v_i, by:

$$n_i(t)=c_N(t)\frac{v_i}{k_v\left(\bar{x}_i\right)^3\Delta x_i} \tag{52}$$

The normalization constant, $c_N(t)$, which is different at each particle size measurement in time, where the normalization of the Malvern, $\sum_i v_i = 100$, is This is then obtained as:

$$c_N(t)=\frac{\sum_i k_v n_i\left(\bar{x}_i\right)^3\Delta x}{\sum_i v_i}=\frac{M_T(t)}{100}=\frac{M_{seeds}+Fc_F MW_{BaSO_4}\,t}{100} \tag{53}$$

Combining equations 8 and 9 then gives the final de-normalization relation:

$$n_i(t) = \frac{M_{seeds} + Fc_F MW_{BaSO_4} t}{100} \frac{v_i}{k_v \left(\bar{x}_i\right)^3 \Delta x_i} \qquad (54)$$

Only by this normalization method the real population density is given as precipitation proceeds during the experiment.

1.6. Barium sulphate reduction to barium sulphide.

The Pipco process, by which elemental sulphur is produced from barium sulphide requires that the barium sulphide be in a highly water-soluble form. This means that the presence of impurities that can hinder the maximum solubility should be avoided. Although the reduction of barium sulphate to barium sulphide, using coal, under thermal conditions, has produced good results, impurities due to the presence of products from burnt coal (i.e. ash) are unavoidable (Volman, 1984).

1.6.1. The need for barium sulphate reduction.

The reduction of barium sulphate to barium sulphide dates a long way back, where it found use in a number of processes. One of the pioneer examples of the use of this process was in the Wet Thiogen Process. In essence, the necessity of having more exact information than was available in the literature on the subject, concerning the reduction of barium sulphate to sulphide, arose in connection with a critical study of the Wet Thiogen Process (Wells, 1917) for the recovery of elemental sulphur from smelter gases. The study of this process was undertaken mainly to deal with the general problem of elimination of waste in the smelting operations.

1.6.2. The Thiogen Process.

The Wet Thiogen Process involves the recovery of sulphur dioxide from smelter gases by passing them up through absorption towers, in which a descending “mother liquor” solution absorbs the sulphur dioxide (Wells, 1917). In carrying out the process, the gases are first cooled and cleared of all dust and fumes, prior to

absorption. Barium sulphide is added, as a powder or suspension, to the solution of sulphur dioxide whereupon a precipitate, consisting of barium sulphite (reaction equation 55), barium thiosulphate (reaction equation 56) and sulphur, are produced.

$$2BaS + 3SO_2 \longrightarrow 2BaSO_3 + 3S \quad (55)$$

$$\text{or } 2BaS + 3SO_2 \longrightarrow 2BaS_2O_3 + S \quad (56)$$

The collection of elemental sulphur is done through distillation of the filtered and dried product at 450 ^{0}C, which is the boiling point of sulphur. In both cases, whether the precipitate consisted of barium sulphite and sulphur or barium thiosulphate and sulphur, the distilled and condensed sulphur is practically pure. The residual from the distillation is barium sulphite and barium sulphate. This means that, upon distillation, the thiosulphate species gets converted to sulphate. Investigations done by the United State Bureau of Mines (Wells, 1917) on the Thiogen Process have shown that the main reaction of these above two reactions is reaction (55), thus barium sulphate is the dominating species of the residual mixture after distillation. This residue is then reduced to sulphide and used again for precipitation, the barium thus being kept in circulation through cycles.

In order for the barium to be most efficient as a precipitant, it is very necessary that the maximum reduction of the sulphate or sulphite to the water-soluble sulphide be attained in each cycle. Thus, it is very necessary to determine the conditions under which the barium sulphite or sulphate was reduced most completely to the sulphide, and considerable experimental work has been conducted on that problem. As barium sulphate must be used in the initial reduction, and was present to a large extent in all precipitates after distillation, and also, as this material could be obtained in quantities much more readily than the sulphite, the greater part of these investigations were concerned with the reduction of the sulphate.

In the reduction of the barium sulphate/sulphite, by mixing the residue with carbon, coke or coal and heating to a temperature between 750 - 1200 ^{0}C there was a tendency for the formation of small amounts of the oxides and carbonates of barium. These impurities made the reduced material to react very slowly with the SO_2 when used as a precipitate in the dilute solution from the absorption towers. The

impurities, therefore, became “inert” substances of the mixture, diluting the active BaS, and increasing in amount in each cycle of operations.

The presence of impurities in the reduced material was attributed to the direct fired furnace where the products of combustion passed over the material. The effect was more pronounced when coal containing a high percentage of ash was used as a reducing agent. The use of high ash coal made it necessary for the reduced material to be leached for the removal of insoluble materials prior to use as a precipitating material. It was only with the addition of this supplementary operation that the technical operation of the process could be carried out successfully.

The Pipco process, which was briefly introduced earlier and which forms part of the integrated barium carbonate process, is a more recent technology which resembles the Wet Thiogen Process in that both processes require the reduction of barium sulphate to barium sulphide as a first step. However, these two processes have significant differences that can be outlined as follows:

1. In the Pipco process H_2S, instead of BaS, is contacted with SO_2 form sulphur thus the Pipco process requires a H_2S stripping step from BaS solution prior to sulphur production.
2. The SO_2 in the Pipco process is generated within the process system unlike in the Wet Thiogen process where the SO_2 is introduced from the external source into the system.
3. Pure liquid sulphur is produced as the product in the Pipco process instead of solid elemental sulphur, as is the case with the Wet Thiogen Process. This means elemental sulphur produced in the Wet Thiogen Process requires an additional distillation step to produce pure sulphur.

A summary of the Pipco process is given in the following section.

1.6.3. The Pipco process.

The description of the Pipco process is detailed in U. S. patent 5,057,298 (Ray *et al.,* 1990) and in a report prepared by Pipco Inc (Gryka, 1992) for the Gas Research Institute. Processes that have been developed by earlier workers serve as a

foundation of knowledge which can be applied to the Pipco process. A schematic diagram of the Pipco process is given in Figure 1.16

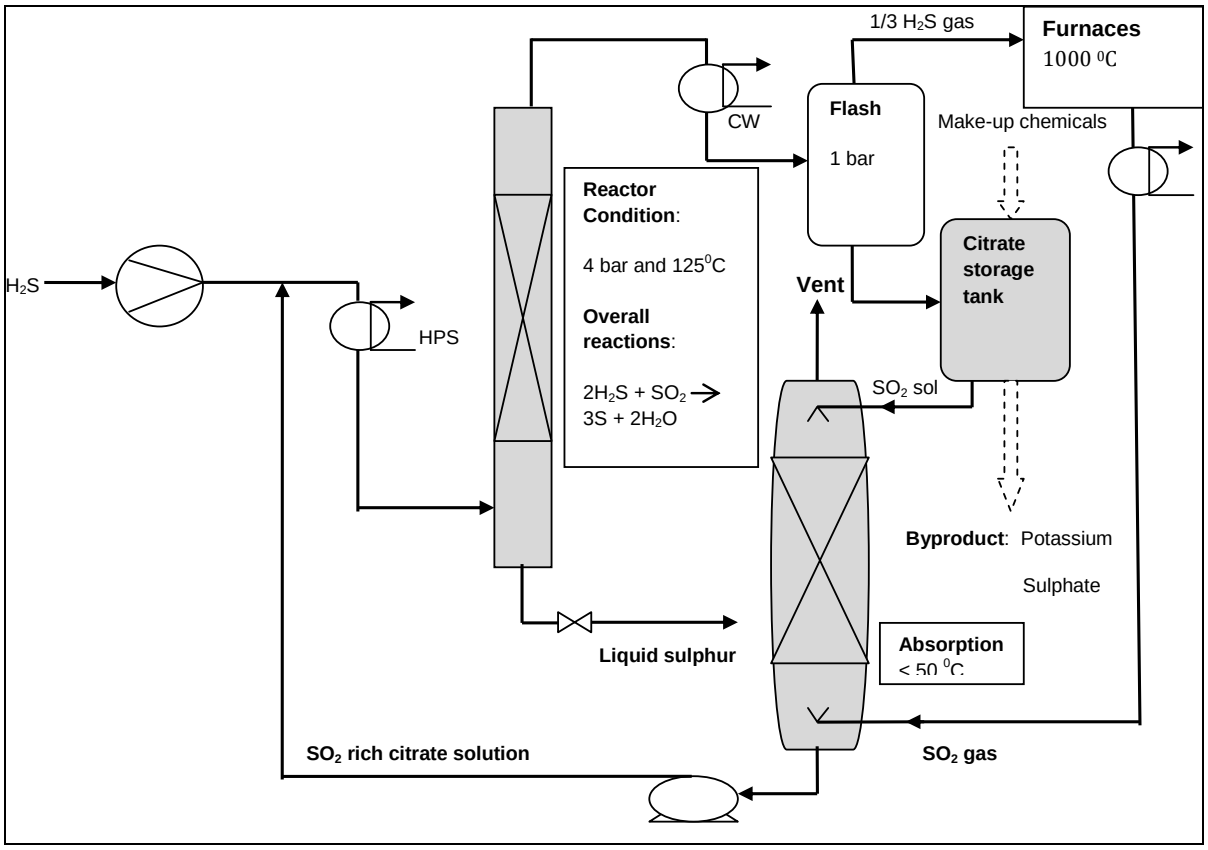

Figure 1.16. The schematic flow diagram of the Pipco process (Ray *et al.,* 1990).

In the reactor, the pressure is elevated to 4 bar and the H_2S – SO_2 rich citrate solution mixture is heated to 125 ^{0}C whereupon sulphur is formed according to the overall reaction equation (57).

$$2H_2S + SO_2 \longrightarrow 3S + H_2O \qquad (57)$$

The formation of sulphur proceeds through reactions which involve several intermediate compounds in the liquid (Vasan, 1975; Rochelle & Gibson, 1982, Rochelle & King, 1979), which are very complex and beyond the scope of discussion in this thesis. The temperature in the reactor is a very delicate parameter as the reaction is carried out at temperature above the melting point of sulphur and below

the temperature where sulphur becomes a very viscous material (in the range of 150 to 160 ^{0}C). The preferred temperature is therefore 125 ^{0}C. The reaction is carried out at an elevated pressure to prevent the potassium citrate solution from boiling. Ideally, only 2/3 of the H_2S that enters the reactor reacts with SO_2 to form sulphur and the remaining 1/3 passes through the reactor to the flash vessel. The formed sulphur, in the reactor, is coalesced and separated from the citrate solution by decantation.

At the top of the reactor a gas liquid mixture leaves the reactor. The gas and the liquid phase are separated in a flash vessel at atmospheric pressure. The gas phase is introduced to a furnace where the unreacted H_2S is converted to SO_2, according to reaction equation (58):

$$2H_2S + 3O_2 \longrightarrow 2H_2O + 2SO_2 \qquad (58)$$

The SO_2 gas is introduced in the bottom of an absorption column as shown in Figure 1.16. The liquid phase is first introduced to a citrate storage tank, where the make-up chemicals can be added and by-products can be removed, before it is added to the top of the absorption column. In the absorption column the potassium citrate solution is again enriched with SO_2 and can be used for the reaction. The absorption of SO_2 in a potassium citrate solution should take place at a temperature as low as possible, preferably below 50 ^{o}C. The unique aspect of a buffered process such as the PIPco process is illustrated by the following: SO_2 solubility in water at 50 ^{o}C is only 0.17 g/l (with 1000 ppm SO_2 in the feed gas), while a solution buffered with citrate has a solubility of 8.7 g/l (at pH = 4.5), which is a fifty-fold increase (Vasan, 1975). The task of a buffering agent like citric acid is to shift the equilibrium to the right as shown in reaction equations (59 – 61) below:

$$SO_2 + H_2O \longrightarrow HSO^{3-} + H^+ \qquad (59)$$

$$Cit^{3-} + H^+ \longrightarrow HCit^{2-} \qquad (60)$$

$$HCit^{2-} + H^+ \longrightarrow H_2Cit^- \qquad (61)$$

From equations (59), (60) and (61) it is also clear that absorption is favoured by a high pH. The concentration of potassium citrate in the solution is preferably as high as possible to increase the buffering capacity, but should be below the concentration at which the potassium citrate would crystallize from the solution at the coldest or most concentrated part of the process. Generally, a concentration in the range of about 1.0 to about 3.5 molar is suitable and about 2 molar is preferred.

The only feedstock for the Pipco process is H_2S gas. For the H_2S source, this process can be coupled with a number of sulphide producing processes. The brine treatment process was the first process to be considered for this purpose, as the gypsum produced from this process is a good source of sulphide when thermally decomposed (Nengovhela, 2007) (reaction equation (62).

$$CaSO_4 + 2C \longrightarrow CaS + 2CO_2 \qquad (62)$$

The calcium sulphide is leached in water to form a CaS slurry. This slurry is then transported to a stripping vessel where H_2S gas is stripped off with CO_2 as follows:

$$CaS_{(s)} + H_2O + CO_{2(s)} \longrightarrow CaCO_{3(s)} + H_2S_{(g)} \qquad (63)$$

Coupling the Pipco process with the barium carbonate process offers an advantage of the use of water soluble BaS instead of a CaS slurry for H_2S stripping. This is because H_2S is stripped quantitatively from a concentrated BaS solution in the barium carbonate process. However, the problems encountered when barium sulphate was reduced to barium sulphide in the Wet Thiogen Process still need to be addressed in order for the Pipco process to be successfully coupled with the barium carbonate process. These problems have opened doors for further research into this technology.

1.6.4. Research into the barium sulphate reduction process.

The studies on the reduction of barium sulphate, by carbon-containing solid reducing agents, to form water-soluble barium sulphide have been carried out by many authors under various experimental conditions (Akhmetov, 1974; NIPOHIM, 1979).

The aim of the research into barium sulphate reduction was mainly concerned with finding optimum conditions for the production of high quality barium sulphide. The knowledge and understanding of the reaction mechanism of this process will lead to possible control of this reaction. This will be beneficial, not only to the sulphur producing industry, but also to industries engaged in the manufacture of barium salts as barium sulphide is used as starting material from which a variety of other barium salts can be formed.

1.6.5. The reaction mechanism behind the barium sulphate reduction.

Investigations by Maree *et al.*(2004), have shown that the barium sulphate reduction process requires the use of a pure carbon source as reducing agent, under inert conditions. The use of pure solid carbon does not, however, guarantee effective reduction of barium sulphate to barium sulphide. The reason for this is that the kinetics of this reaction is also affected by the gas composition of the reaction environment, as it is assumed that the solid reducers are initially gasified to CO, which then interacts with barium sulphate (NIPOHIM, 1979; Pelovski & Taniguchi, 1981). Even though the experimental data to verify this mechanism is scanty, Pelovski and Taniguchi, (1988) have, by simultaneous application of thermogravimetric analysis under nitrogen and solid electrolyte systems for purifying and measuring the partial pressure of O_2 in the gas phase, elucidated additional information on this process mechanism.

In these studies, sequential changes of the oxygen partial pressure (observed as the oxygen potential on the solid electrolyte) were associated with rapid changes in the reaction mixture at the beginning of the reaction process. The initial rapid decrease in oxygen partial pressure was assumed to be due to the adsorption and chemisorptions of oxygen, while the rapid increase in the oxygen partial pressure was assumed to be determined by the occurrence of the following reactions:

$$BaSO_4 \longrightarrow BaS + 2O_2 \quad (64)$$

$$BaSO_4 + 2C \longrightarrow BaS + 2CO_2 \quad (65)$$

$$BaSO_4 + 4C \longrightarrow BaS + 4CO_2 \quad (66)$$

$$CO_2 + C \longrightarrow 2CO \quad (67)$$

$$CO_2 \longrightarrow CO + 0.5O_2 \quad (68)$$

$$CO_2 \longrightarrow CO + O_2 \quad (69)$$

$$BaSO_4 + 4CO \longrightarrow BaS + 4CO_2 \quad (70)$$

The second oxygen partial pressure decrease that was observed, was most probably due to the dominating effect of reactions (55) and (56) for a definite period of time, after which reaction (70) predominated. A temporary high oxygen partial pressure was observed at 955 ^{0}C and this was explained in terms of the rapid accumulation of carbon monoxide in the system from reaction (70) and the establishment of equilibrium in reactions (66-68). It was further concluded in this studies that the initial reduction period depends on the temperature, as the reaction degree does not exceed 10% during this period.

Furthermore, the development of the process was outlined by the establishment of a constant oxygen potential, determining the constancy of the ratio of the partial pressures of CO and CO_2 within 0.13 – 0.20. This fact motivates the conclusion that the reduction process proceeds mainly with a definite ratio of the rate constants of reactions (64 – 70). These studies have supported the assumption of gasification of the solid reducer prior to $BaSO_4$ reduction to BaS i.e the above reaction equations.

1.6.6 Kinetics of solid state thermal reactions

The kinetics of solid state reactions is a very broad subject. For the purpose of this thesis it has been narrowed down. Generally, two objectives are common to the vast majority of kinetic studies of chemical reactions and they are as follows: (Brown & Gawley, 2006).

- The determination of the rate equation that satisfactorily describes the extent of conversion of reactant(s) or formation of product(s) with time as the reactions proceeds, usually, but not necessarily, at a constant temperature.

Experimental data are compared with values predicted from a range of theoretical kinetic expressions to determine which rate equation describes the experimental measurements most precisely. The form of this kinetic expression enables inferences to be made concerning the reaction mechanism through which reactants are converted into products

- The determination of the influence of temperature on the reaction rate. The parameter(s) in the rate equation which are most affected by temperature are the rate constant(s) (or rate coefficient(s)). The temperature dependence of the rate constant(s) is usually expressed quantitatively by the Arrhenius equation as follows:

$$k = A \exp(-E_a/RT) \qquad (71)$$

where E_a is the activation energy and A the frequency factor. These parameters provide a convenient and widely-used method for the concise reporting of kinetic data, for comparison of reactivities of different systems, and for use to estimate reactivities or stabilities at temperatures outside the interval of the experimental measurements.

These two objectives are attained by use of a quantitative thermal analytical tool known as thermogravimetry (TG). An internationally accepted definition of TG is the technique whereby the weight of a substance, in an environment heated or cooled at a controlled rate, is recorded as a function of time or temperature (McKenzie,1969). The development and readily availability of reliable and accurate electronic microbalances in TG have led to their wide application in kinetic studies of solid reactions (Garn, 1965). Two alternative methods are used in kinetic investigations of the solid state reactions, isothermal and non-isothermal, the results of which elucidate the information required for the above mentioned two objectives.

1.6.7. Isothermal method of TG.

In the isothermal method yield-time measurements are made while the reactants are maintained at a known constant temperature (Garner, 1955). This kind of experiment yields curves of either α-time or $(d\alpha/dt)$-time. α is the fractional reaction which, by definition, changes progressively from reactants (α = 0.00) to products (α = 1.00) (Brown & Galwey, 2006). Techniques for measuring α include determinations of the changes of pressure of a gaseous product evolved during reaction in a constant volume, changes in reactant mass, evolved gases analyses, chemical and/ or X-ray diffraction measurements on partly reacted material, determination of heat evolved, etc. For example, if a reaction yields one or more gaseous products (and the evolved gas composition is constant) α values can be calculated from the mass loss up to time t, $m_o - m_t$, related to the overall mass loss corresponding to completion of reaction, $m_o - m_f$, by $\alpha = (m_o - m_t)/(m_o - m_f)$. Analogous expressions are applicable to measurements using other techniques.

Experimentally, isothermal kinetic analysis requires the measurement of a set of (α,t) values for the reaction selected for investigation at a known, constant temperature (T). These data are then tested for accuracy of fit to the equations shown in Table 1.5 to identify which expression represents most precisely the systematic changes of α with time (Criado & Morales, 1980). For many (but not all) solid state reactions, the expression giving the best fit to the α-time data is often independent of temperature, while the magnitudes of the rate constants increase with temperature.

Table 1.5. The most important rate equations used in the kinetic analysis of solid state reactions (Brown & Galwey, 2006).

The name	***g(α)=k(t'–t₀)=kt***	***f(α)=(1/k)(dα/dt)***	***A= h(t)***
Acceleratory *α*-time			
P1 power law	$\alpha^{1/n}$	$n(\alpha)^{(n-1)/n}$	
E1 exponential law	Ln*α*	*A*	
Sigmoid *α*-time curves			
A2 Avrami-Erofeev	$[-\ln(1-\alpha)]^{1/2}$	$2(1-\alpha)(-\ln(1-\alpha))^{1/2}$	
A3 Avrami-Erofeev	$[-\ln(1-\alpha)]^{1/3}$	$2(1-\alpha)(-\ln(1-\alpha))^{2/3}$	
A4 Avrami-Erofeev	$[-\ln(1-\alpha)]^{1/4}$	$2(1-\alpha)(-\ln(1-\alpha))^{3/4}$	
An Avrami-Erofeev	$[-\ln(1-\alpha)]^{1/n}$	$n(1-\alpha)(-\ln(1-\alpha))^{(n-1)/n}$	$1-\exp[-(kt)^n]$
B1 Prout-Tompkins	$\ln[\alpha/(1-\alpha)]$	$\alpha(1-\alpha)$	$\{1+1/[\exp(kt)]\}^{-1}$
Deceleratory *α*-time			
Geometrical methods			
R2 contracting area	$1-(1-\alpha)^{1/2}$	$2(1-\alpha)^{1/2}$	$1-(1-kt)^2$
R3 contracting volume	$1-(1-\alpha)^{1/3}$	$3(1-\alpha)^{1/3}$	$1-(1-kt)^3$
Diffusion model			
D1 one-dimensional	α^2	$1/2\alpha$	$(kt)^{1/2}$
D2 two-dimensional	$(1-\alpha)\ln(1-\alpha)+\alpha$	$[1-\ln(1-\alpha)]^{-1}$	
D3 three-dimensional	$[1-(1-\alpha)^{1/3}]^2$	$3/2(1-\alpha)^{2/3}[1-(1-)^{1/3}]$	$1-(1-(kt)^{1/2})^3$
D4Ginstling-Brounshtein	$1-(2\alpha/3)-(1-\alpha)^{2/3}$	$3/2[(1-\alpha)^{-1/3}-1]^{-1}$	
Order of the reaction models			
F0 zero order	*A*	1	Kt
F1 first order	$-\ln(1-\alpha)$	$1-\alpha$	$1-\exp(-kt)$
F2 second order	$[1/(1-\alpha)]-1$	$(1-\alpha)^2$	$1-(kt+1)^{-1}$
F3	$[1/(1-\alpha)^2]-1$	$(1-\alpha)^3$	$1-(kt+1)^{-1/2}$

In these equations, the rate coefficients, *k* are different in each expression and times, *t*, are assumed to have been corrected for any induction period, t_0. The units of *k* are always expressed as $(\text{time})^{-1}$. The accurate determination of the final product is very important, particularly in distinguishing between the fit of data to alternative kinetic expressions e.g. the contracting volume (R3) model (where the rate process ceases when advancing interface reaches the particle centre) and the first order (F1) model

(where the rate continually diminishes). It is also important to allow sufficient time in order for the reaction to reach completion (Brown & Galwey, 2006).

In order for the data to be reliable, they must be accurate and reproducible. However, while the criteria for reproducibility have not been agreed upon, the variation in α-time values between similar experiments can be determined and reported. Data for isothermal kinetic analyses thus consist of sets inter-convertible values of: $\alpha,t;$ $(d\alpha/dt)$, $t;$ $(d\alpha/dt)$, $\alpha,$ *etc.* Some experimental techniques may yield relatively noisy sets of $\alpha,t;$ $(d\alpha/dt)$, $t;$ $(d\alpha/dt)$, $\alpha,$ *(etc)* values and some smoothing of data may be necessary.

As mentioned earlier, the initial objective in kinetic analysis is to identify which, if any, of the rate equations in Table 1.5 provides the most acceptable description of each experimental (α,t) data set. In deciding what constitutes an acceptable description, at least three aspects of the problem need to be considered:

1. The accuracy of the mathematical fit of the experimental values to the relationship between α and $t;$ $(d\alpha/dt)$ and $t;$ or $(d\alpha/dt)$, and $\alpha,$ expressed by the equations listed in Table 1.5.

2. The range of α across which the acceptable fit extends. It is acceptable that two different equations may apply across successive α ranges, but it is essential to demonstrate first that a single rate expression does not represent the overall rate process.

3. Evidence in support of the reaction model identified as applicable must be sought through complimentary experimental techniques, including optical and electron microscopy, X-ray diffraction (XRD) measurements, spectroscopy etc.

The most important methods that have been used in the kinetic analysis of data from isothermal experiments include the following:

(i). Examination of the linearity of plots of $g(\alpha)$ (from Table 1.5) against time.

(ii). Comparison of plots of α against reduced-time with curves given by the rate equations in Table 1.5. (Dimensionless reduced-time values, t_{red}, are

obtained by scaling the measured time values, t, appropriately to give a common point on all curves, usually $t_{0.5}$ = 1.0 at α = 0.5, with allowance for any induction period, so that $t_{red} = t/t_{0.5}$)

(iii). Comparison of plots of measured ($d\alpha/dt$) values against reduced-time or α with curves given by the rate equations in Table 1.5

(iv). Examination of the linearity of plots of measured ($d\alpha/dt$) values against $f(\alpha)$ (from Table 1.5). This may give better discrimination amongst kinetic models than method (i) above.

The decision as to which of the available rate equations provides the most acceptable description of a given set of data requires consideration of the following:

(i). The α-time ranges over which the different reaction models can be most clearly distinguished, and

(ii). The effects of experimental errors, including random scatter in the measured values of α, which may reduce distinguishability.

There is, however, no general agreement on the range of α over which a perceived fit can be regarded as acceptable.

1.6.8. Testing the linearity of the plots of g(α) against time.

The deviation from the linearity of g(α) – time plots can be used to identify which equations merit more detailed consideration (Brown & Gawley, 2006). The decision as to which kinetic expression provides the best fit is frequently a compromise between the maximum α range applicable and the deviations at the limits. Once a satisfactory fit has been obtained, identifying the applicable rate equation, $g(\alpha) = k(t - t_0)$, the value of k, at that recorded temperature, and its standard error can be determined from the slope of the plot. For those rate expressions containing exponents, n, for example the Avrami-Erofeev equations (equation 3) in Table 1.5, plots of $\ln[-\ln(1 - \alpha)]$ against $\ln(t)$ should provide the most direct method for the determination of the value of n. Such plots are, however, notoriously insensitive and an error in t_0 can significantly influence the apparent value of n (Criado & Moralez, 1976).

1.6.9. The influence of temperature on reaction rate.

The Arrhenius equation, mentioned earlier, is almost exclusively used as the functional relationship between k and T. Irrespective of any physical and theoretical importance to be attached to the parameters A and E_a, their magnitudes represent an important established method of reporting and comparing kinetic data.

The data from isothermal experiments are analysed, as described above, to yield a set of values of k_i at each temperature T_i. These values are usually presented in the form of a plot of ln k_i against $1/T_i$ (reffered to as an Arrhenius plot). Linear regression (with suitable weighting for the ln function) yields values for (E_a/R) and ln$A$, together with their standard errors (Brown & Gawley, 2006).

Kinetic analysis of non-isothermal experiments

As in isothermal kinetic studies, the analysis of non-isothermal kinetic data is directed towards identifying the rate equation and the Arrhenius parameters which most satisfactorily describe the observations. In a typical non-isothermal kinetic experiment the temperature of the environment of the reactant sample is systematically changed according to the defined programme (usually, but not necessarily, a linear increase of T with time) (Brown & Gawley, 2006).

A technique referred to as constant rate thermal analysis (CRTA) in which the sample is heated in such a way that reaction takes place at a constant rate has been developed. A temperature-jump or step-wise programme has also been suggested in which, during which a single experiment, the temperature is rapidly changed ("jumped") from one value to another and the rates at the two (or more) temperatures are measured and used to calculate Arrhenius parameters for that particular α value (Brown & Gawley, 2006). This method assumes that α does not change significantly during the time taken to measure the two rate values. The formulation of the kinetic analysis models (via the inverse kinetic problem) is discussed in the following section.

The "inverse kinetic problem (IKP)"

The usual starting point for kinetic analysis of non-isothermal data is to use the following equation to determine the kinetic parameters of the reaction:

$$d\alpha/dT = (d\alpha/dt).(dt/dT) = (d\alpha/dt).(1/\beta) \quad (72)$$

where $\beta = (dT/dt)$, is the heating rate.

On the assumption that the Arrhenius equation is applicable to the rate processes being studied, the above equation may be expanded to:

$$dt/dT = (1/\beta).(d\alpha/dt) = (A/\beta)\exp(-E_a/RT)\, f(\alpha) \quad (73)$$

where $f(\alpha)$ is a kinetic expression in Table 1.5.

Separating the variables in equation (73) lead to:

$$d\alpha/f(\alpha) = (A/\beta)\exp(-E_a/RT)\, dT$$

Integrating between the limits, $\alpha = 0$ at $T = T_0$ and $\alpha = \alpha$ at $T = T$, gives:

$$\int_0^{\alpha} (f(\alpha))^{-1} d\alpha = \int_{T_0}^{T} (A/\beta)\exp(-E_a/RT)\, dT$$

$$g(\alpha) = \int_{T_0}^{T} (A/\beta)\exp(-E_a/RT)\, dT = \int_0^{T} (A/\beta)\exp(E_a/RT)\, dT \quad (74)$$

For any reaction under investigation, experimental measurements, obtained at a known heating rate, β, are converted to values of α and/or dα/dt at temperatures T. The "inverse kinetic problem" as the necessity to determine up to six unknown constants, *b1, b2, b3, d1, d2,* and *d3* can be expressed as follows (Brown & Gawley 2006)*:*

$$d\alpha/dt = b1T^{b2}\exp(-b3/RT)\, \alpha^{d1}(1-\alpha)^{d2}[-\ln(1-\alpha)]^{d3}$$

Often, in the analysis the rate equations familiar from homogeneous kinetics are used, in that *d1* and *d3* are taken to be zero, so that f(α) is assumed to be $(1 - \alpha)^n$. (n = *d2*). The apparent reaction order then becomes the unknown. The simpler form of the Arrhenius, i.e. *b2* = 0, is generally used because a temperature dependent term in the pre-exponential factor only adds a further adjustable parameter. When d3 is zero, $f(\alpha) = \alpha^{d1}(1 - \alpha)^{d2}$, is known as the Sestá-Berggren (SB) equation, or if *d1* = *d2* = 1, as the Prout-Tomkins or Austin-Ricket equation (Criado *et al.,* 1975).

It is usually assumed that a single rate equation expression, f(α) or g(α), applies over a wide range of α values (ideally $0 < \alpha < 1.0$ and that the values of the Arrhenius parameters, A and E_a, are constant over at least that α range. If the expression and/or the Arrhenius parameters vary with α, i.e. the reaction mechanism changes, the kinetic analysis becomes very complicated and hence the results of such analysis become less reliable and less useful.

Whether rate measurements from a single experiment, extending across a range of temperatures are, in principle, capable of providing a complete kinetic analysis (the form of f(α) or g(α) and the magnitudes of E_a and A) has been debated. Criado & Moralez (1980) have shown that the same TG curve can be generated using three different kinetic models with different Arrhenius parameters.

Isothermal studies represent one limit of the numerous possibilities for temperature changes which can, in principle, be employed in non-isothermal studies. Both isothermal and non-isothermal approaches have their advantages and disadvantages and attempts to downplay or ignore the importance of either one are unproductive.

1.7. Kinetic studies of the reduction of barium sulphate using solid carbon reducing agent.

Kinetic studies of thermal reactions are aimed at finding reaction conditions that will lower the activation energy and increase the rate of the reaction. Such studies are done following a systematic approach whereby one parameter is kept constant while the other is varied.

The literature on the kinetic studies of the barium reduction is very scanty. To the best of our knowledge the initial investigation, which forms preliminary studies in this area of research, is the work reported by Pevloski and Taniguchi (1988). In addition to the elucidation of additional information supporting the gas phase composition reaction mechanism, these studies have also demonstrated the effect of temperature on the process kinetics. The results from these investigations have shown that the effect is particularly strong in the temperature range 723 – 825 ^{0}C. Thus while 48 hours was required for a complete barium sulphate reduction at 723 ^{0}C, about 3 hours was required at 825^{0}C, less than 2 hours in the range 825 – 955 ^{0}C. All experiments were carried out under inert atmosphere using N_2 that was purified from O_2 and H_2O and the ratio C / $BaSO_4$ = 2.5.

The kinetic parameters of the process were obtained by treating the data by means of the Kekam Equation and the Arrhenius Equation:

$-\ln[-\ln(1-\alpha)]$ *vs*. ln *t*

The activation energy, E_a, of 10.26 kcal/mol, was obtained under the conditions that these studies were carried out. These studies have open doors to further research into the kinetics of this reaction.

Further investigations on the kinetics of the reduction of barium sulphate were carried out by Pelovski *et al.,* (1987). In these studies the effect of additives (Na_2CO_3) to the barium sulphate sample on the kinetics of the reaction was investigated as was suggested by Pelovski and Taniguchi (1981). The results showed that the addition of 0.3% Na_2CO_3 to the barium sulphate samples promotes the reduction process at different temperatures ranging from 786 to 871 ^{0}C. The reduction of barium sulphate in the presence of 0.3% sodium carbonate was completed in 15 -25 minutes at temperatures ranging from 842 to 871^{0}C. Such a degree of decomposition could only be achieved in 50 – 100 minutes under identical conditions but in the absence of additives. The experimental data from these studies were closely fitted by the equation of Erofeeff:

$\alpha = 1-e^{-ktn}$

The values of –ln*k* obtained for temperatures ranging from 786 to 871 ^{0}C varied from 5.15 to 3.37, respectively. The apparent energy of activation determined in the above temperature range amounted to 59.30 kcal/mol (248.3 kJ/mol) (Pelovski & Taniguchi, 1981).

A similar activating action on the process of reduction of barium sulphate by carbon was found when sodium chloride and calcium chloride were used as additives. This suggested that the observed activating action cannot be ascribed to a given chemical component but it is probably determined by the appearance of microeutectic centres where the energy level and the crystal structure of the solid substances are changed. These investigations have been carried out to confirm the possibility of decreasing the energy consumption during barium sulphate reduction by carbon through the introduction of a suitable additive into the initial mixture.

1.8. The reduction of barium sulphate using a gaseous reducing agent.

As far as we are aware, no literature has reported the results of studies conducted on the reduction of $BaSO_4$ using CO gas as a reducing agent, instead of solid carbon. However, Kuusik et al. (1985) reported results on the decomposition of the calcium analogue of $BaSO_4$ i.e $CaSO_4$ in the CO atmosphere. Using TGA and DTA, the kinetic studies of this reaction concentrated on the effect of the CO concentration in the gaseous phase, temperature and the heating rate on the reduction of $CaSO_4$.

It was concluded from these studies that by slow heating, in a gaseous medium containing 20 – 100% of CO, $CaSO_4$ is completely reduced to CaS with maximal rate just below 865^{0}C. With CO content lower than 20% in the gas phase and at temperatures above 1050 – 1100^{0}C, the formation of CaO, SO_2 and CO_2 becomes dominant and, correspondingly, the overall exothermic effect becomes an endothermic effect. It was further concluded that application of inhibitors such as CO_2 or O_2 in the gas phase would prevent the formation of CaS and hence promote the formation of CaO and SO_2

Just like it is the case with the reduction of calcium sulphate, as discussed here, investigations in the barium sulphate reduction reaction are done with the aim of up-

scaling the process for industrial use. It is equally important for the reaction kinetics of the reduction of barium sulphate to be elucidated.

1.9. Aims of the current study.

The general aim of the current study was to demonstrate the performance of the integrated barium carbonate process (Figure 1.11), close the gaps opened by previous research through optimization of the different stages of this process with particular attention given to barium sulphate precipitation, thermal reduction of barium sulphate to barium sulphide and H_2S stripping.

These studies were designed in such a way that most of the questions regarding the viability of this process could be answered and open further research avenues which would bring improved applicability of this process. The results obtained from these studies should be useful in making recommendations for the design and operation of a pilot plant scale. In order to achieve this aim, a closer look at the fundamentals of the different stages was required. This has led to the formulation of the following specific aims:

- Study the effects of different parameters ($BaCO_3$ concentration, the presence of Mg in the treated water and alkalinity) on the sulphate removal rate.

- Develop a system that can be used to establish the influence of supersaturation and mixing on nucleation rate (B) and particle growth rate (G) by varying parameters such as barium feed concentration, number of feed points into the reactor and the stirrer speed. The information gathered from the optimization of these parameters, to favour particle growth over nucleation, is important for controlling $BaSO_4$ precipitation in order to yield particles with improved settling properties and for recommendations on the design of the precipitation reactor to be used.

- To evaluate the effect of reaction time, temperature, sample mass and the presence of $CaCO_3$ in $BaSO_4$ on the reduction yield of $BaSO_4$ to BaS in a furnace, when solid carbon is used as a reducing agent and to establish the effect of the furnace dimensions (tube vs muffle) on the reduction yield.

- To elucidate the kinetic parameters (E_a values, K and q-values) of the reduction of $BaSO_4$ to BaS using CO as a reducing agent in the TGA. The parameters of concern in these studies were the CO concentration (in v/v%) and the reaction temperature. Ultimately, to find the kinetic model that fits the data which will aid during the design of the furnace to be used on an industrial scle.

- The evaluation of the effect of different parameters (CO_2 flow and BaS concentration) on effective H_2S stripping from the BaS solution and the absorption thereof into the Zn acetate solution.

1.9.1. Research approach.

The research approach outlines the planned activities to be undertaken in order to meet the aims of the study. These were as follows:

1. The sulphate removal process.

    - Conduct laboratory beaker tests aimed at the identification of the parameters affecting the sulphate removal step and the optimization thereof.

2. Controlled $BaSO_4$ precipitation process.

    - Design an experimental setup that will help identify the parameters influencing the precipitation of $BaSO_4$ from two solutions.

    - Calculate and compare average growth rates and nucleation rates obtained under different reaction conditions and reactor set-ups, in order to make recommendations for the design and operation of the pilot scale plant

3. The reduction of barium sulphate to barium sulphide using a solid carbon reducing agent in industrial furnaces.

    - Conduct furnace studies on the reduction of $BaSO_4$ to BaS, using solid carbon as a reducing agent, with the aim of identifying the reaction

conditions and type of reactor which will help improve the reduction yield.

4. TGA studies on the reduction of $BaSO_4$ using CO as a reducing agent

    - Carry out non-isothermal studies on the reduction of $BaSO_4$ to BaS using CO as reducing agent.
    - Determine the reaction kinetic parameters of this reaction under variable reaction conditions.
    - Determine the kinetic model which fits the data obtained from these studies.
    - The kinetic information obtained from the TGA studies will form the basis on which the optimization of the full scale operation of the $BaSO_4$ reduction to BaS process will be based.

5. H_2S stripping process.

    - Using a laboratory set-up, conduct a study of the H_2S stripping system and absorption efficiency of the stripped gas into a zinc acetate solution, and relate the quantity of the absorbed H_2S to the elemental sulphur that will be produced from the solution by the Pipco process.

6. Estimate the running cost for the operation of the integrated barium carbonate process for sulphate and metal removal.

CHAPTER 2

EXPERIMENTAL

Introduction

The experimental apparatus and the experimental methods employed, as well as the materials used to conduct the necessary experimental work are described in this Chapter. In Section 2.1 the laboratory apparatus, setup and materials used for the sulphate removal studies are described. Methods and varied conditions applied are tabulated in this section. Section 2.2 describes the laboratory setup, apparatus, the materials used and the experimental procedures followed for the controlled precipitation studies. The laboratory setup for the H_2S stripping process studies and the corresponding experimental procedures are outlined in section 2.3. The thermal reduction of barium sulphate to barium sulphide was studied using a furnace and a TGA system. The furnace systems were used mainly for preliminary studies and to demonstrate the practical industrial application of this technology, while the TGA system was used to study the reaction kinetics of the technology. The laboratory setups, apparatus, materials and experimental procedures for these studies are described in Section 2.4.

2.1. The water treatment studies.

The water treatment studies were done to demonstrate the effects of a number of parameters on the rate of sulphate removal by barium carbonate.

2.1.1 Apparatus used for the water treatment studies

All the experiments were carried out using a laboratory set-up which consisted of 1000 mL plastic beakers and IKA RW 20 digital stirrers as shown in Figure 2.1.

Figure 2.1. A picture of the beaker study set-up that used for water treatment studies.

2.1.2 Experimental methods and materials

In sub-section 2.2.2.1 of the methods used for the preparation of the SO_4^{2-} solution are outlined, where $CaCO_3$ and $MgSO_4$ were used in a solid form. The procedures followed to carry out the different studies and the experimental programs are given in sub-section 2.1.2.2.

2.1.2.1 The preparation of the stock solutions

Sulphate stock solution

A reagent grade (specially purified) $CaSO_4$ (Merck) (2508 mg) was dissolved in 1000 mL deionised water to yield a 1400 mg/L SO_4^{2-} solution. This solution was stirred

overnight in a sealed volumetric flask prior to use.

2.1.2.2 Experimental methods and different conditions for the sulphate removal studies

A general procedure for all the experiments for sulphate removal studies involved addition of the required amount of $BaCO_3$ to the 1400 mg/L SO_4^{2-} solution in a 1000 mL beaker, followed by stirring at 150 rpm. The reduction in the sulphate concentration was monitored by taking samples at 30, 60, 120, 180 and 240 minutes intervals and analysis of the sample for sulphate concentration using a spectrophotometer.

The different experimental conditions for the evaluation of the effect of the different parameters on the rate of sulphate removal are given in Tables 2.1 to 2.4.

Experiment 1(a)

Table 2.1. Experimental conditions for the evaluation of the effect of the different $BaCO_3$ concentration on the sulphate removal rate.

Beaker	**$BaCO_3$ (mg)**	**$BaCO_3/SO_4^{2-}$ molar ratio**	**SO_4^{2-} solution (mL)**	**Stirrer speed (rpm)**
1	0	0	1000	150
2	1436	0.5	1000	150
3	2873	1	1000	150
4	5746	2	1000	150
5	11492	4	1000	150

Experiment 1(b)

Table 2.2. Experimental conditions for the evaluation of the effect of varied alkalinity on the sulphate removal, when $BaCO_3/SO_4^{2-} = 1$

Beaker	$Ca(OH)_2$ (mg)	Alkalinity (mg/L $CaCO_3$)	$BaCO_3$ (mg)	SO_4^{2-} solution (mL)	Stirrer speed (rpm)
1	0	0	2 873	1000	150
2	74	100	2 873	1000	150
3	370	500	2 873	1000	150
4	1 480	2000	2 873	1000	150

Experiment 1(c)

Table 2.3. Experimental conditions for the evaluation of the effect of varied alkalinity on the sulphate removal rate, when $BaCO_3/SO_4^{2-} = 2$

Beaker	$Ca(OH)_2$ (mg)	Alkalinity (mg/L $CaCO_3$)	$BaCO_3$ (mg)	SO_4^{2-} solution (mL)	Stirrer speed (rpm)
1	0	0	5 746	1000	150
2	74	100	5 746	1000	150
3	370	500	5 746	1000	150
4	1 480	2000	5 746	1000	150

Experiment 1(d)

Table 2.4. Experimental conditions for the evaluation of the effect of Mg (as $MgCl_2$ and $MgSO_4$) on the sulphate removal.

Beaker	$MgSO_4$ (mg/L)	$MgCl_2$ (mg/L)	[Mg] (mg/L)	SO_4^{2-} (mL)	Stirrer speed (rpm)
1	0	808	100	1000	150
2	0	2423	300	1000	150
3	1014	0	100	1000	150
4	3041	0	300	1000	150

2.2. The controlled precipitation studies.

A brief description of the apparatus used for these studies is outlined in the sub-sections of section 2.2.1. The materials, experimental methods and experimental program are given in section 2.2.2.

2.2.1 Apparatus used in the controlled precipitation studies

The studies on controlled precipitation were carried out using the laboratory set-up as depicted in Figure 2.2. This setup consisted of a precipitator system (multi-dose Gilson peristaltic pump and a tube reactor) and a particle size analyzer (Malvern Mastersizer 2000).

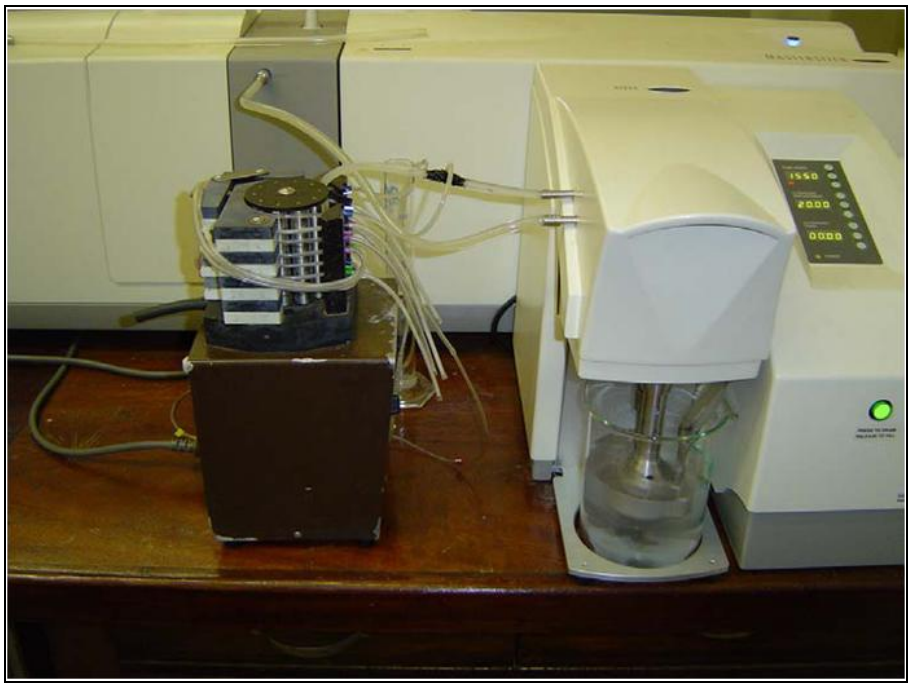

Figure 2.2. The depiction of the laboratory set-up used in the controlled precipitation studies.

The precipitator system

A Gilson multi-dose peristaltic pump and a tube reactor were used. Holes were punched in the reactor tube through which the barium reactant solution could be

administered in a multi-dose mode using the Gilson multi-dose pump (Figure 2.3). In the tube reactor, the barium reactant solution reacts with the sulphate solution from the slurry tank to form a $BaSO_4$ precipitate. The Gilson multi-dose pump has a minimum flow-rate of 10 mL/min hence was ideal for the current studies as very low flow-rates were required to carry out the experiments.

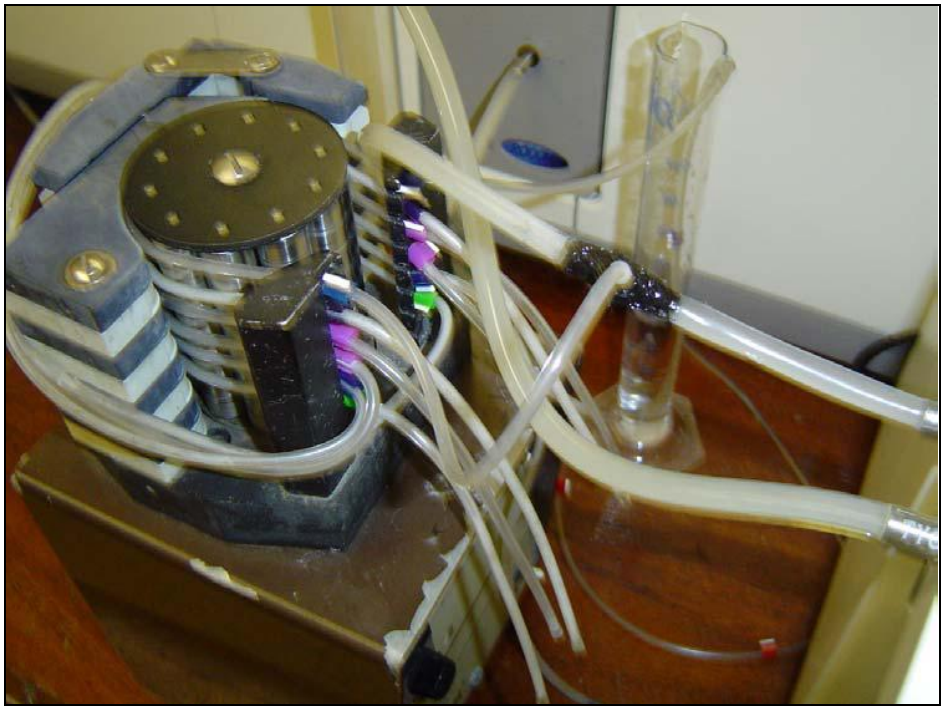

Figure 2.3. The depiction of the Gilson Multi-dose peristaltic pump that was used in the controlled precipitation studies.

The Malvern Mastersizer 2000

The Mastersizer 2000 particle size analyzer is a laser diffraction system from Malvern Instruments, offering advanced technology that is simple and straightforward in operation. It has the ability to measure particles over a wide size range, from submicron to a few millimetres, accurately and non-destructively, for both wet and dry dispersions. The Malvern Mastersizer 2000 consists of an optical section (laser, cell and a signal detector), a data acquisition section and a slurry section (1L vessel with circulation pump and 5 mm diameter tube).

For the current studies, a Malvern Mastersizer 2000 was used as an inline analyser of the $BaSO_4$ precipitate CSD, as shown by the shematic diagram of the experimental set-up in Figure 2.4. In this set-up the suspension from the slurry tank flowed through the optical cell of the unit where the particle sizes were analysed through laser diffraction and the data sent to the computer data acquisiton section of the system.

The slurry was recycled back into the slurry tank, via the circulation tube, where it was stirred. The stirrer speed of the Malvern Mastersizer 2000 was adjusted to give different Reynolds numbers, hence it made the evaluation of the effect of the Reynold's number possible.

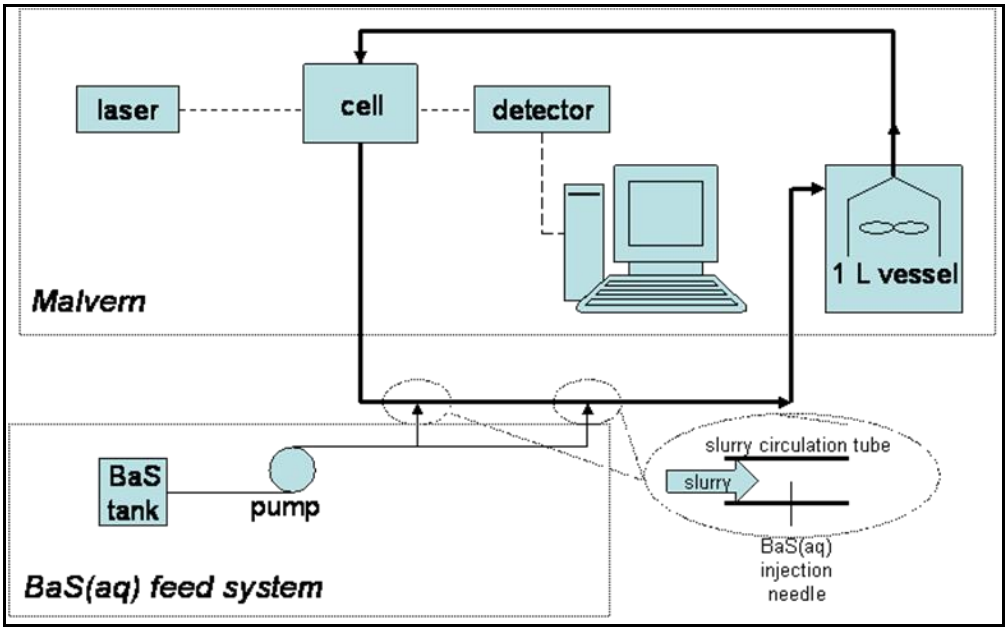

Figure 2.4. The schematic diagram of the laboratory set-up that was used for the controlled precipitation studies.

Experimental calibration.

Experiments had to be conducted to establish the window of operation for the experimental setup prior to the execution of the planned studies. Air bubbles are, inevitably, introduced into the mixing unit of the Malvern Mastersizer during stirring and if not taken care of, these bubbles influence the CSD data obtained. It is for this

reason that an experiment was conducted to ascertain the stirrer speed at which the effect due to bubbles was minimized. In this experiment the stirrer speed was varied, while the CSD data was collected and related to the volume concentration of the bubbles in the system.

An accurate flow-rate of the fluid administered by the dosage pump into the precipitator tube is essential as the mass balance used in the calculation of the growth and nucleation rates are based on this flow-rate. The calibration of the flow-rate was done by plotting the flow-rate of the fluid, measured using a pipette, versus the pump setting.

Data was also obtained for the flow-rate of the fluid through the dosage tube versus the stirrer pump setting. The reason for this experiment was to eliminate the discrepancy that is caused by the turbulent effect of the flow of fluid through the tube on the calculated Reynolds number. From the fluid flow-rate and stirrer pump settingaccurate Reynolds could be calculated and be used to classify if the flow through the tube was laminar or turbulent.

2.2.2 Experimental methods and materials

The methods used for the preparation of the stock solutions that were used for these studies are outlined in sub-section 2.2.2.1 and the general experimental methods for the studies are outlined in sub-section 2.2.2.2. The experimental conditions that were varied and those that were kept constant during the examination of the effect of certain parameters on nucleation and particle growth rate are given in Tables 2.5 and 2.6 respectively.

2.2.2.1 The preparation of stock solutions

$Ba(NO_3)_2$ solution

A $Ba(NO_3)_2$ solution was prepared by dissolving a required amount of reagent grade (99.7% pure) $Ba(NO_3)_2$ (ADH) in double distilled water, to give a solution with a

desired Ba^{2+} concentration for a specific experiment. This was followed by filtration of the solution over a 0.5 µm Teflon filter to give a well defined and clear solution.

Na_2SO_4 solution

A 10.4 mmol/L solution of Na_2SO_4 was prepared by dissolving 1480 mg of a reagent grade (99.8% pure) Na_2SO_4 (Merck) in double distilled water, followed by filtration through a 0.5 µm TEFLON filter to give a well defined and clear solution.

2.2.2.2 Experimental methods

The general experimental method followed for all the experiments for controlled precipitation studies was as follows:

1. The 1L vessel of the Malvern Mastersizer 2000 was filled with 600 mL Na_2SO_4 (10.4 mmol/L) solution. This solution was pumped through the cell, the reading of which was used as the CSD background. The Malvern Mastersizer pump was set in a fixed position, which in combination with the tube diameter determined the Reynolds number and thus the turbulence at the mixing points.

2. $BaSO_4$ (60.00 mg) was added to the 1L vessel as seeds and the CSD was recorded. Observation of the CSD indicated a change of the CSD pattern, which was due to de-agglomeration of the seeds. Typically after 5 minutes the CSD pattern remained constant and 15 minutes after introduction of the seeds the starting CSD was stored in the data acquisition system.

3. At time zero the $Ba(NO_3)_2$ solution was fed in-line to the Na_2SO_4 system through the multi-dose feed system at the rate of 10 mL/h and the CSD was recorded at preset time intervals.

Under these conditions the total amount of $BaSO_4$ precipitated at the end amounted to 1460 mg in the vessel, which implied that the particle size of the seeds, assuming negligible nucleation, will increase with a factor:

$$\frac{d_{end}}{d_0} = \left(\frac{m_{precip} + m_{seeds}}{m_{seeds}} \right)^{1/3} = 2.9 \qquad (75)$$

2.2.2.3 Experimental conditions

The number of variables in the precipitation systems is usually large. However, constraints are defined by both the experimental method and the application of mine water treatment. An overview of the experimental conditions that were kept constant is given in Table 2.5.

Table 2.5. Experimental conditions that were not varied during the controlled precipitation studies

Variable	**Value**	**Unit**
Starting volume	600	mL
$[Na_2SO_4]$	10.42±0.02	mmol/L
Amount of seeds	60.0±0.3	Mg
$Ba(NO_3)_2$ feed rate	10	mL/h
Temperature	20±2	^0C

The experimental conditions that were varied in this study were further focused on the question: How does the way of mixing change the separation characteristics of the precipitate?

This was a change large enough to be accurately detected with the CSD analyzer. The feed rate of the $Ba(NO_3)_2$ solution was kept constant at 10 mL/h, but the concentration as well as the number of feed points were varied in order to optimize the $BaSO_4$ production rate, without reducing the separation properties of the precipitate.

The conditions that were varied in the different experiments are given in Table 2.6. In the last column the objective of the specific experiments are given: the feed concentration of the Ba-source was changed, the number of feed points was doubled

and the effect of turbulence was investigated. It should be noted that all experiments were conducted in the turbulent regime (Re>2100).

Table 2.6. The experimental conditions that were varied during the controlled precipitation studies.

Run	[$Ba(NO_3)_2$/ mmol/L	Number of feed points	Re (-)	Objective
1	156	1	3098	Central experiment
2	156	1	3098	Reproducability
3	78.1	1	3098	Lower Ba-concentration
4	78.1	2	3098	Number of feed points
5	8.73	2	3098	Lower Ba-concentration
6	8.73	2	3810	Turbulence effect
7	8.73	2	4642	Turbulence effect

Furthermore, during the experimental runs two conditions that have a distinct influence on supersaturation were expected to change. On the one hand, the number of crystals and the total $BaSO_4$ surface area were expected to increase. Secondly, the sulphate concentration was expected to decrease and with it the supersaturation ratio, expressed as:

$$S_F = \sqrt{\frac{\left(Ba^{2+}\right)\left(SO_4^{2-}\right)}{K_{sp}}} \qquad (76)$$

Both phenomena would lead to a continuous decrease in a supersaturation ratio and thus a decrease in crystal growth rate as well as nucleation rate.

2.3. The thermal reduction of barium sulphate to barium sulphide using solid carbon.

The studies on the thermal reduction of barium sulphate to barium sulphide, using solid carbon as a reducing agent, were carried out in tube and muffle furnaces.

2.3.1 Furnace studies on the reduction of barium sulphate with solid carbon.

In this section the descriptions of the furnaces and the accompanying apparatus that were used for the reduction of barium sulphate with solid carbon are outlined. Two furnaces, the tube furnace and the muffle furnace, were used in these studies

The tube furnace

A Carbolite tube furnace (Lenton) was used in these studies (see Figure 2.5).

Figure 2.5. A picture of the Carbolite tube furnace used for the barium sulphate reduction studies.

The tube furnace consists of a 40 mm diameter and 530 mm long cylindrical furnace and a digital temperature control unit. A quartz tube is fitted into a cylindrical furnace and this was used to avoid a direct contact between the furnace walls and the sample. The sample was placed in a small porcelain boat and, using an insulated rod, it was pushed up to the middle of the quartz tube. The digital temperature control unit was used to program the temperature and could be programmed up to a maximum temperature of 1200 ^{0}C.

The muffle furnace

An Elite muffle furnace (Lenton) was used for these studies (Figure 2.6).

Fiure 2.6. A picture of the Lenton muffle furnace used for the reduction of the barium sulphate.

The muffle furnace consists of a 25.8 L rectangular oven and a digital temperature control unit. The inside of the furnace is covered with refractory material to help reduce energy consumption. The furnace is insulated with ceramic fibre which improves furnace temperature uniformity. The sample was introduced in a porcelain dish using a pair of tongs with heat resistant handles. The temperature control unit can be operated in both manual and automatic modes and like the tube furnace a maximum temperature of 1200 ^{0}C can be attained.

2.3.2 *Experimental methods and materials*

Sub-sections 2.3.2.1 and 2.3.2.2 outline the experimental methods followed for the experiments carried out in the tube and the muffle furnaces, respectively.

2.3.2.1 *The tube furnace experimental methods and materials*

The experiments carried out in the tube furnace were aimed at evaluating the following parameters:

1. The effect of temperature on the reaction yield.
2. The effect of $CaCO_3/BaSO_4$ ratio on the reaction yield.
3. The effect of reaction time on the reaction yield.

The methods for the experiments carried out in the tube furnace are given in Experiments 2(a) to 2(c).

Experiment 2(a). The effect of temperature on the percentage yield of BaS.

A mass of 4000 mg (17.17 mmol) reagent grade $BaSO_4$ (Merck), was thoroughly mixed with 620 mg (51.17 mmol) of activated carbon (100% carbon). This mixture was placed into a porcelain boat which was then pushed up to the middle of the pre-heated (800 ^{0}C) tube furnace, using the insulated rod. Using a stop watch, the reaction was left to continue for 20 minutes under a N_2 (100 mL/min) atmosphere, after which the product was removed from the furnace and left to cool under a N_2 atmosphere for 20 minutes. An amount of 500 mg of the product was mortared and dissolved in 100 mL distilled water after which the solution was analyzed for the sulphide content using the iodine method of sulphide analysis (APHA, 1997*).* This procedure was repeated for different temperatures (900, 950 and 1050 ^{0}C).

Experiment 2(b) The effect of $CaCO_3/BaSO_4$ ratio on the percentage yield of BaS.

A mass of 5000 mg (21.46 mmol) reagent grade $BaSO_4$ (Merck), was thoroughly mixed with 770 mg (64.38 mmol) activated carbon (100% carbon). This mixture was placed into a porcelain boat which was then pushed to the middle of the pre-heated (1050 ^{0}C) tube furnace, using the insulated rod. Using a stop watch the reaction was left to continue for 20 minutes under a N_2 (100 mL/min) atmosphere, after which the product was removed from the furnace and left to cool under a N_2 atmosphere for 20 minutes. A mass of 500 mg sample of the product was mortared and dissolved in 100 mL distilled water after which the solution was analyzed for sulphide content

using the iodine method (APHA, 1997*).* This procedure was repeated while different amounts of $CaCO_3$ were added to the mixture to give different $CaCO_3/BaSO_4$ ratios (0.2, 0.5 and 1.0). Qualitative and quantitative XRD analysis were done for the products of the reactions with pure $BaSO_4$ and with $CaCO_3/BaSO_4$ ratio = 1.

Experiment 2(c). The effect of the reaction time on the percentage yield of BaS.

A mass of 4000 mg (17.17 mmol) reagent grade $BaSO_4$ (Merck) and 1720 mg (17.17 mmol) $CaCO_3$ (Merck) were thoroughly mixed with 620.00 mg (51.17 mmol) of activated carbon (100% carbon). This mixture was placed into a porcelain boat which was then pushed to the middle of the pre-heated (800 ^{0}C) tube furnace, using the insulated rod. Using a stop watch the reaction was left to continue for 5 minutes under a N_2 (100 mL/min) atmosphere, after which the product was removed from the furnace and left to cool under a N_2 atmosphere for 20 minutes. A mass of 500.00 mg of the product was mortared and dissolved in 100 mL distilled water after which the solution was analyzed for the sulphide content using the iodine method of sulphide analysis (APHA, 1997*).* This procedure was repeated for different reaction times (10, 15, 20 and 30 minutes).

2.3.2.2 *The muffle furnace experimental methods and materials*

The experiments carried out in the muffle furnace were aimed at evaluating the following parameters:

4. The effect of time on the reaction yield.
5. The effect of sample mass on the reaction yield.

The experimental methods for the experiments carried out in the tube furnace are given in 2(d) to 2(e).

Experiment 2(d). The effect of time on the reaction yield in the muffle furnace

A mass of 30 000 mg (1.29×10^5 mmol) $BaSO_4$ (Merck), of reagent grade and 12 900 mg (1.29×10^5 mmol) $CaCO_3$ (Merck) of reagent grade were thoroughly mixed with 46 500 mg (3.86×10^3 mmol) activated carbon (100% carbon) in a porcelain dish. Using a pair of thongs, with insulated handles, this mixture was put into a pre-

heated muffle furnace (1050 ^{0}C), which was purged with N_2 prior to heating. The sample mixture was left to react for 15 minutes after which it was removed and left to cool under a N_2 atmosphere for 20 minutes. A mass of 500 mg of the product was mortared and dissolved in 100 mL distilled water after which the solution was analyzed for sulphide content using the iodine method of sulphide analysis (APHA, 1997*).* This procedure was repeated for different reaction times (20, 30, 60 and 100 minutes).

Experiment 2(e). The effect of sample mass on the reaction yield in the muffle furnace

A mass of 5 000 mg (21.45 mmol) $BaSO_4$ (Merck), of reagent grade and 2 150 mg (2.45 mmol) $CaCO_3$ (Merck) of reagent grade were thoroughly mixed with 770 mg (64.35 mmol) activated carbon (100% carbon) in a porcelain dish. Using a pair of thongs, with insulated handles, this mixture was put into a pre-heated muffle furnace (1050 ^{0}C), which was purged with N_2 prior to heating. The sample mixture was left to react for 100 minutes after which it was removed and left to cool under a N_2 atmosphere for 20 minutes. A mass of 500 mg of the product was mortared and dissolved in 100 mL distilled water after which the solution was analyzed for the sulphide content using the iodine method of sulphide analysis (APHA, 1997*).* This procedure was repeated for different sample masses (20 000 mg, 30 000 mg, 50 000 mg, 300 000 mg and 500 000 mg) while the ratios $CaCO_3/BaSO_4$ = 1 and $C/BaSO_4$ = 3 were kept constant.

2.4. TGA studies on the reduction of $BaSO_4$ using a gaseous reducing agent.

The studies on the thermal reduction of barium sulphate to barium sulphide using CO as a reducing agent were done in the TGA system.

In section 2.4.1 the experimental set-up that was used to carry out the TGA studies is described. Attention is given to the main apparatus used for these studies, hence a brief description and operation of these apparatus are also outlined in the sub-sections of section 2.4.1. The materials, experimental methods and program are given in section 2.4.2.

2.4.1 *The apparatus that was used for the TGA studies for the reduction of barium sulphate to barium sulphide, using CO as a reducing agent*

- A schematic diagram for the experimental setup is depicted in Figure 2.7. The system consisted of a 9.60% CO in N_2, a 99.99% CO_2 and a 99.98% N_2, gas cylinders (G1, G2 and G3 respectively), mass flow control system, a gas flow-meter, thermogravimetric analyser (TGA), and data and signal output.

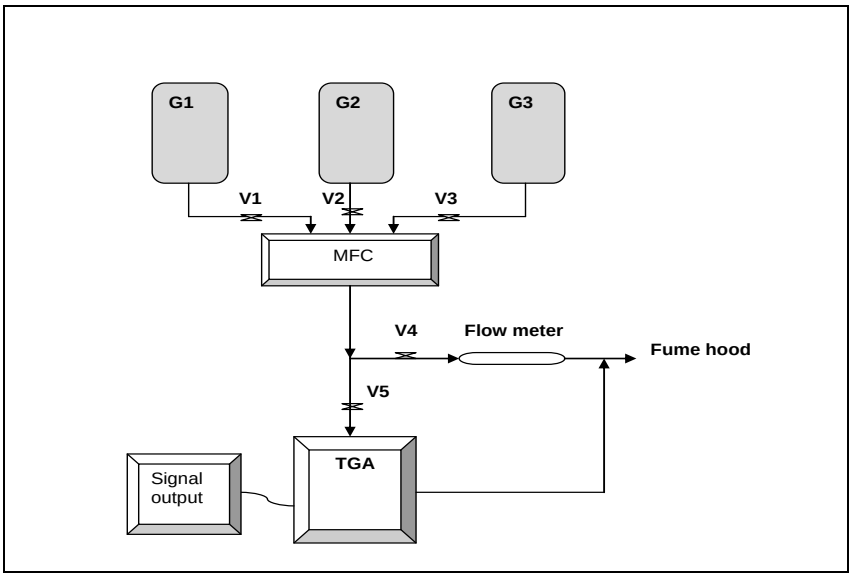

Figure 2.7. The schematic diagram of the experimental set-up used for the TGA studies of the reduction of barium sulphate with CO.

The 2050 Du Pont TGA.

The thermogravimetric analyzer is the apparatus most commonly used in studies on the kinetics of solid reactions. This analyzer measures and logs the weight of the sample along with the time and the temperature at which the reaction takes place. It can be operated isothermally or non-isothermally and is very accurate in data collection and temperature regulation.

The TGA has a feed gas tube, which allows reactant or inert gases to be fed to the reactor. The flow of these gases can be controlled via flow-meters in order to control the gaseous environment in which the reaction takes place. A photometer is

installed and acts to measure the slightest movement of the balance beam in order to measure the change of the sample mass as the reaction proceeds. This photometer is very accurate and is able to detect and record mass changes as small as 0.01mg.

The thermogravimetric analyzer used in this study was the TGA 2050 (Du Pont). This apparatus was used to heat the sample, while simultaneously measuring the mass and temperature of the sample. This mass-temperature-time data was logged by a computer using associated software. The specifications of the 2050 Du Pont TGA are given in Table 2.7.

Table 2.7. TGA 2050 Du Pont Thermogravimetric Analyzer specifications.

Maximum weighing capacity	1.0 g
Temperature range	Ambient - 1000˚C
Sensitivity/resolution.	0.2 µg
Balance accuracy	< 0.1%
Purge gas rate	Furnace: 90 ml/min Balance: 10 ml/min
Temperature calibration	1 to 5 points (metal standards)
Heating rate	0.1 ˚C/min to 50 ˚C/min
Furnace cooling	Forced air
Sample pans	Platinum: 50µL, 100µL Alumina: 100µL, 250µL, 500µL Aluminum: 100µL
Thermocouple	Platinel II
Operating line voltage	115 volts, 50/60 Hz
Energy consumption	1.5 kVA
100 mg range	10 mg-100 mg
1000 mg range	100 mg-1000 mg
Furnace atmosphere purge gases	He, N_2, O_2, Air, Ar
Furnace atmosphere purge rates	Up to 100 ml/min

Figure 2.8 shows a schematic diagram of the TGA 2050 and Figure 2.9 depicts the TGA as used in this study.

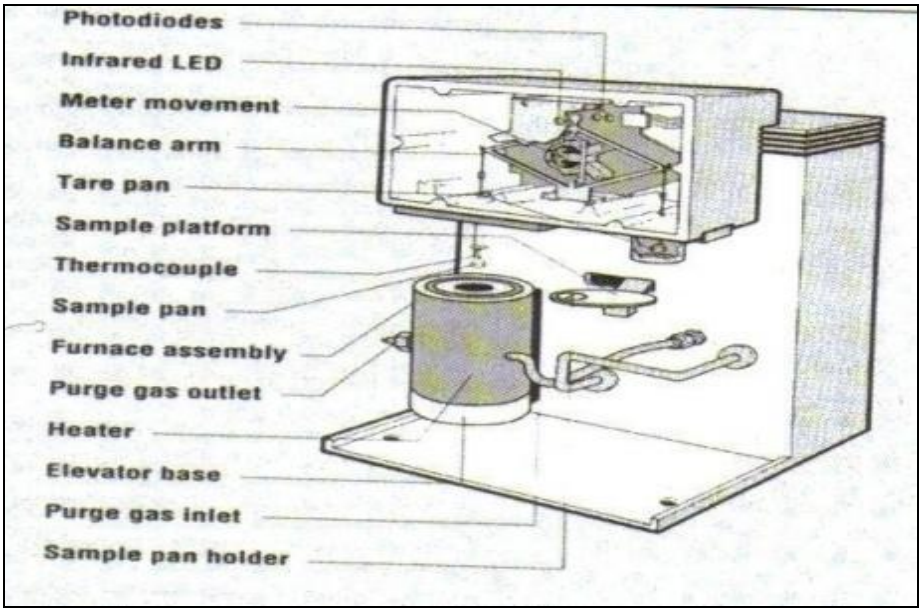

Figure 2.8. The schematic diagram of the 2050 Du Pont Thermogravimetric Analyzer.

Figure 2.9. A picture of the 2050 Du Pont Thermogravimetric analyzer.

The Sartorius 1800 laboratory balance.

The weighing of the $BaSO_4$ samples was done using a Sartorius 1800 laboratory balance shown in Figure 2.10.

Figure 2.10. A picture of the Sartorius 1800 laboratory balance used to weigh $BaSO_4$ samples for TGA studies.

This balance allows a maximum mass of 110 g to be weighed with an accuracy of 0.1 mg.

The Brooker Mass Flow Controller system.

This is a digital flow measuring apparatus which has the ability to record specific gas flow, taking into account the difference in densities of different gases. It therefore corrects the slight deviations from the exact gas flow, which is due to its specific density, when the gas flow is measured using the gas flow-meter. Each channel had to be calibrated for a specific gas and that channel was used for that specific gas

only in all different experiments. Calibration of the mass flow control system for each gas was done by plotting mass flow values vs flow-rate from the gas flow-meter.

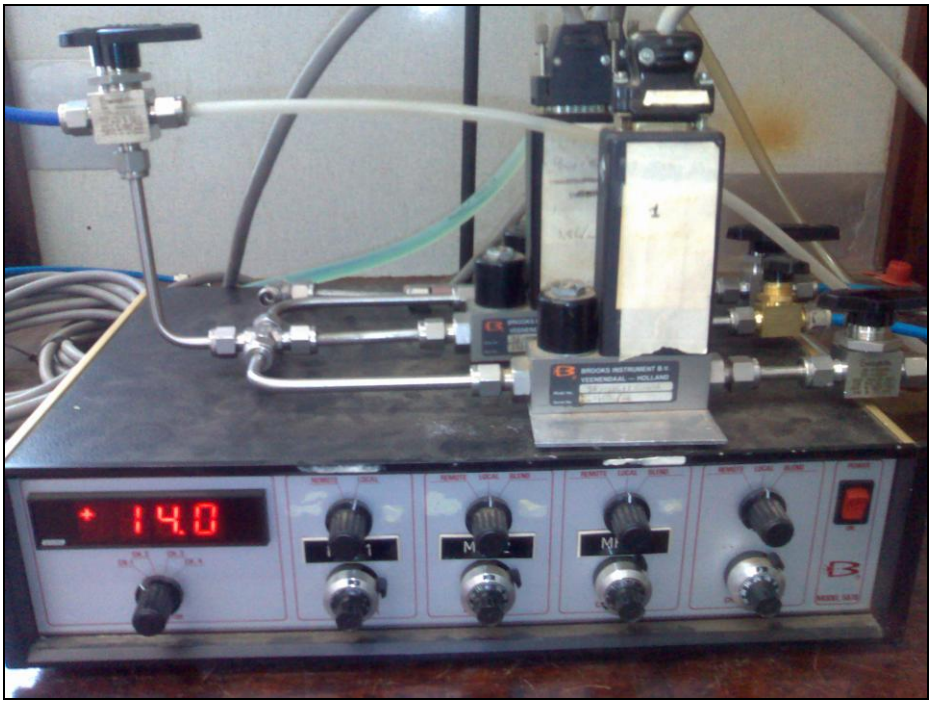

Figure 2.11. A picture of the Brooker mass flow controller system used to control gas flow during TGA studies.

2.4.2 Experimental methods and materials

An isothermal method of determining the reaction kinetics parameters was employed for these studies and the following general experimental procedure was followed for all experiments.

A 13.0 mg (0.043 mmol) mass of a reagent grade $BaSO_4$ (Merck), was accurately weighed using the Sartorius 1800 laboratory weighing balance and placed on the aluminium TGA pan. The TGA furnace temperature was set to rise at the rate of 30^0C/min under N_2 flow (200 ml/min) until the desired temperature, according to the experimental conditions, was reached. On reaching the desired temperature, the reactant gases (CO and CO_2) valves were opened at flows according to the specific experimental conditions. The pressure gauge on each cylinder was kept constant at 500 kpa while valves V1, V2 and V3 were used to open and close the gas flow to the mass flow control system. The gas composition mixture was done by varying the

gas flows (according to experimental conditions) using the calibrated mass flow control system and the total gas flow was maintained at 200 mL/min for all experiments. The reaction was left to run until completion, which was observed as a flattening (plateau) of the mass vs time plot curve on the display window of the TGA apparatus.

Experimental conditions were varied in order to evaluate the following:

1. The effect of temperature on the reduction of barium sulphate to barium sulphide with CO – Experiments 1 - 4 in Table 2.8
2. The effect of CO concentration on the reduction rate of barium sulphate to barium sulphide – Experiments 1 - 12 in Table 2.8
3. The possibility of CO_2 to act as a reducing agent in the reduction of barium sulphate to barium sulphide – Experiment 13 in Table 2.8
4. The effect of CO_2 on the reduction rate of barium sulphate to barium sulphide at different temperatures and different CO concentrations – Experiments 14 - 21 in Table 2.8.

Table 2.8. The reaction conditions for the isothermal experimental runs.

Experiment	% CO	% N_2	% CO_2	Temp ^{0}C
1	9.6	90.4	0	850
2	9.6	90.4	0	900
3	9.6	90.4	0	950
4	9.6	90.4	0	1000
5	4.8	95.2	0	850
6	4.8	95.2	0	900
7	4.8	95.2	0	950
8	4.8	95.2	0	1000
9	2.4	97.6	0	850
10	2.4	97.6	0	900
11	2.4	97.6	0	950
12	2.4	97.6	0	1000
13	0	0	100	1000
14	4.8	45.2	50	850
15	4.8	45.2	50	900
16	4.8	45.2	50	950
17	4.8	45.2	50	1000
18	2.4	47.6	50	850
19	2.4	47.6	50	900
20	2.4	47.6	50	950
21	2.4	47.6	50	1000

2.5. Hydrogen sulphide stripping studies.

The laboratory set-up that was used for the H_2S stripping is shown in Figure 2.12. The set-up consisted of two 5000 mL columns for H_2S-stripping and H_2S-absorption respectively, connected via a 5 mm diameter silicone tube. Three quarters of the volume of the first column, in which H_2S-stripping took place, was filled with BaS solution leaving the other quarter empty for the accumulation of H_2S. The connecting tube was submerged three quarters below the Zn acetate solution in the second column, where H_2S-absorption took place. The purpose of the Zn acetate solution in this system was to absorb and concentrate the H_2S sulphide from the stripping column in preparation for the sulphur production in the Pipco process.

A CO_2 gas cylinder was connected to the H_2S-stripping column via a gas flow -meter, which was used to regulate the CO_2 flow-rate into the column. Theoretically, the flow-rate of the H_2S/CO_2 mixture leaving the H_2S-stripping column should be equal to the flow-rate of CO_2 entering the column, after the pressure balance has been reached in the column. Therefore, the flow-rate of the H_2S/CO_2 entering the H_2S-absorptin column can be regulated using the CO_2 flow-rate into the H_2S-stripping.

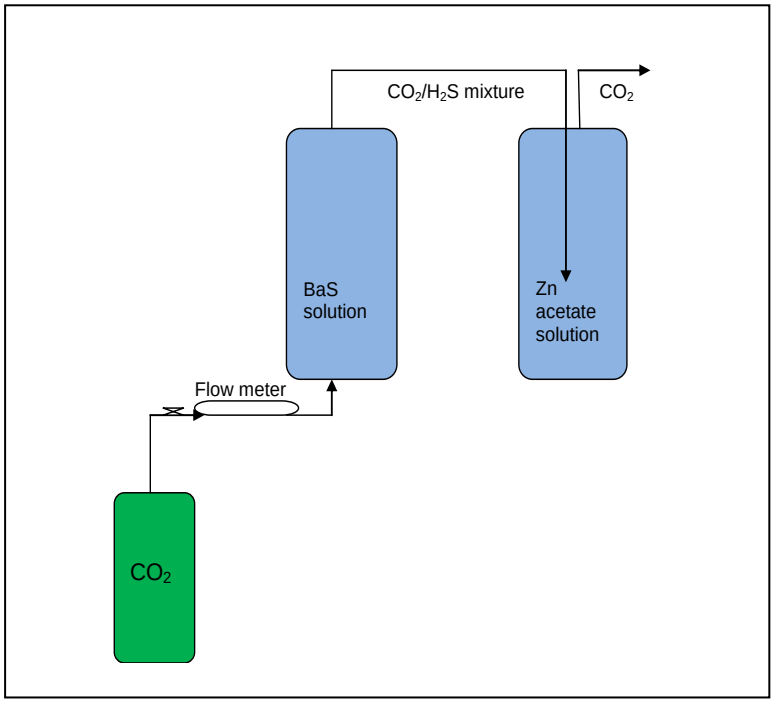

Figure 2.12. The schematic diagram of the laboratory set-up used for the H_2S stripping and absorption studies.

2.5.1 Experimental methods and materials

Sub-section 2.5.1.1 outlines the methods used for the preparation of the BaS and the Zn acetate stock solutions and sub-section 2.5.1.2 outlines the experimental methods and the experimental programs followed to carry out the different studies on the H_2S stripping and absorption processes.

2.5.1.1 The preparation of solutions

A 2*N* Zn acetate was used in all the experiments with the BaS solution concentration varied according to the experimental requirements. A fresh BaS solution was prepared and used immediately for each experiment in order to avoid excessive loss of sulphide from the solution into air.

Zn acetate stock solution

Zn acetate (6 000 000 mg) was dissolved in 5000 mL deionised water to give a 2*N* Zn acetate solution. The solution was stirred overnight in a closed container, to ensure full dissolution of the Zn acetate.

BaS solution

For each experiment, the BaS solution was prepared by weighing the correct mass of BaS and dissolving it in the required volume of deionised water to give the required concentration in mmol/L of BaS. The solution was stirred in a tightly sealed container to avoid loss of sulphide, and was used immediately after stirring.

2.5.1.2 Experimental methods and programs followed for the H_2S stripping and absorption studies

The aims of the following experiments were to:

1. Confirm the sulphide stripping from BaS solution using CO_2 and the absorption of H_2S into the Zn acetate solution.

2. Evaluate the effect of the (CO_2 flow-rate)/(Initial [S^{-2}]) ratio on the H_2S stripping and absorption.

2.5.1.2.1 The confirmation of H_2S stripping from BaS solution with CO_2 and the absorption of H_2S into Zn acetate

BaS (150 000 mg, 89 mmol) was dissolved in 5000 mL deoinised water. The analysis of this solution, using the iodine method of sulphide analysis (APHA, 1997*),* indicated a sulphide concentration of 150 mmol/L. Excess CO_2 was passed through the solution at a flow-rate of 148.8 mL/min (6.64 mmol CO_2/min) over a period of 90 minutes while 5 mL samples were taken from the H_2S stripping and the H_2S absorption columns and analyzed, immediately, for sulphide content and pH at increasing time intervals.

2.5.1.2.2 The evaluation of the effect of the (CO_2 flow-rate)/(Initial [S^{-2}]) ratio on the H_2S stripping and absorption.

The experimental program for the evaluation of the effect of the the (CO_2 flow-rate)/(Initial [S^{-2}]) ratio on the H_2S stripping and absorption is given in Table 2.9. All the experiments were carried out following the method outlined in 2.5.1.2.1 under the experimental conditions given in Table 2.9.

Table 2.9. The experimental conditions used for the evaluation of the effect of (CO_2 flow-rate)/(Initial [S^{2-}]) ratio on the H_2S stripping and absorption.

(CO_2 flow-rate)/(Initial[S^{2-}])	**7.96**	**2.80**	**1.29**
CO_2 flow-rate (mL/min)	149	52	105
CO_2 flow-rate (mmole/min)	6.6	2.3	4.7
Period of run (min)	90	90	90
CO_2 load (mmole)	598	421	421
BaS column:			
Initial [S^{2-}] (mmole/L)	75	150	325
Reactor volume (mL)	1000	1000	1000
Zn acetate column:			
Initial [S] at (mg/L)	0	0	0
Reactor volume (mL)	5000	5000	5000

CHAPTER 3

RESULTS AND DISCUSSION

Introduction

In this Chapter the results obtained from the different experiments that were carried out as outlined in Chapter 2, are presented. The results for each experiment, followed by the corresponding discussion, are presented in the order in which they were executed, as described in Chapter 2.

3.1. Water treatment.

The results for the batch studies on sulphate removal are depicted graphically representing the decrease in sulphate concentration with time, when the sulphate-rich water was treated with barium carbonate under different experimental conditions. Only qualitative and quantitative results of the water treatment studies are presented and no further modelling of the results was done, as it was beyond the scope of this thesis.

3.1.1 The effect of the barium carbonate concentration on the sulphate removal rate

Figure 3.1 is a graphical representation of the decrease in sulphate concentration with time, when the different amounts of barium carbonate were dosed, batchwise, into sulphate-rich water. The different amounts of barium carbonate are shown as the $BaCO_3/SO_4^{2-}$ ratio. The errors in the sulphate concentration measurements were < 10%.

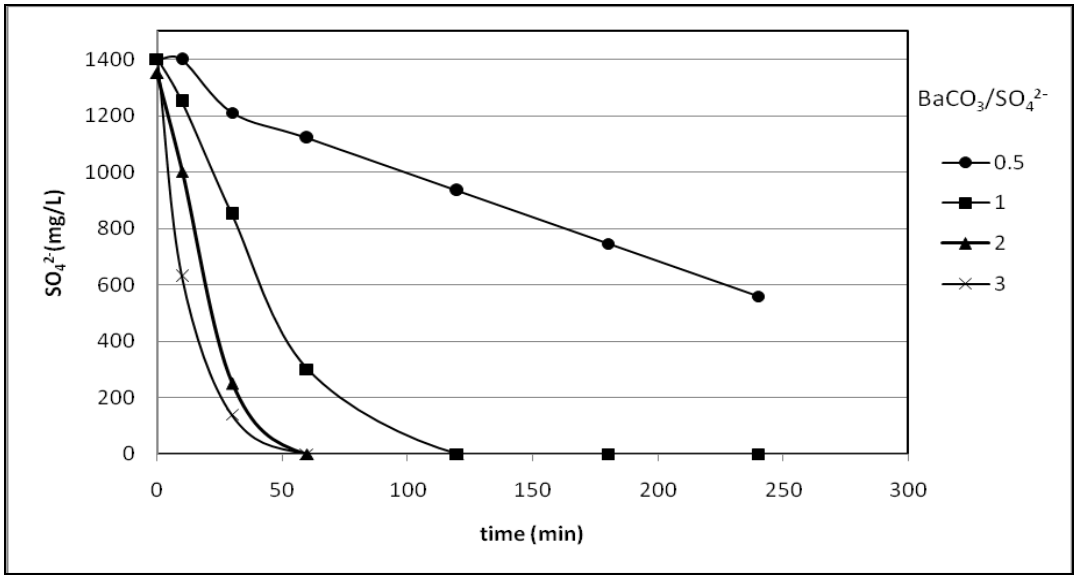

Figure 3.1. A graphical representation of the sulphate removal using different barium carbonate concentrations.

An increase in the sulphate removal rate with increased barium carbonate concentration in the solution, as indicated by the plots in Figure 3.1, was observed and explained in terms of the amount of Ba^{2+} ions available for the reaction with the SO_4^{2-} in solution and the supersaturation level. At higher $BaCO_3/SO_4^{2-}$ ratio there is, relatively, a higher initial concentration of Ba^{2+} which leads to higher supersaturation levels on interaction with the SO_4^{2-} present in the solution. As was discussed in Chapter 1, supersaturation is the driver of precipitation. Therefore at high barium carbonate concentration there is a relatively constant supply of Ba^{2+} for a longer period, which in turn keeps the supersaturation level almost constant leading to a higher nucleation rate.

Furthermore, the results showed that the sulphate removal follows the same trend for all barium carbonate concentrations with $BaCO_3/SO_4^{2-} \geq 1.0$. For all these ratios the trend is such that the sulphate removal starts off linearly followed by a slowing down as the Ba^{2+} ions become depleted in the solution. This indicates that the reaction is faster at high levels of barium carbonate concentrations and slows down gently with the depletion of the barium carbonate.

A different trend was observed with a barium concentration below the stoichiometric amount ($BaCO_3/SO_4^{2-}$ = 0.5). In this case the reaction rate still seems to be faster at the beginning of the reaction and slower towards the depletion of the Ba^{2+} ions. The sulphate removal follows a linear trend towards the end of the reaction. indicating that the sulphate removal rate remains constant as the supersaturation is not mainly controlled by the supply of Ba^{2+} ions in this case.

The reaction rates for the different barium carbonate concentrations were calculated for the linear parts of the curves and from these rates the order of the reaction was calculated. The determination of the reaction order for this reaction was done by plotting the log of the reaction rates for the sulphate removal for different $BaCO_3/SO_4^{2-}$ ratios against the log of the corresponding barium carbonate concentrations as shown in Figure 3.2. The order for this reaction, as reflected by the slope of the best straight line of this graph, was found to be a first order relationship (rate order >0), which is an indication of the concentration dependent rate.

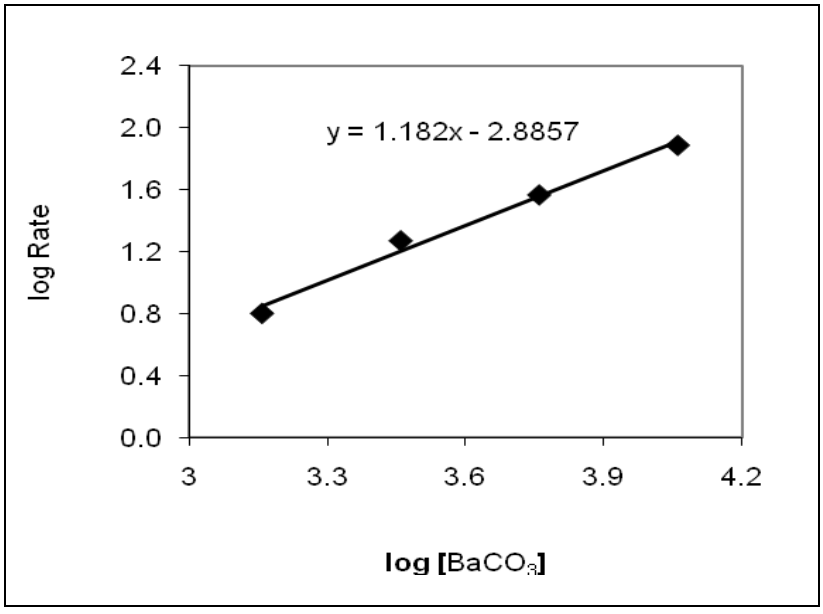

Figure 3.2. A graphical representation of the log of the reaction rates against the log of the barium carbonate concentrations.

3.1.2 The effect of alkalinity on the sulphate removal rate

Figure 3.3 shows graphical representations of sulphate removals when stoichiometric amounts of barium carbonate (mol ratio, $BaCO_3/SO_4^{2-}$ = 1) were added to beakers containing sulphate rich water having different alkalinity levels.

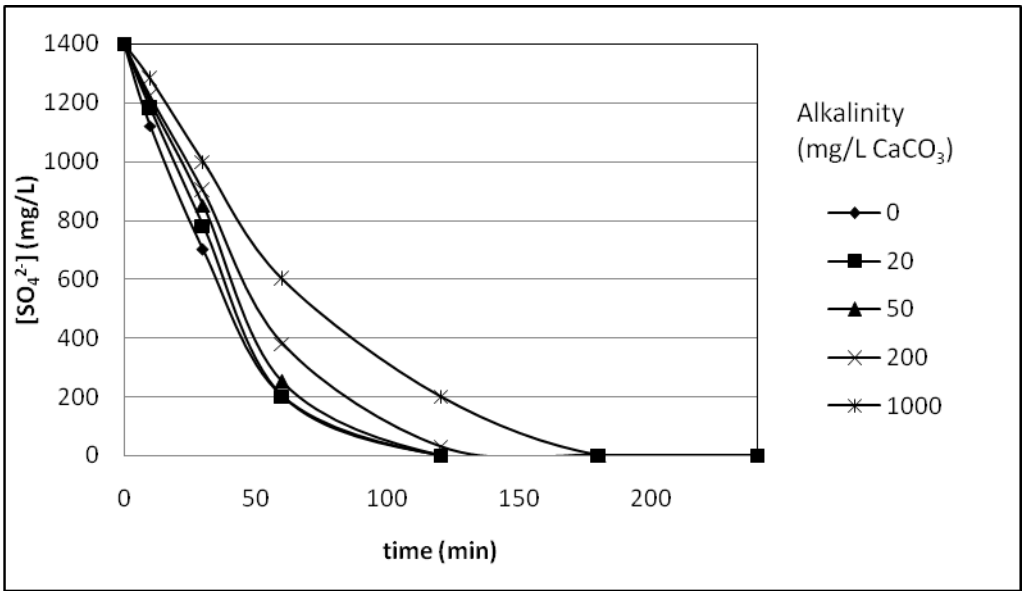

Figure 3.3. A graphical representation of the sulphate removal from water with different alkalinity levels.

Comparison of the results from the different experiments, carried out under increasing alkalinity levels, indicated that the effect of alkalinity is only pronounced at alkalinity levels above 200 mg/L $CaCO_3$.

There was no significant decrease in the sulphate removal rate when the alkalinity was increased from 0 – 200 mg/L $CaCO_3$. However, an increase in the alkalinity of the treated water to 1000 mg/L $CaCO_3$ resulted in a significant decrease in the sulphate removal rate. Graphical representation of the decrease in the sulphate concentration with time, when the alkalinity was 1000 mg/L $CaCO_3$, indicated that an additional 60 minutes were required for a complete removal of sulphate to be attained as compared to water with < 200 mg/L $CaCO_3$ alkalinity.

The decrease in sulphate removal rate with increased alkalinity can be ascribed to the decrease in solubility of the barium carbonate in high alkalinity environments. The precipitation of $BaSO_4$ from the solution requires $BaCO_3$ to dissolve in order to provide Ba^{2+} ions. However, as it has been mentioned in Chapter 1, $BaCO_3$ has a relatively low solubility hence it only undergoes a partial dissolution in water. The dissolution of $BaCO_3$ in this case is enhanced by the constant removal of the Ba^{2+} ions from solution, through $BaSO_4$ precipitation, and constant removal of CO_3^{2-}, via $CaCO_3$ precipitation. It is clear that this phenomenon requires that the treated water be rich in dissolved SO_4^{2-} ions, which in turn renders it acidic. An alkaline environment implies high concentration of CO_3^{2-} in the solution which, through the common ion effect, will inhibit further dissolution of the $BaCO_3$. The presence of CO_3^{2-} in solution also makes the Ca^{2+} ions unavailable for precipitation with CO_3^{2-} from the partial dissociation of $BaCO_3$ and consequently further inhibits the dissolution of $BaCO_3$.

The decreased sulphate removal from water with very high alkalinity levels does not pose any problem to sulphate removal using the barium carbonate process as AMD is normally high in acidity and low in alkalinity. In the case of high alkalinity water, the sulphate will still be completely removed. However, the biggest problem is the long time period needed for complete precipitation of $BaSO_4$.

3.1.3 The effect of magnesium on sulphate removal

The current studies have shown that the anion associated with the magnesium in water dictates the effect that magnesium will have on the sulphate removal rate during treatment with barium carbonate. Figures 3.4 and 3.5 show graphical representations of the results of the sulphate removal experiments with $BaCO_3$ ($BaCO_3/SO4^{2-} = 2$) in the presence of $MgCl_2$ and $MgSO_4$, respectively.

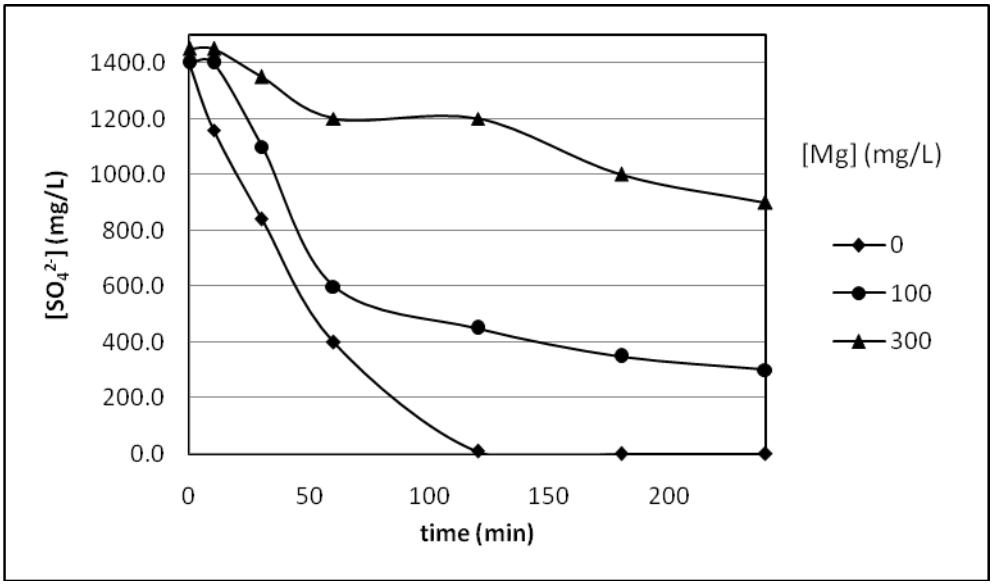

Figure 3.4. A graphical representation of sulphate removal from water, containing different concentrations of $MgSO_4$, using $BaCO_3$.

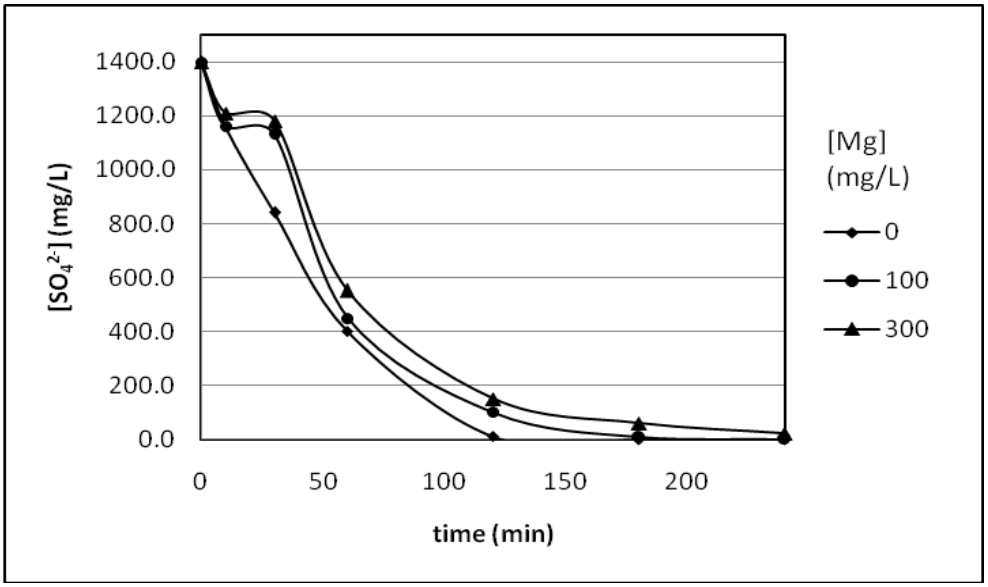

Figure 3.5. A graphical representation of sulphate removal from water, containing different concentrations of $MgCl_2$, using $BaCO_3$.

A significant negative effect on the sulphate removal rate was observed when the water contained increasing amounts of $MgSO_4$. On the other hand, only a negligible decrease in the sulphate removal rate was observed when the $MgCl_2$ equivalent amounts were added to the water being treated. This finding led to a re-evaluation

of the general conclusion made by Trusler (1988) that the presence of magnesium in water to be treated has a negative effect on the sulphate removal when barium carbonate is used to treat the AMD, containing large amounts of sulphate ions.

It must be noted that in the case of sulphate removal in the presence of $MgSO_4$, the sulphate content associated with magnesium forms part of the total sulphate to be removed. Graphical representation of the effect of $MgSO_4$ on the sulphate removal from water, as shown by Figure 3.4, suggests that only the sulphate which is not associated with magnesium can be completely removed and that which is associated with magnesium remains in the treated water. This effect was shown by the slowing of the sulphate removal rate as the remaining sulphate in solution reached the sulphate equivalent in concentration to the added $MgSO_4$. The more $MgSO_4$ was added, the slower was the observed sulphate removal rate.

On the other hand, as shown by the Figure 3.5, the presence of $MgCl_2$ in the treated water did not have a significant effect on the sulphate removal using $BaCO_3$, irrespective of the magnesium concentration in the solution. This showed that magnesium does not, necessarily, inhibit the interaction between the Ba^{2+} and SO_4^{2-} ions, as was suggested by Trusler (1988), but the negative effect, caused by the presence of magnesium in solution is due to the type of ion associated with the Mg^{2+} ion in solution, in this case the SO_4^{2-} ion. Therefore, only sulphate-rich water with high magnesium concentrations and less/no chloride will pose difficulties if the barium carbonate process is used for sulphate removal.

In the light of the above explanation, a deduction could be made that water that contains high concentrations of Mg^{2+} or Na^{+} ions, that are associated with the SO_4^{2-} ion, will have a residual sulphate concentration, which is stoichiometrically equivalent to the sum of the Mg^{2+} and Na^{+} concentrations, after treatment with barium carbonate. On the other hand, in the case of high concentrations of Mg^{2+} and Na^{+} that are associated with the Cl^{-} ion, complete removal of sulphate from the solution will be possible.

3.2. Controlled precipitation studies.

The experiments conducted for the calibration of the experimental setup showed that there was a pronounced air bubble uptake into the solution at stirrer speeds below 2200 rpm. This was shown by an increase in volume concentration of the air bubbles at 2200 rpm and below. The volume concentration values of air bubbles at these stirrer speeds varied between 0 and 0.38%. These values were extremely low but taking into account that the solids concentration in the solution was between 0 and 1% the effect of the bubbles could not be neglected.

In order to eliminate the effect of air bubbles on the CSD data obtained at stirrer speeds below 2200 rpm, the CSD data was normalized over the size interval 0 to 200 microns. The air bubble volume percentage peaks appeared in the CSD data in the region 250 microns and above, hence the effect was more pronounced in these regions.

A number of experiments were conducted to establish consistency and trends in the controlled precipitation studies, in order to assure that the methodology was correct. The results and discussion of these experiments are outlined in the methodology optimization section.

Methodology optimization.

The initial experiments that were conducted using BaS and $CaSO_4 \cdot 2H_2O$ solutions as reagents were done in order to mimic the industrial process as closely as possible. From the SEM analysis (Figure 3.6) it appeared that both $BaSO_4$ and $CaSO_4 \cdot 2H_2O$ were precipitated and some residual BaS still remained undissolved. The SEM scan showed $BaSO_4$ as large and light crystals wheras the $CaSO_4 \cdot 2H_2O$ were larger and darker particles. The barium sulphide was seen as small, lighter particles on the surface of the darker and larger calcium sulphate particles.

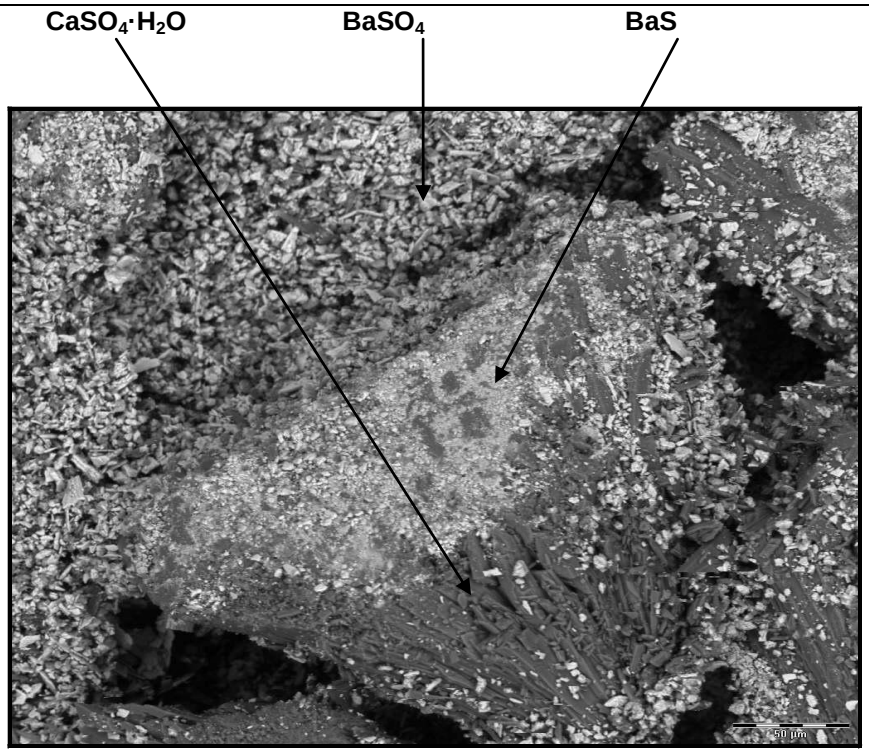

Figure 3.6. The SE photomicrophotograph of the product obtained from the reaction between BaS and $CaSO_4$, showing the presence of a mixture of compounds.

Although the co-precipitation of $BaSO_4$ and $CaSO_4{\cdot}2H_2O$ is not a problem in the integrated barium carbonate process, as both $BaSO_4$ and $CaSO_4{\cdot}2H_2O$ are reduced to the sulphides in the kiln, the simultaneous presence of these compounds in the product made the CSD analysis and the study of the controlled precipitation by an in-line dosing system complicated. It was for this reason that $Ba(NO_3)_2$ and Na_2SO_4 solutions were selected as reagent streams for all other experiments that were conducted in these studies.

Figure 3.7 depicts the SEM scan of the $BaSO_4$ product particle from the reaction between $Ba(NO_3)_2$ and Na_2SO_4 at the end of the reaction. Very large $BaSO_4$ crystals, of the order of 30 microns, were obtained as the product, compared to those reported in the literature, which were usually of the order of 2-5 microns, indicating the effectiveness of this precipitation system in enhancing growth of the particles over nucleation.

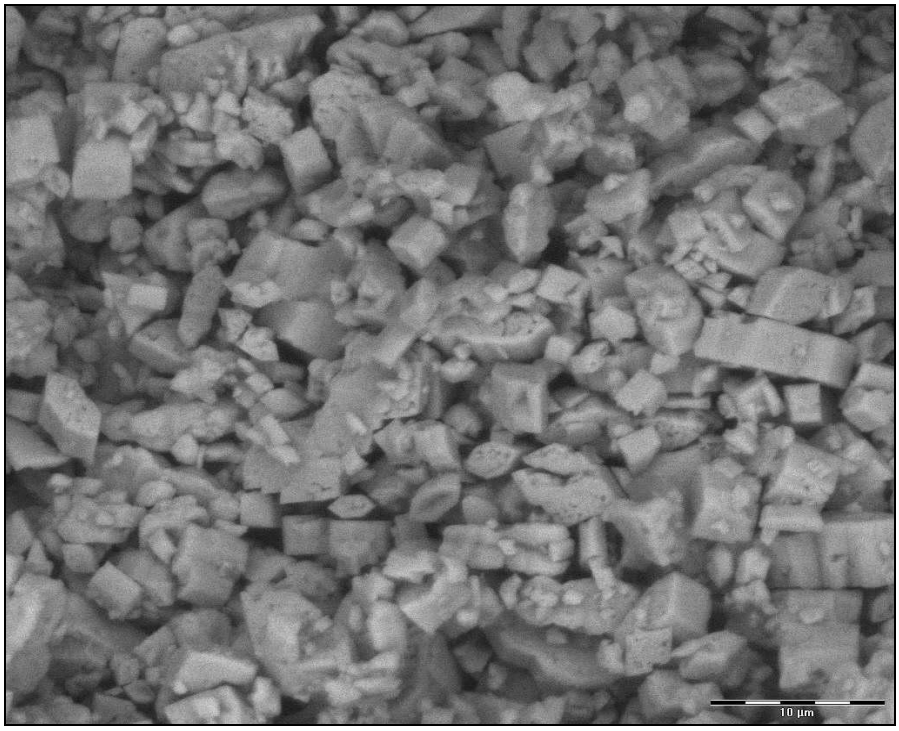

Figure 3.7. The SE photomicrophotograph of the $BaSO_4$ product obtained from the reaction between $Ba(NO_3)_2$ and Na_2SO_4.

The other factor, which had to be optimized, was the position of the feed needle into the precipitator tube. The position of the $Ba(NO_3)_2$ feed needle, relative to the end of the tube was varied in order to be sure that the precipitation-mixing-dilution was occurring predominantly in the tube and not where the recirculation tube enters the 1 L vessel. It appeared that the CSD pattern was not affected by changing this distance between 10 and 30 cm and a downstream mixing length of 20 cm was used in all experiments.

3.2.1 The central experiment

The central experiment, herein referred to as Experimental Run 1, serves as reference for all other experiments that were carried out. The particle size analysis of the $BaSO_4$ seed was done prior to the execution of Experimental Run 1 and the CSD of these particles is shown in Figure 3.8. This CSD shows that the seed particle size has a bimodal pattern with the two maxima at 0.63 and 3.99 microns.

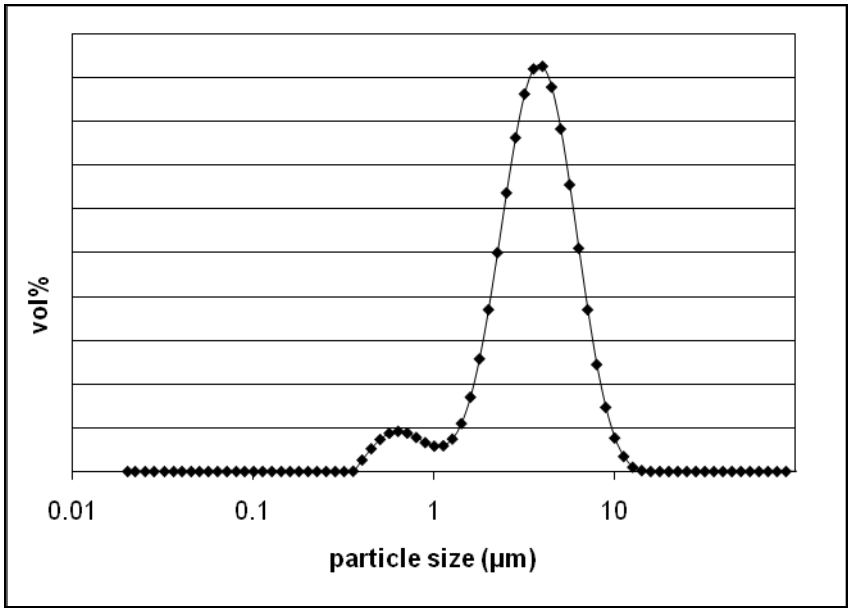

Figure 3.8. The bimodal CSD pattern of the $BaSO_4$ seeds.

The seeds having a size below 1 micron, in Figure 3.8, represent only 5.6% of the mass of seeds that were present, but represent 85% of the number of seed crystals. Figure 3.9 is a SEM photomicrograph of the seeds, qualitatively confirming the CSD analysis.

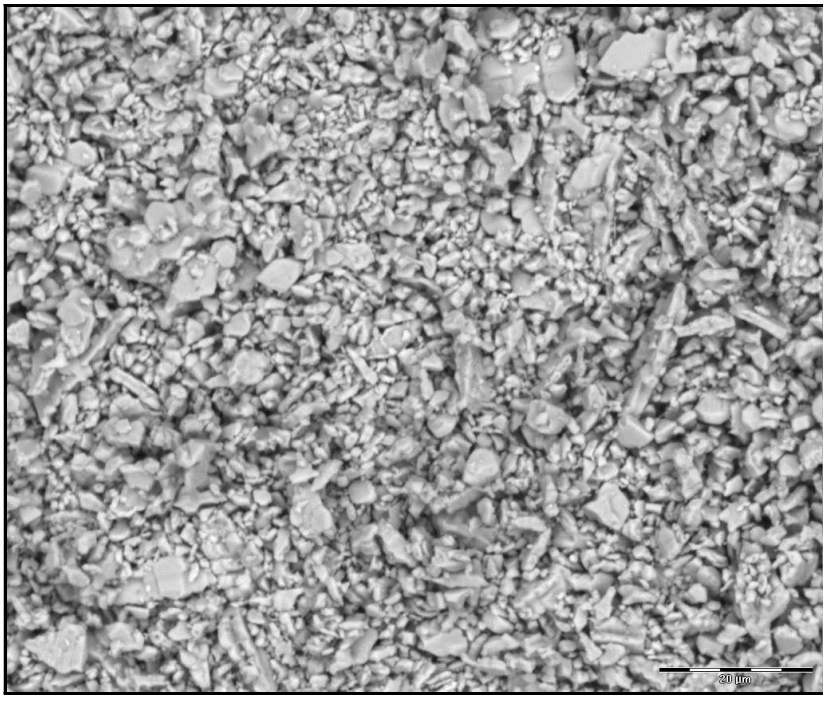

Figure 3.9. The SE photomicrograph of the $BaSO_4$ seed particles.

Experimental Run 1

The precipitation of the $BaSO_4$ particles were indicated by an increase in obscuration, (as dimensionless quantity) as the particles were formed as shown in Figure 3.10. The development of the plateau indicated the depletion of the reactant ions in solution as the reaction reached completion.

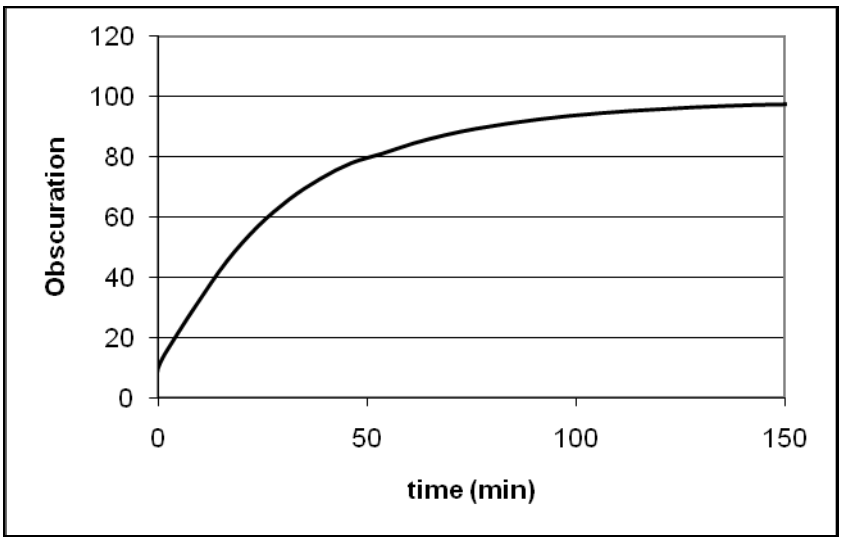

Figure 3.10 The development of obscuration as the number of precipitated $BaSO_4$ particles increased.

The development of the normalized CSD pattern with time, as the barium nitrate solution was dosed into the system, for experimental run 1 is depicted in Figure 3.11. The graphs include particle sizes of the seeds, nucleation and the final product. The number of CSD data points used for this graph is in the order of 10,000. The data are for 7 experimental runs with 25 measurements per run and 60 non-zero data points per analysis. Due to the huge amount of points obtained from such a run not all data points can be shown, however the trend remains the same.

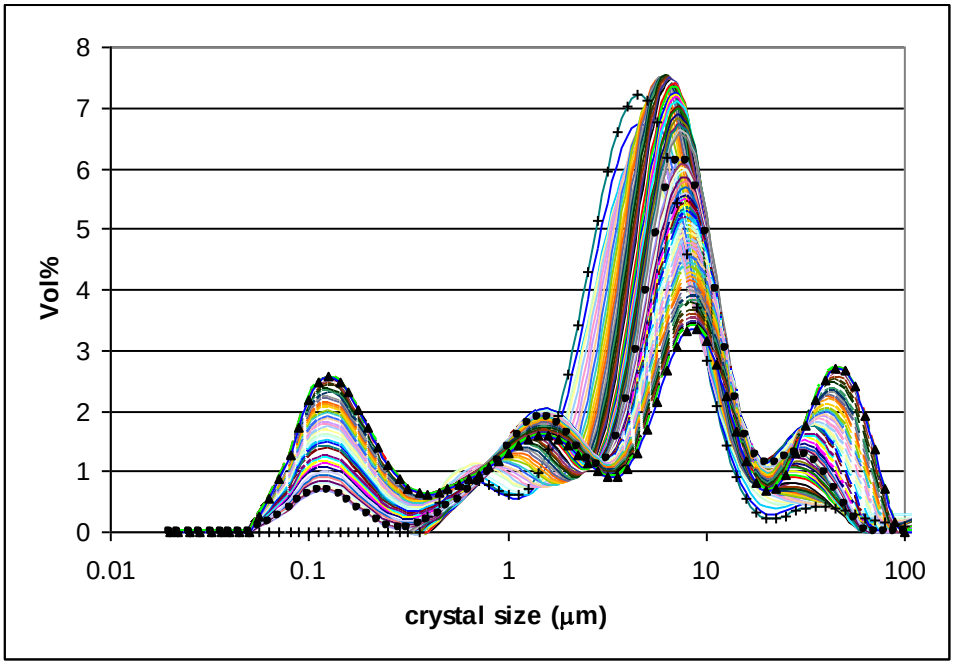

Figure 3.11. The CSD pattern for Experimental Run 1: seeds:+, first observed nucleation: ● and the final product:▲.

A closer observation of this CSD pattern indicated a shift of the CSD modes to larger particle sizes, as the $Ba(NO_3)_2$ was fed to the solution. The CSD formation was checked by monitoring the CSD after stopping the $Ba(NO_3)_2$ feed. It appeared that no visible change in the CSD pattern was observed after stopping the $Ba(NO_3)_2$ feed. The overall mass balance was confirmed by the observation that the CSD pattern stopped shifting to larger sizes once the stoichiometric amount of $Ba(NO_3)_2$ was added.

Finally, from the CSD data consistency it became clear that:

- The growth rates in each size class decreased with time due to the decreasing supersaturation and the increasing available crystal surface area.
- The growth increased with larger particles, either due to growth rate dispersion or to size dependent growth (discussed below).
- The nucleation occurred with continuous addition of $Ba(NO_3)_2$.

3.2.2 Reproducibility

Experimental Run 2 was carried out to confirm the reproducibility of Experimental Run 1. The CSD obtained from this run was found to be similar to that of Experimental Run 1, with negligible differences. Figure 3.12 depicts the two normalized CSDs obtained from Runs 1 and 2, respectively.

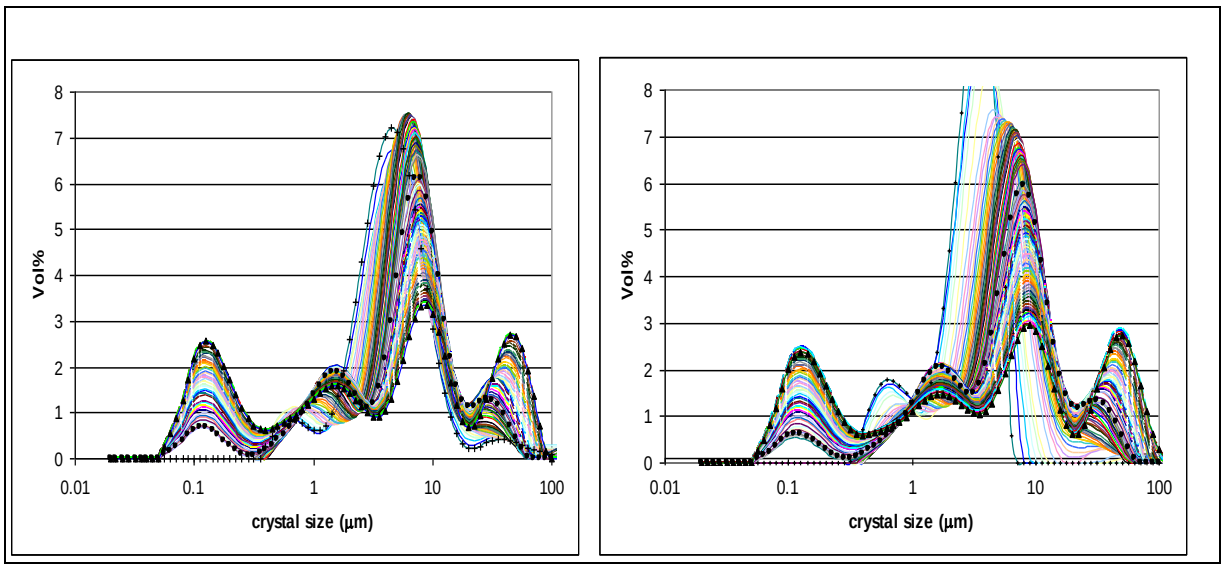

Figure 3.12. The CSD patterns for Experimental Runs 1 and 2, respectively, showing the reproducibility of the experiment.

The main difference in this reproducibility test was the size distribution of the starting seeds, which was narrower in Experimental Run 1, and thus higher in Experimental Run 2. The developing pattern showed, however, a very great similarity in how the original bimodal distribution developed into a broad distribution with four maxima in the final product.

The following phenomena were observed:

1. In the first 73 minutes the seeds grew, where the larger crystals with a maximum at 4 micron clearly grew faster, than those with a maximum at 0.6 micron. From the start a peak developed with a maximum of 50-70 microns, which quickly increased in relative importance

2. After 73 minutes, in both runs, particles with a size in the order of 0.05-0.4 micron were formed. These nuclei increased in volume and number, but hardly grew. The relative importance increased, and at the end of the run these particles made out 25% of the total mass (volume).
3. After 150 minutes, the stoichiometric amount of sulphate has been added and the CSD pattern remained constant

Figure 3.13 shows the relative amount of crystals that formed in the three size ranges: < 0.4 micron (the nuclei), 0.4-10 microns (the seeds), and >10 microns (the crystals).

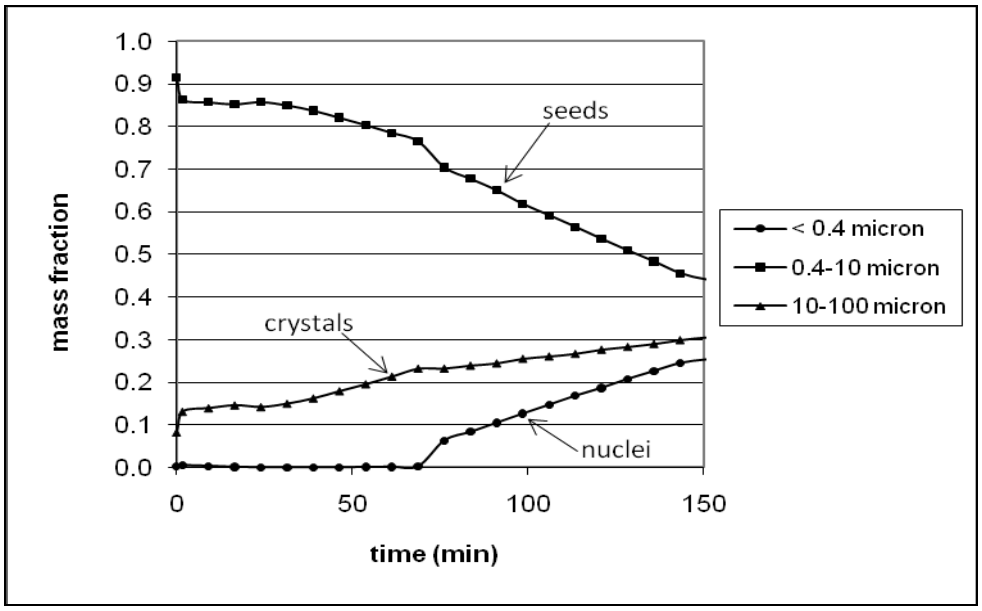

Figure 3.13. The graph of the mass fractions of seeds (0.4-10 microns), crystals (10-100 microns) and nuclei (<0.4 microns) produced in Experimental Run 1.

From Figure 3.13 it was clear that although large $BaSO_4$ crystals in the range larger than 10 microns were produced, the large volume of nuclei formed smaller than 0.4 microns, a product that is difficult to separate. The question then is: What caused the formation of these small crystals after 73 minutes and what is the best way to prevent their formation?

In most precipitation processes of salts with low solubility, such as $BaSO_4$, the phenomenon that causes nucleation bursts are heterogeneous and in some cases homogeneous nucleation. In this case this seemed not to be the case, considering:

- The size of the new particles, which were much larger than the sizes of the primary nuclei, the latter being undetectable with the size analyzer used.
- The relative width of the size distribution of the new particles.
- That the particles were not formed at the start when the supersaturation was higher
- That the particles did not tend to grow, which indicates that these particles contained a lot of crystallographic stress

All these observations indicated that new particles were formed rather by secondary abrasive nucleation. This is usually not encountered in $BaSO_4$ precipitation, but apparently the methodology applied here to harvest a coarse product, played a role. In the crystallization of readily soluble salts, these phenomena have been observed, typically at a crystal size larger than a few hundred microns (Mersmann, 1990; Kramer, 2003).

The graph of the number of particles that formed with time showed the time that elapses before initiation of nucleation, after the start of the $Ba(NO_3)_2$ dosage into the system. Figure 3.14 indicates that, for Experimental Run 1, nucleation initiated 69 minutes after $Ba(NO_3)_2$ dosing commenced.

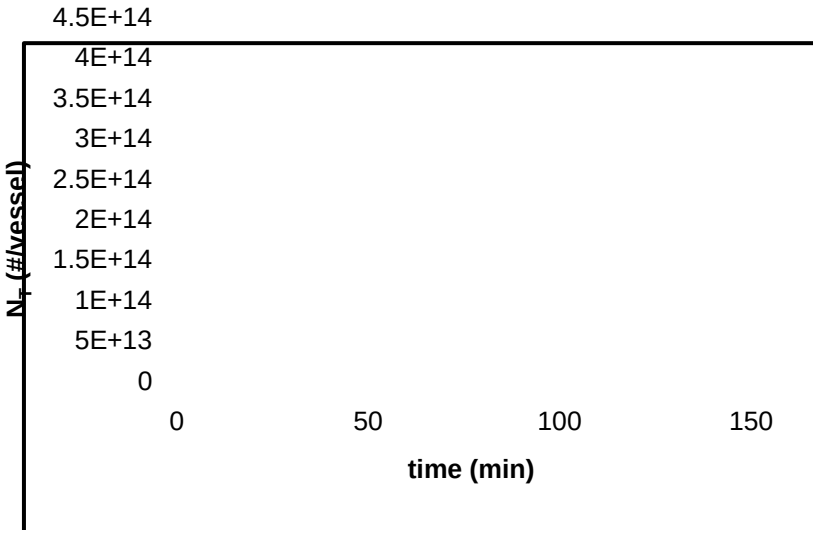

Figure 3.14. A graphical representation of the total number of particles ($\mathbf{N}_T$) present as a function of time, as nucleation took place (Experimental Run 1).

The graph of nucleation (B) with time, in Figure 3.15, indicates that maximum nucleation took place 76 min after $Ba(NO_3)_2$ dosing.

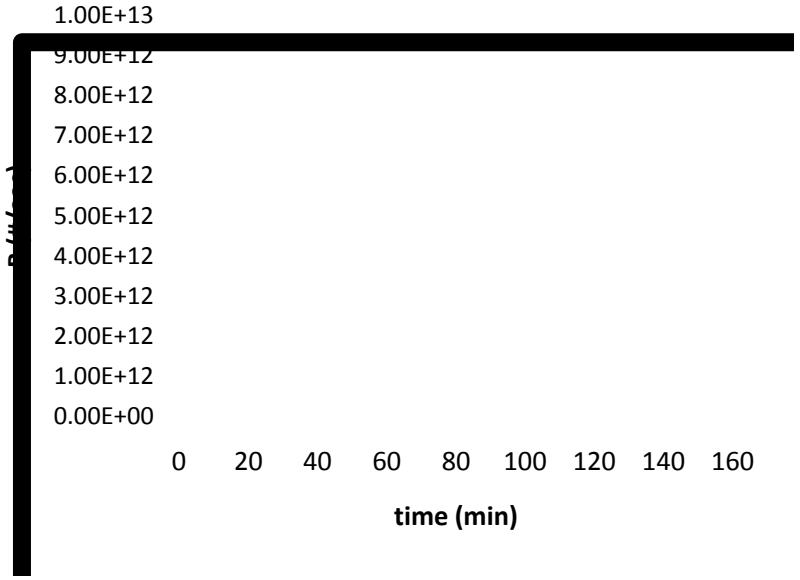

Figure 3.15. The development of nucleation with time, for Experimental Run 1.

Figure 3.16 shows the CSD patterns that developed with time after the nucleation event from Experimental Run 1. A closer look at the trends in the changes of the

CSD showed that there is an interconnection between the new formed particles (nucleation) and the particles in the crystal size larger than 10 microns, indicating secondary nucleation. This was shown by a corresponding rise in the large particle size range above 10 microns with the rise of the nuclei peak with time, after the start of the reaction.

These patterns showed that the rise in the nuclei peak corresponded with the rise in the large particle size range above 10 microns, indicating secondary nucleation. Furthermore, the slopes of the arrows showed that larger particles grew much faster than smaller particles, suggesting a size dependent growth.

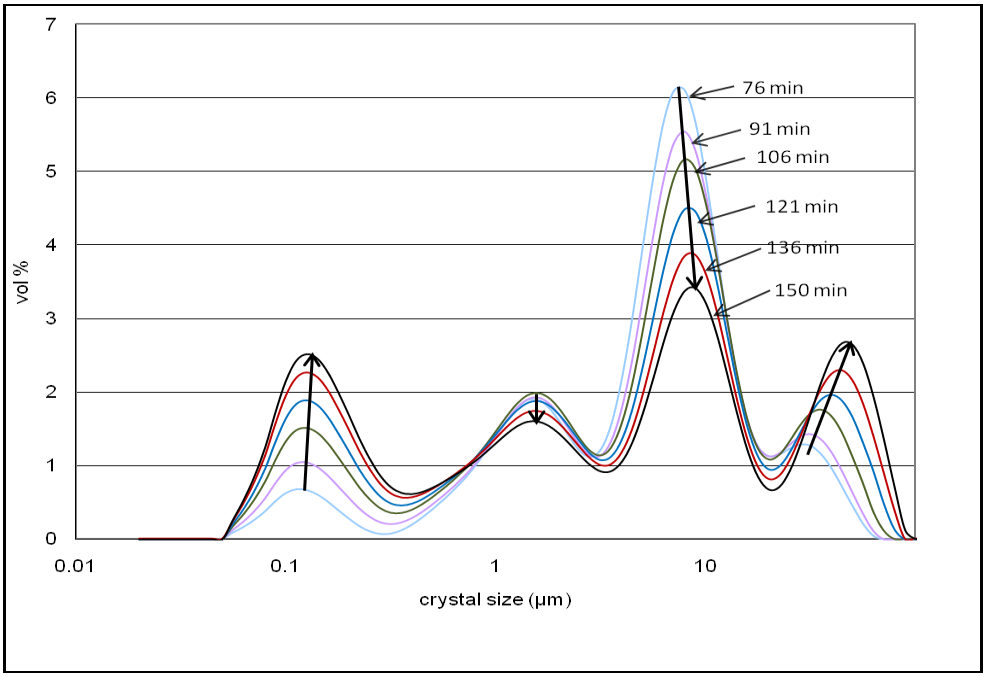

Figure 3.16 The CSD pattern development in Experimental Run 1, indicating the time after the start of the reaction.

The average growth rate, (G), was calculated for every particle size interval, according to Equation 46 (p. 53). In the calculation procedure, the data where the slope of the CSD curve was steep, gave erratic results for the growth rate. The data for these points have been omitted. The reason why it was logical to plot the average value of G(x)/G(1) is that, although the growth rates during the run

decreased, the supersaturation that the crystals experienced at a given time, was the same for each crystal.

The average growth rate of crystals with size x were calculated relative to the average growth rate of particles with a size of 1 micron. The calculated average growth rate showed that the average growth rate remained relatively constant for crystal sizes below 7 microns and thereafter increased with the crystal size. This observation suggested a size dependent growth and thus supported the observation from the CSD above. Figure 3.17 shows a graph of the average growth rate of crystals of size x relative to the growth rate of crystal particles with a size of 1 micron for Experimental Run 1.

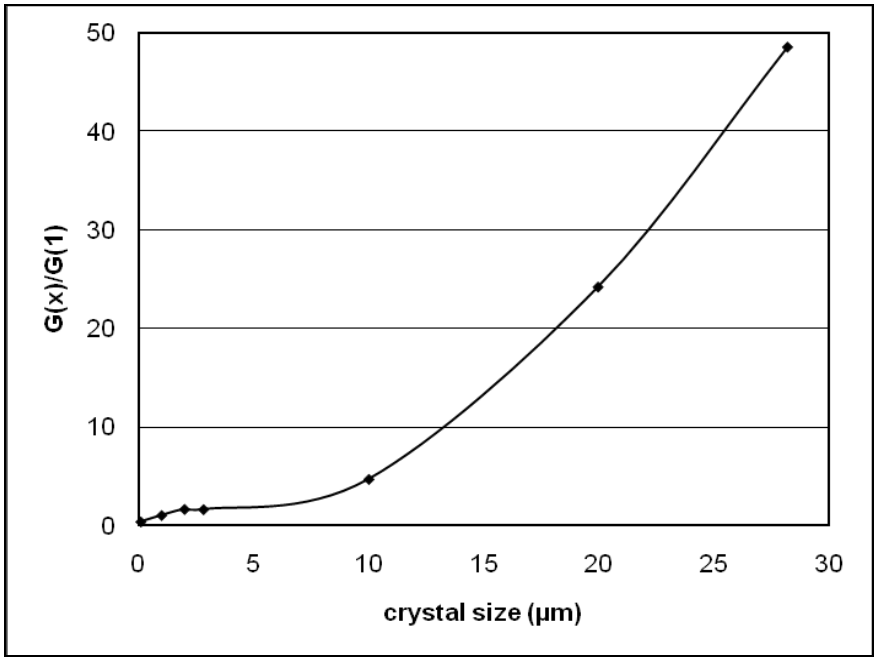

Figure 3.17. A graphical representation of the average growth rate of crystals of size x, relative to the growth rate of particles with a crystal size of 1 micron for Experimental Run 1.

3.2.3 The effect of lower Ba-concentration on the crystal growth rate

Reducing the $Ba(NO_3)_2$ concentration by half (Experimental Run 3), thus lowering the supersaturation ratio at the feed point, led to an increased growth rate for crystal

sizes above 7 microns, relative to the average growth rate in Experimental Run 1. The decrease in the supersaturation ratio decreased the nucleation rate and increased the precipitation period. The overall effect was an increased growth, which resulted in the formation of larger crystals. Even though size-dependent growth was still observed, the trend changed for crystal sizes above 20 micron. In this case a decline in the growth rate was observed for crystal sizes above 20 µm. This observation could be explained in terms of the depletion of Ba^{+2} ions in solution and also indicated that secondary nucleation was involved. Figure 3.18 shows the comparison between the average growth rates in Experimental Run 1 and Experimental Run 3.

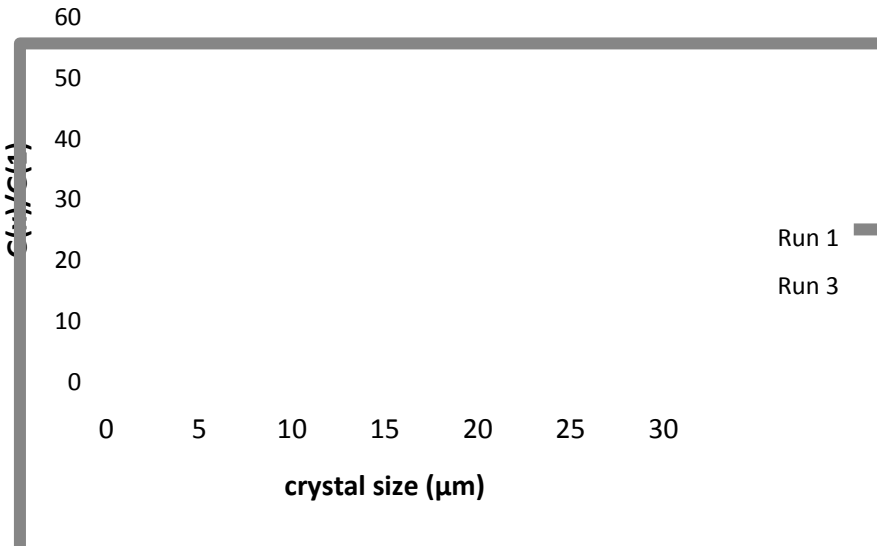

Figure 3.18 A graphical representation of the increase in the average growth rate (G) as the $Ba(NO_3)_2$ concentration was lowered by a half (Experimental Run 3), relative to the average growth rate in Experimental Run 1.

A consideration of the total number of particles ($\mathbf{N}_T$) that formed, as the precipitation progressed, showed that there was a decrease in the number of particles formed in Experimental Run 3 compared to the number of particles formed in Experimental Run 1, as indicated by Figure 3.19. This observation suggested that fewer and larger particles were formed faster in Experimental Run 3 as compared to those formed in Experimental Run 1.

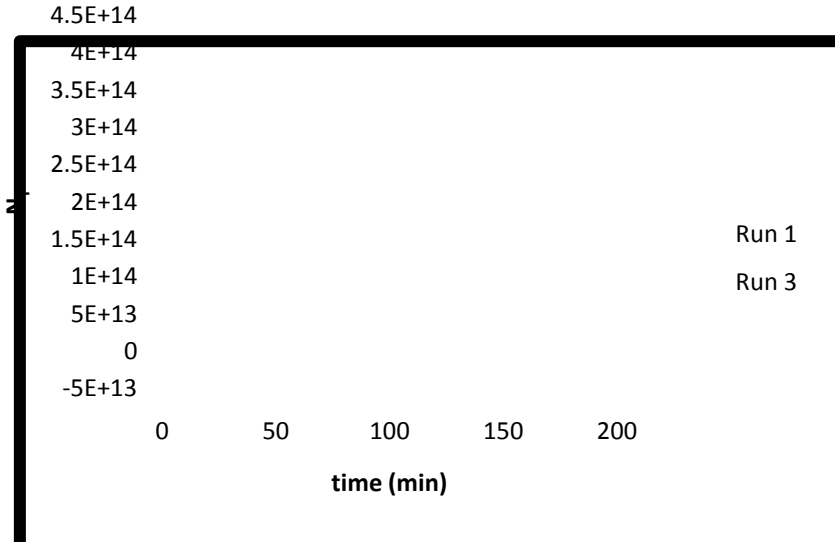

Figure 3.19. A comparison between the number of particles that formed in Experimental Run 1 and the number of particles formed in Experimental Run 3, as precipitation progressed.

3.2.4 The effect of the number of feed points on the crystal growth-rate

A further increase in the average growth rate relative to Experimental Run 1 was observed when the number of feed points into the precipitator tube was increased to 2 while the $Ba(NO_3)_2$ concentration from Experimental Run 1 was halved (Experimental Run 4). Doubling the number of feed points and halving of $Ba(NO_3)_2$ meant that the supersaturation around the feed points was still as low as that in Experimental Run 3, but the precipitation period was reduced to the value of Experimental Run 1. However an increase in the number of feed points from 1 to 2 enhanced the fluid turbulence in the precipitator tube, thus leading to improved mixing in the precipitator tube. The nuclei that formed in the first feed-point quickly collided with the nuclei formed in the closest feeding point, as the nucleation flames overlap, enhancing crystal growth, as illustrated by Figure 3.20.

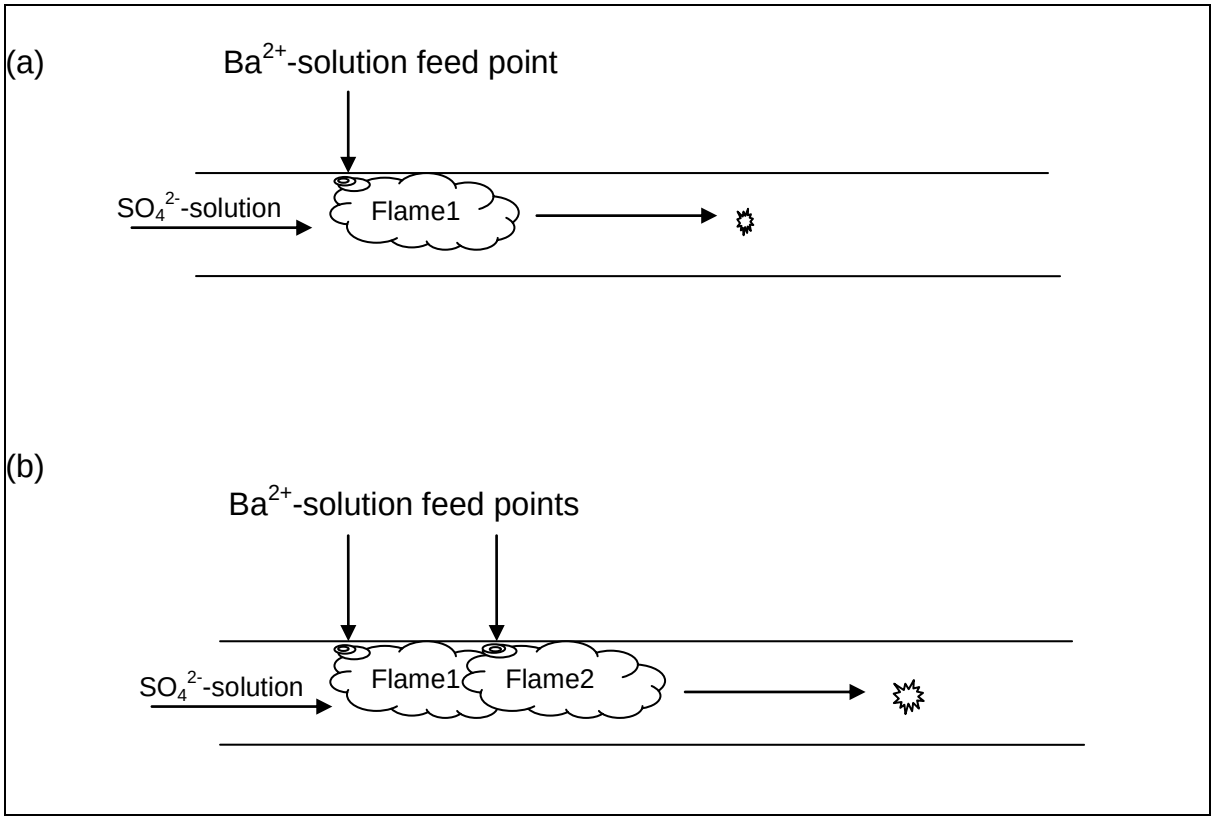

Figure 3.20. An illustration of the enhanced crystal growth due to overlapping nucleation flames from a double feed point system.

This effect, together with the lowered supersaturation, led to a further increase in the average growth rate relative to the average growth rate in Experimental Run 3. Figure 3.21 shows the further increase in the average growth rate as the number of feed points was increased.

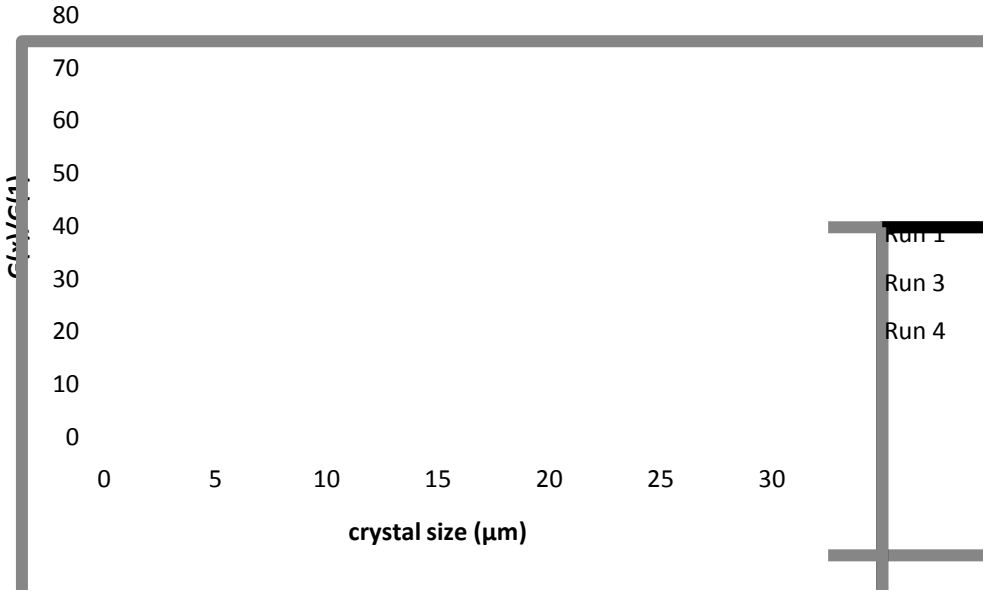

Figure 3.21. A graphical representation of the increased average growth rate due to an increased number of Ba^{2+} feed points and halved $Ba(NO_3)_2$ concentration (Experimental Run 4).

A comparison between Experimental Run 3 and Experimental Run 4 showed that a similar growth-rate trend was followed for these two experiments. In both cases the growth rate continued to increase within the 4 - 20 micron crystal size interval, followed by a decline in average growth rate for crystal sizes above 20 microns. The difference in the average growth rate between Experimental Run 3 and Experimental Run 4 was the additional increase in growth rate due to improved mixing in the precipitator tube.

Figure 3.22 revealed a decreased number of particles formed during precipitation in Experimental Run 4 compared to Experimental Run 3. The flattening of the curve in the graph of the number of particles that formed vs time, indicated a decrease in both the nucleation and the particle growth as the supersaturation around the feed points decreased and the particle size reached a certain limit.

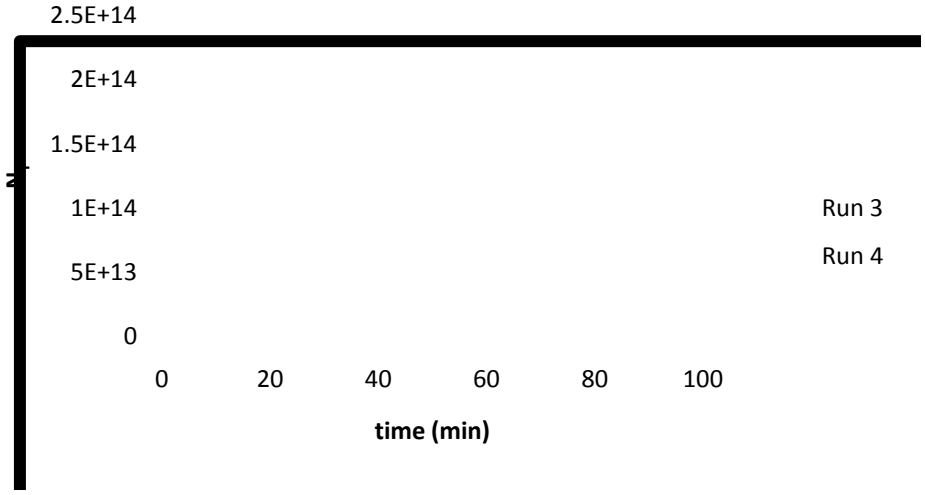

Figure 3.22. A graphical comparison between the number of particles formed in Experimental Run 3 (1 feed point) and the number of particles formed in Experimental Run 4 (2 feed points).

3.2.5 The effect of a further lowered Ba-concentration, employing two feed points, on the crystal growth rate

A reduction of the $Ba(NO_3)_2$ concentration to 5.5% of the $Ba(NO_3)_2$ concentration in Experimental Run 1, while the feed point number was maintained at 2 (Experimental Run 5), showed a more pronounced influence on the average growth rate. In this experiment the supersaturation ratio around the feed points was reduced by a factor of approximately 18 and the precipitation period was further increased, compared to that of Experimental Run 4. The effect of the change in these two parameters led to slow nucleation, which resulted in the formation of larger particles with time. The drastic drop in average growth-rate for Experimental Run 5 (Figure 3.23) indicates the rapid depletion in Ba^{2+} ions as the reaction approached completion.

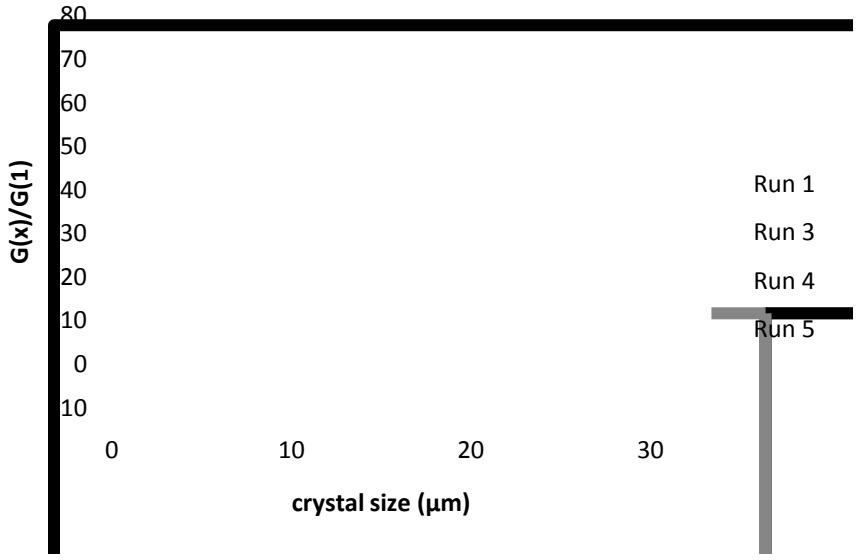

Figure 3.23. A comparison between the number of particles formed in Experimental Run 3 (one feed point) and the number of particles formed in Experimental Run 4 (two feed points).

Associated with the drop in nucleation rate was the lower number of total particles formed in Experimental Run 5 when compared to the total number of particles formed in Experimental Run 4, as shown in Figure 3.24.

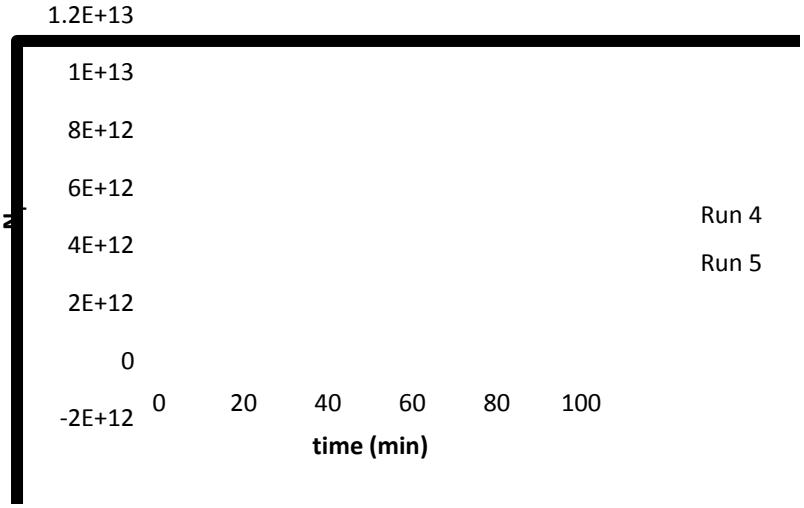

Figure 3.24 A graphical comparison of the total number of particles formed in Experimental Run 4 with the total number of particles that formed in Experimental Run 5.

3.2.6 The effect of an increased Reynolds Number (Re(-)) *on the average growth rate*

In Experimental Run 6, the $Ba(NO_3)_2$ concentration and the number of feed points were retained as in Experimental Run 5, and by adjusting the speed of the stirrer, the Re(-) was increased from 3098 to 3810. The adjustment of the Re(-) to a higher value was accompanied by a further increase in the average growth rate as shown in Figure 3.25. The supersaturation around the feed points remained the same as in Experimental Run 5. The increased Re(-) led to increased turbulence which, in turn, resulted in improved mixing in the precipitator tube. Improved mixing due to increased turbulence increases the chance of interaction between nuclei and results in the formation of larger crystals, as nucleation is slowed by the low supersaturation ratio.

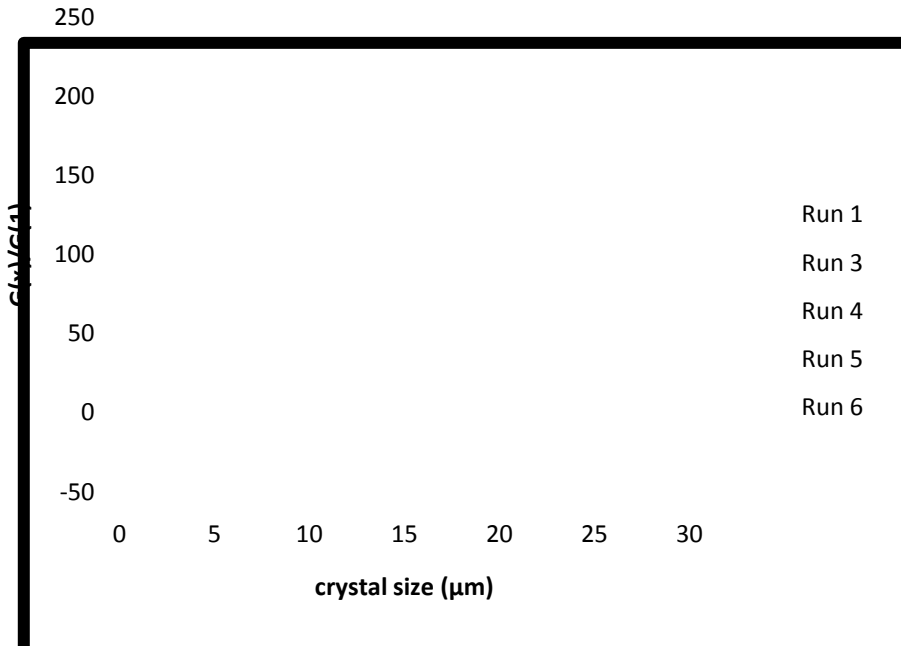

Figure 3.25. A graphical representation of an increased average growth due to improved turbulence in the reactor tube when Re(-) was increased from 3098 to 3810 (Experimental Run 6).

A further decrease in the number of particles was observed for Experimental Run 6 when compared to Experimental Run 5 as shown in Figure 3.26.

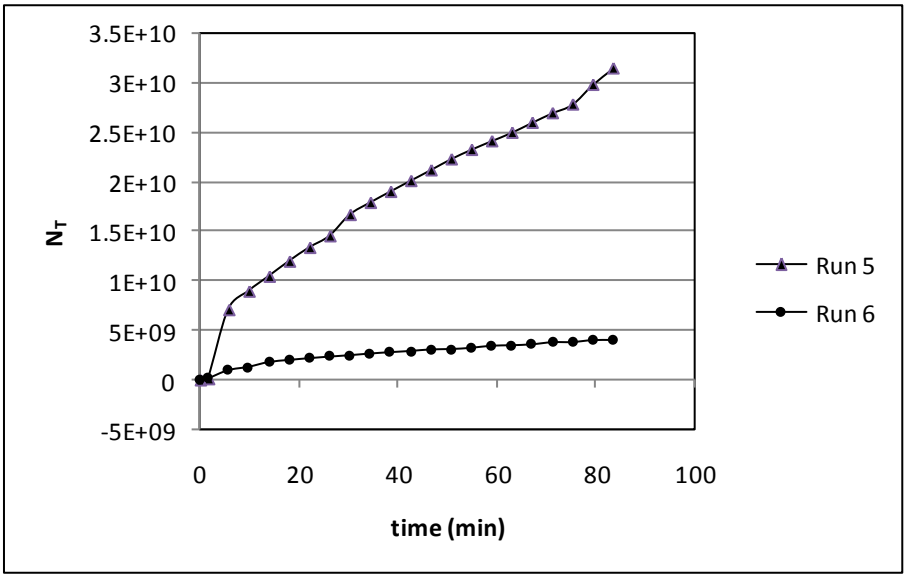

Figure 3.26. A graphical comparison between the number of particles formed in Experimental Run 5 and the number of particles formed in Experimental Run 6.

3.2.7 The effect of a further increase in the Re(-) *on the average growth rate*

A further adjustment of the Re(-) to 4642 (in Experimental Run 7) reduced the average growth rate significantly. In this experiment the growth rate seemed to increase within the 4 - 9 microns crystal size interval, beyond which it started to decrease until it reached zero (see Figure 3.27). This was explained in terms of the breakage of larger crystals due to attrition, as a result of the high stirrer speed.

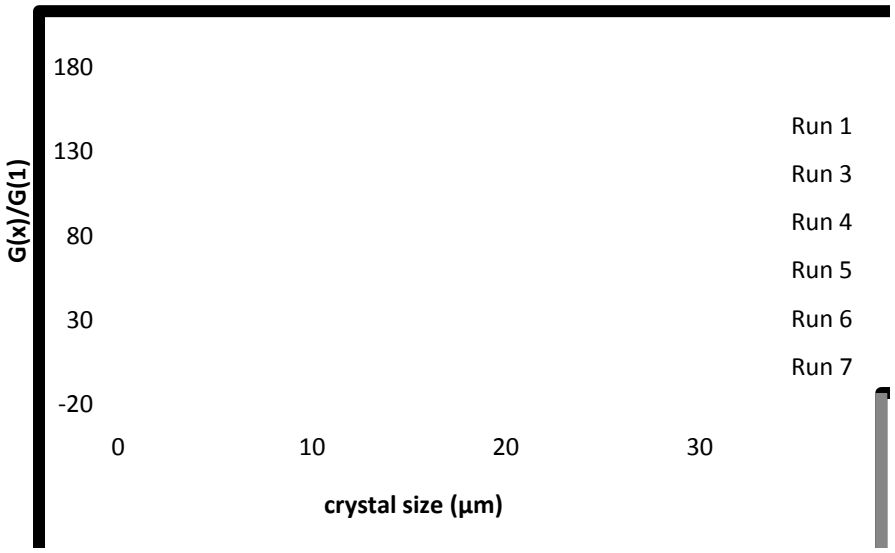

Figure 3.27. A graphical representation showing a decline in average growth-rate due to attrition when Re(-) was increased to 4642 from 3810, (Fig. 3.25).

As can be seen in Figure 3.28, the CSD of this run at any time resembled that of the seed (Figure 3.8), with two maxima at 0.7 and 4.1 micronsand, not showing any significant shift to larger particle sizes, but increased number of particles.

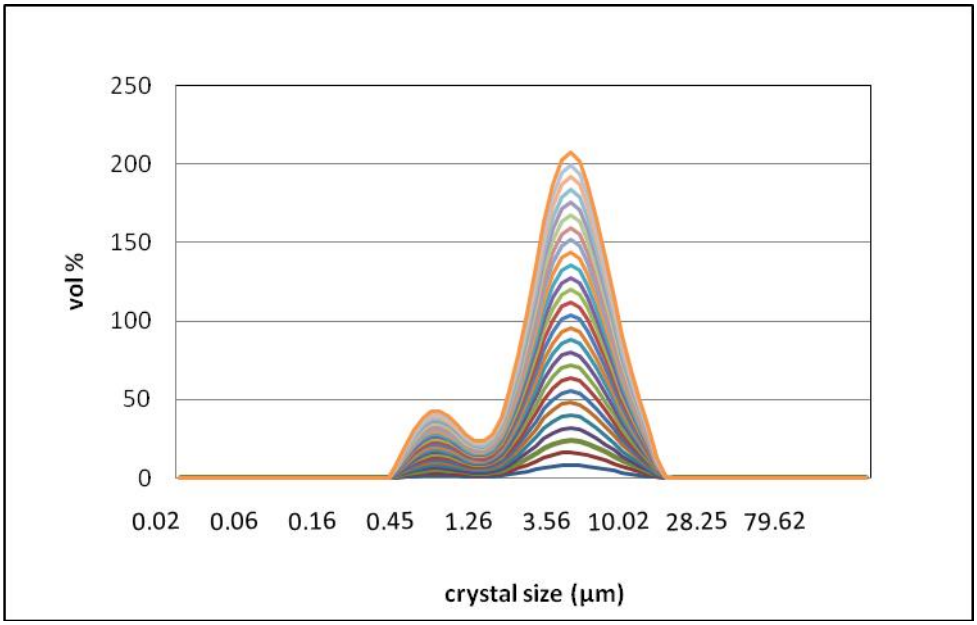

Figure 3.28. The CSD pattern obtained when Re(-) was further increased to 4642 (Experimental Run 7), showing a stunted growth of particles in the system.

The number of particles that formed in Experimental Run 7 was higher than the number of particles that formed in Experimental Runs 5 and 6, as seen in Figure 3.29. This was because, in addition to primary nucleation, there was a fourth nucleation type resulting from the breakage of larger particles to smaller ones in Experimental Run 7.

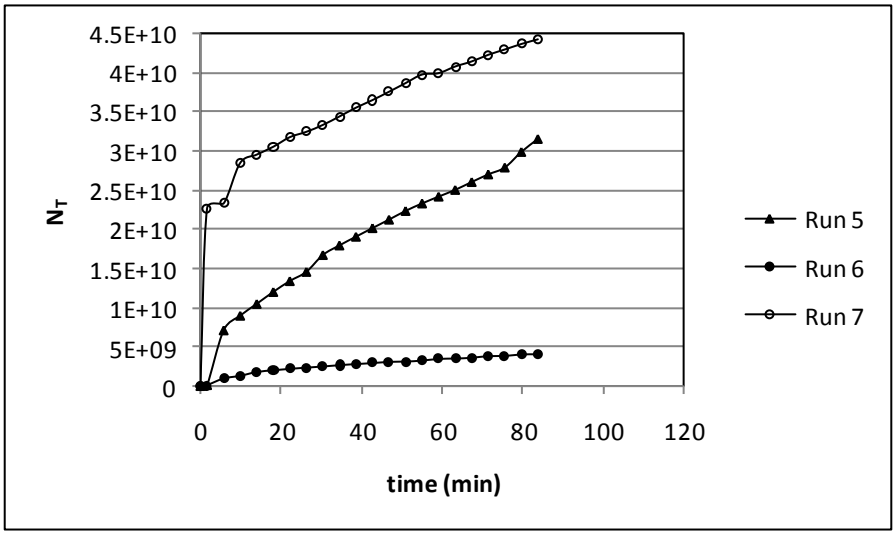

Figure 3.29. Ian increased number of particles that formed in Experimental Run 7 relative to Experimental Runs 5 and 6, which is attributed to the breakage of larger particles due to the high Re(-).

3.3. Barium sulphate reduction studies using solid carbon as reducing agent.

The results from these studies are presented as graphs of the BaS % yield vs Time or BaS % yield vs Temperature. In all the experiments the calculation of the BaS % yield was done according to the calculation procedure used by Maree et al. (2004).

3.3.1 *The effect of temperature on the yield of BaS in the tube furnace*

These studies have shown that the optimum temperature range for the reduction of $BaSO_4$ (5.00 mg), with activated carbon ($C/BaSO_4$ = 3), for a 1:1 $CaCO_3$-$BaSO_4$ mixture ratio is 900 to 1050^0C. The reduction of this mixture at 800 ^{0}C was insignificant after 20 minutes, hence was considered to be zero. Figure 3.30 shows the BaS yield trend as a function of temperature (800 - 1050 ^{0}C) in the tube furnace.

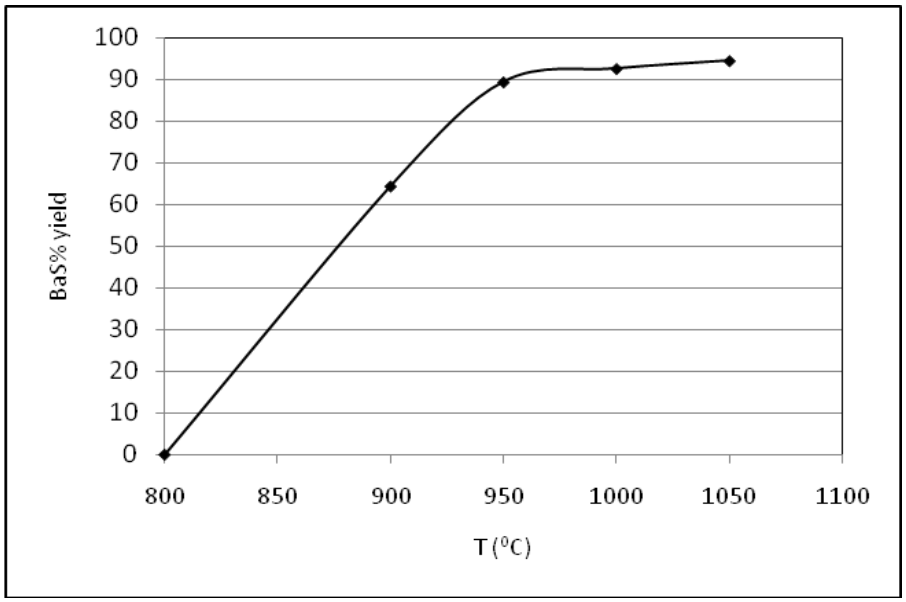

Figure 3.30. A graphical representation of the BaS% yield, from the reduction of $BaSO_4$ with activated carbon, in the tube furnace, under different temperatures.

Similar results were obtained by *Maree et al. (2004)* when reduction of $BaSO_4$ was carried out under the same conditions. A closer look at the curve of the BaS % yield showed that the effect of change in temperature was insignificant between 950 - 1050^0C. This observation suggested that this reaction has a temperature limit, above which the rise in temperature has no effect on the yield.

3.3.2 *The effect of the $CaCO_3/BaSO_4$ ratio on the BaS % yield*

From Figure 3.31 it was clear that the BaS % yield was lowered by about 10% (from 95 to 85%) when the $CaCO_3/BaSO_4$ ratio was increased to 1 under the same temperature conditions.

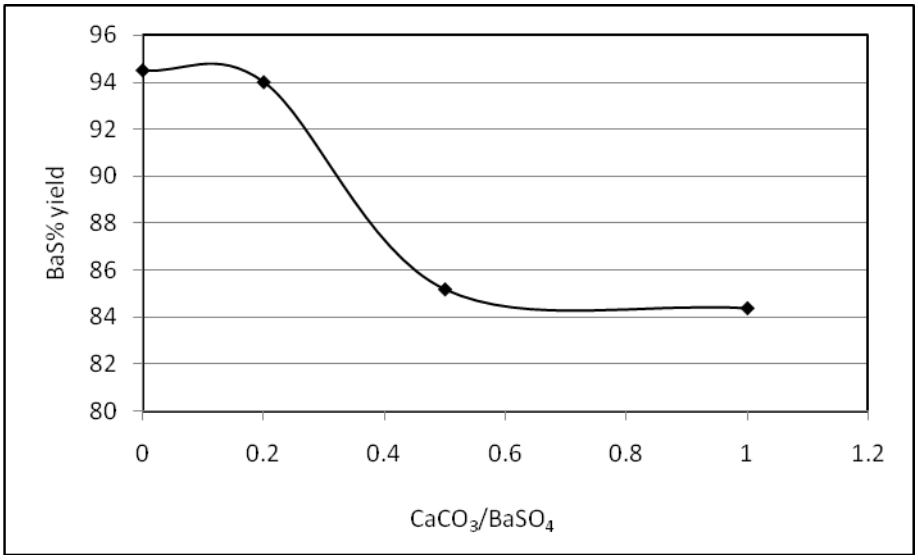

Figure 3.31 A graph of the BaS% yield from the reduction of different $CaCO_3/BaSO_4$ mixtures ratios.

At this stage it makes sense to mention that the presence of $CaCO_3$ in the reaction mixture has a limited influence on the reduction of $BaSO_4$ to BaS, with activated carbon in a tube furnace.

The XRD analysis of the product obtained from the reduction of an equimolar $BaSO_4$ + $CaCO_3$ mixture.

The product obtained from the reduction of an equimolar mixture of $BaSO_4$ and $CaCO_3$ at 1050 ^{0}C was analysed by an XRD method in order to establish the composition of the product. For reference purposes, the XRD analysis was also done on the product from the reduction of the pure $BaSO_4$ sample at 1050 ^{0}C.

Qualitative results

The XRD results for the reduction of the mixture, as shown by the XRD scan in Figure 3.32, indicated the presence of BaS, $BaSO_4$, CaO and CaS, all in significant percentages. The presence of CaO in the product mixture was ascribed to the thermal decomposition of $CaCO_3$ according to reaction equation (77).

$$CaCO_3 \longrightarrow CaO + CO_2 \qquad (77)$$

The reaction mechanism for the formation of CaS is not clear at this stage, however the presence of this compound in the product mixture contributes to the total sulphide content, as it is also soluble in water. The formation of CaS, when $BaSO_4$ is reduced to BaS in the presence of $CaCO_3$, is therefore an added advantage of the integrated barium carbonate process.

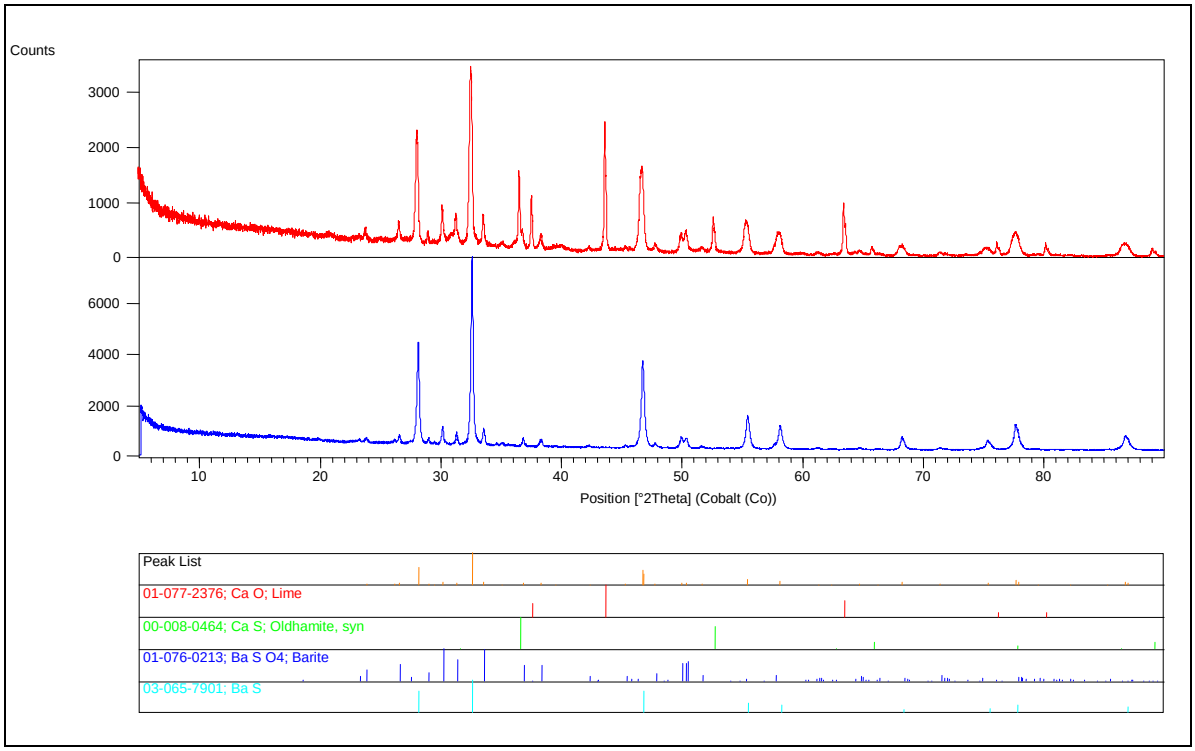

Figure 3.32. The XRD spectra of the product obtained from the reduction of the equimolar $CaCO_3$-$BaSO_4$ mixture (red) and the product obtained from the reduction of pure $BaSO_4$ (blue) in the tube furnace.

Quantitative results

Table 3.1 shows the relative mass percentages of the different compounds present in the two products. These results showed that while BaS is the only solid product from the reduction of pure $BaSO_4$, BaS, CaO and CaS are produced when the $BaSO_4$ + $CaSO_4$ mixture was thermally reduced, with activated carbon, in the tube furnace.

Table 3.1. The relative mass percentages of different compounds in the products from the thermal reduction of the equimolar $CaCO_3$ + /$BaSO_4$ mixture and pure $BaSO_4$, in the tube furnace.

$BaSO_4$+$CaCO_3$	**%**	**pure $BaSO_4$**	**%**
BaS	37.9	BaS	97.8
$BaSO_4$	18.6	$BaSO_4$	2.2
CaO	31.3	CaO	0
CaS	12.2	CaS	0

The results in Table 3.1 suggest that only about 38% of the total mass of the product mixture was BaS. However, the stoichiometric %BaS yield, from the initial amount of $BaSO_4$ which was present in the reaction mixture prior to the reduction, is in fact 48% and not 85% as suggested by the iodine method, in Figure 3.31. This led to the conclusion that the %BaS yield was only lowered by 10% when $BaSO_4$ was reduced in the presence of $CaCO_3$. This was because the iodine method cannot discriminate between sulphide content due to BaS and sulphide due to CaS, but takes into account the total sulphide concentration present in the product mixture. These results showed that while it was previously suggested by Hlabela *et al*., (2007) that the reduction of $BaSO_4$ to BaS in the presence of activated carbon is not significantly influenced by the presence of $CaCO_3$ in the reaction mixture, this is not necessarily true. According to the XRD analysis results, the presence of $CaCO_3$ in $BaSO_4$, in a 1:1 molar ratio, lowers the %BaS yield by about 50%.

3.3.3 *The effect of reaction time on the yield of BaS, obtained in the tube furnace*

Figure 3.33 shows the percentage yields of BaS for different reaction periods, at 1050^0C, in both tube and muffle furnaces.

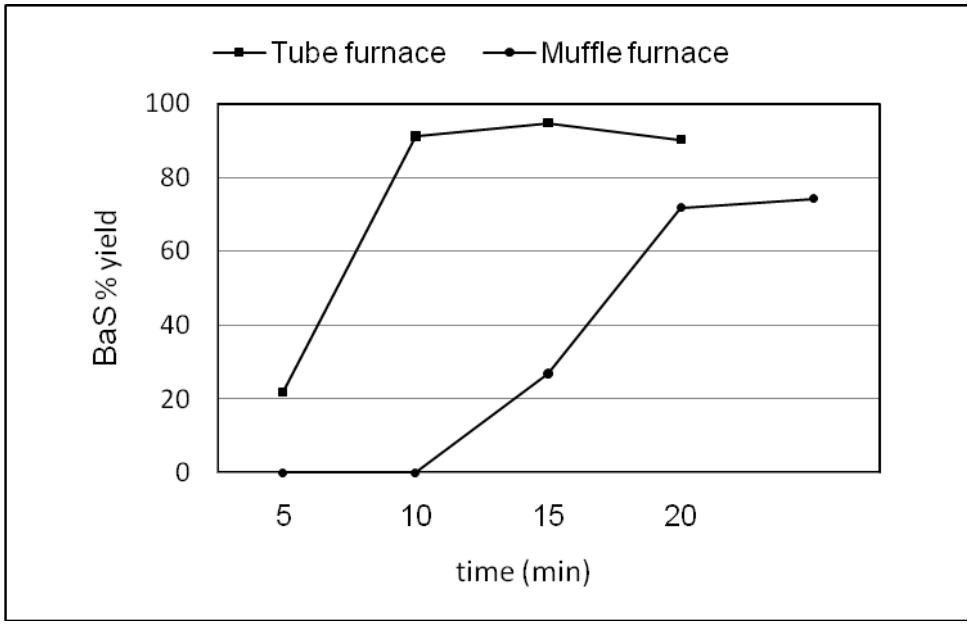

Figure 3.33. The graphical representations of the % BaS yields for different reaction periods in the tube and muffle furnaces, respectively, at 1050^0C.

As indicated in Figure 3.33, the maximum BaS yield, in the tube furnace was obtained when the reaction was allowed to take place for 15 minutes. A decline in BaS yield was observed when the reaction was allowed to take place over longer periods. This decline in the % BaS yield was attributable to either formation of a new barium compound or a reverse reaction i.e. re-oxidation of the BaS. Owing to time constraints, this aspect of the reaction was not explored further and 15 minutes was taken to be the optimum reaction period for the reduction in the tube furnace at 1050^0C.

3.3.4 The effect of reaction time in the muffle furnace

The reduction of $BaSO_4$ in the muffle furnace was slower when compared to that in the tube furnace (Figure 3.33). There was no detectable reduction when the reaction was left to take place for 10 or 20 minutes in the muffle furnace. It was only when the reaction was allowed to take place for 60 minutes that a significant reduction, with 72% BaS yield, was obtained in the muffle furnace.

These results have revealed preliminary information about the molecular interaction between the reducing agent and the $BaSO_4$. Previous researchers (NIPOHIM, 1979;

Pelovski & Taniguchi, 1988) showed that, during the reduction of $BaSO_4$ using a solid carbon reducing agent, the reducing agent is initially gasified to CO, which then interacts with the $BaSO_4$ as shown by reaction equation (70) in Chapter 1. It was also mentioned in Chapter 1 that several reactions (67- 69) are involved in this reduction and these can be influenced by the oxygen partial pressure, thus affecting the overall kinetics of the $BaSO_4$ reduction with solid carbon (Pelovski & Taniguchi, 1988).

A high oxygen partial pressure in the system will inhibit the formation of CO by pushing the reaction equilibrium in reaction (67) to the left, resulting in the formation of CO_2. The oxidation of the solid carbon (reverse of reaction 68) leads to the formation of CO_2 at elevated temperatures and depletes the solid carbon present in the system. Pelovski & Taniguchi, (1988) demonstrated, by using TGA experiments, that the constant removal of oxygen from the system leads to improved kinetics of the $BaSO_4$ reduction with solid carbon.

In the current studies the smaller volume in the tube furnace, compared to the muffle furnace volume and the controlled N_2 purging minimized the oxygen partial pressure in the system. The result is that the forward reactions in the reactions 68 and 69 are favoured and the residual O_2 in the system is replaced by the CO_2 from reaction 67. The efficient gasification of the solid carbon to CO resulted in a constant availability of CO to react with the $BaSO_4$. This was enhanced by the large surface area interaction between the CO and $BaSO_4$ due to the sample occupying the largest part of the total volume of the tube reactor.

In contrast, the larger volume and the poorly controlled N_2 purging system in the muffle furnace led to a poor reduction of $BaSO_4$. In order to verify the effect of the surface area/mass ratio, Experiment 2(e was carried out.), in which different sample masses were used.

3.3.5 *The effect of sample mass on the yield of BaS in the muffle furnace*

The results, as shown in Figure 3.34, indicated that the reduction yield increased with the mass of the sample, when different masses of $BaSO_4$ were subjected to reduction in the muffle furnace for 20 minutes.

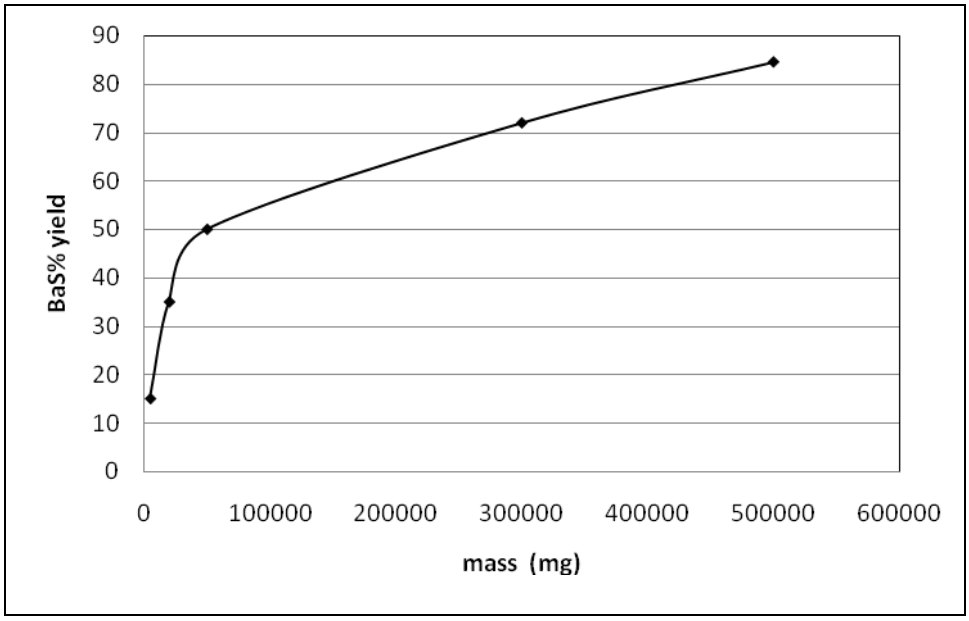

Figure 3.34. A graphical representation of the increase in BaS% yield, with increased sample mass, in the muffle furnace.

These results demonstrated that a larger sample mass, which means a larger surface area, allows an effective interaction between the $BaSO_4$ particles and the CO, resulting in a better BaS% yield, as was suggested in Sub-section 3.3.4. This deduction suggested that, in designing an effective furnace for the reduction of $BaSO_4$, the sample-volume : sample-mass ratio and the control of the oxygen partial pressure are important factors.

3.4. TGA studies on the reduction of $BaSO_4$ using gaseous reducing agent.

An example of the raw data that was obtained from TGA in the conversion of $BaSO_4$ to BaS, at a final temperature of 850^{o}C, in a 4.8% CO in N_2 mixture, is given in Figure 3.35.

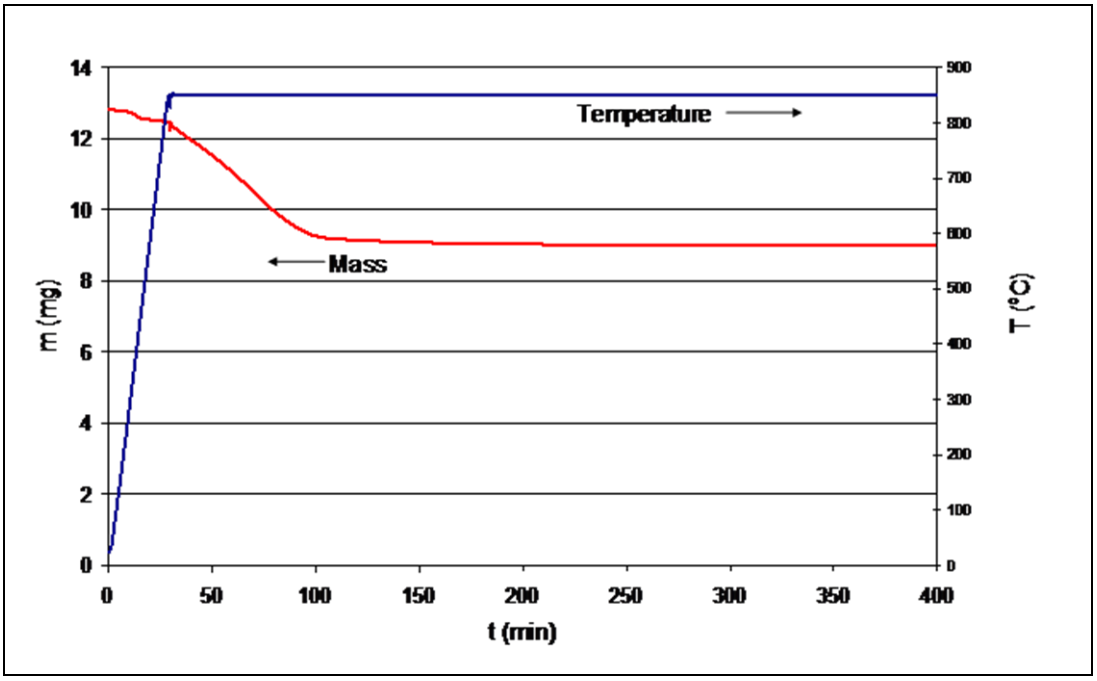

Figure 3.35. A graphical representation, showing the reduction of $BaSO_4$ with CO, in a 4.8% CO/N_2 mixture at 850^{o}C.

Initially the gas atmosphere consisted of N_2 only, and the temperature was raised linearly to the desired temperature, 850^{o}C. During heating, the mass of the sample decreased slightly, possibly due to the release of moisture and other impurities. As the temperature reached a constant value, the gas supply was changed to a 4.8%CO in N_2 mixture. The change of gas caused an abrupt but small change in both mass and temperature, seen in Figure 3.35. Since the mass of the $BaSO_4$ sample was not exactly constant and some mass loss was observed during heating, a comparison between different experiments was done, by comparing the relative mass (m/m_0), where m_0 was taken at the time of the change in gas atmosphere. A comparison of three experiments, all carried out at 950^{o}C is given in Figure 3.36.

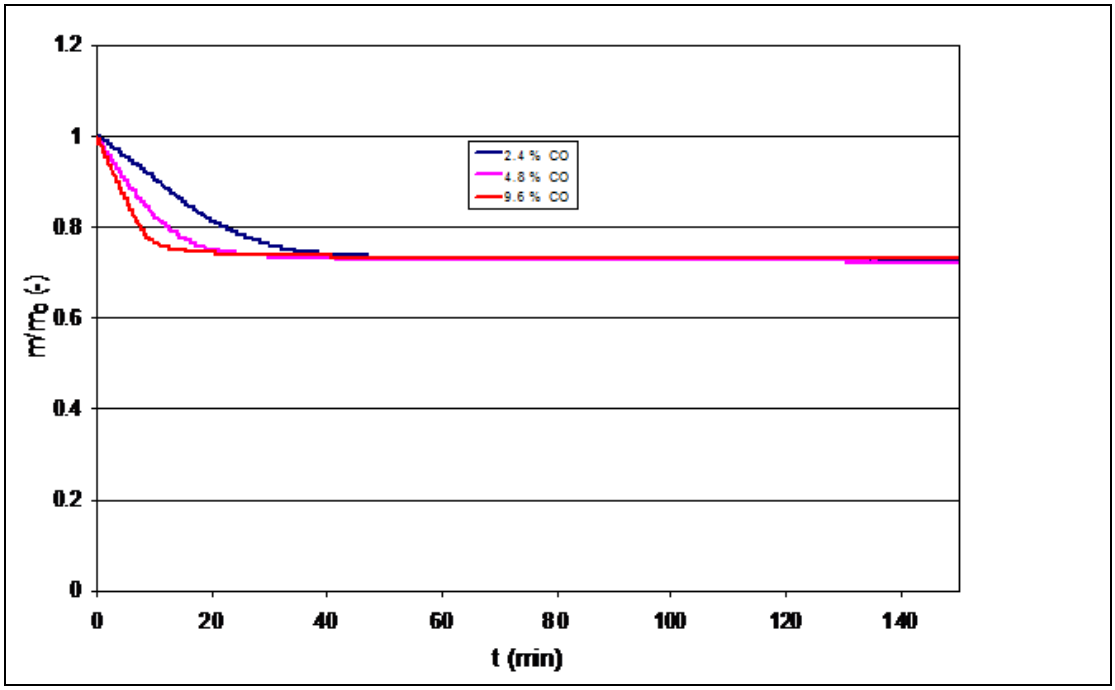

Figure 3.36. A graphical representation, showing the reduction of $BaSO_4$ with CO at 950^0C, for different fractions of CO.

From Figure 3.36, it was seen that the mass loss, and hence the reaction rate, increased with the CO partial pressure. It was also observed that the equilibrium m/m_0 values converged, and a final m/m_0 value, termed q, of 0.730, 0.719 and 0.722 were obtained for the 9.6, 4.8 and 2.4% CO experiments, respectively. These values were in good agreement with the theoretical value of 0.726, which is the ratio of the molecular masses of BaS and $BaSO_4$. Various values of q are given in Table 3.2.

Table 3.2. Observed q-values for all isothermal experiments

Xco	**9.6%**	**4.8%**	**2.4%**
T(^{0}C)			
850	0.749	0.757	0.716
900	0.729	0.702	0.693
950	0.730	0.719	0.722
1000	0.712	0.719	0.684

From Table 3.2, it was concluded that the experiments were all carried out between a final q value of 0.72 (± 0.04). The differences in the observed q values were mainly ascribed to the noise that was introduced by the switching of the gases. To overcome this, and to specifically look at the conversion of $BaSO_4$, X was defined for each experiment as:

$$X = \frac{m_o - m_t}{m_o - m_f} \qquad (78)$$

The values of the conversions as functions of time and temperature are given in Figure 3.37(a), 3.37(b) and 3.37(c) for 2.4, 4.8 and 9.6% CO reducing agent, respectively.

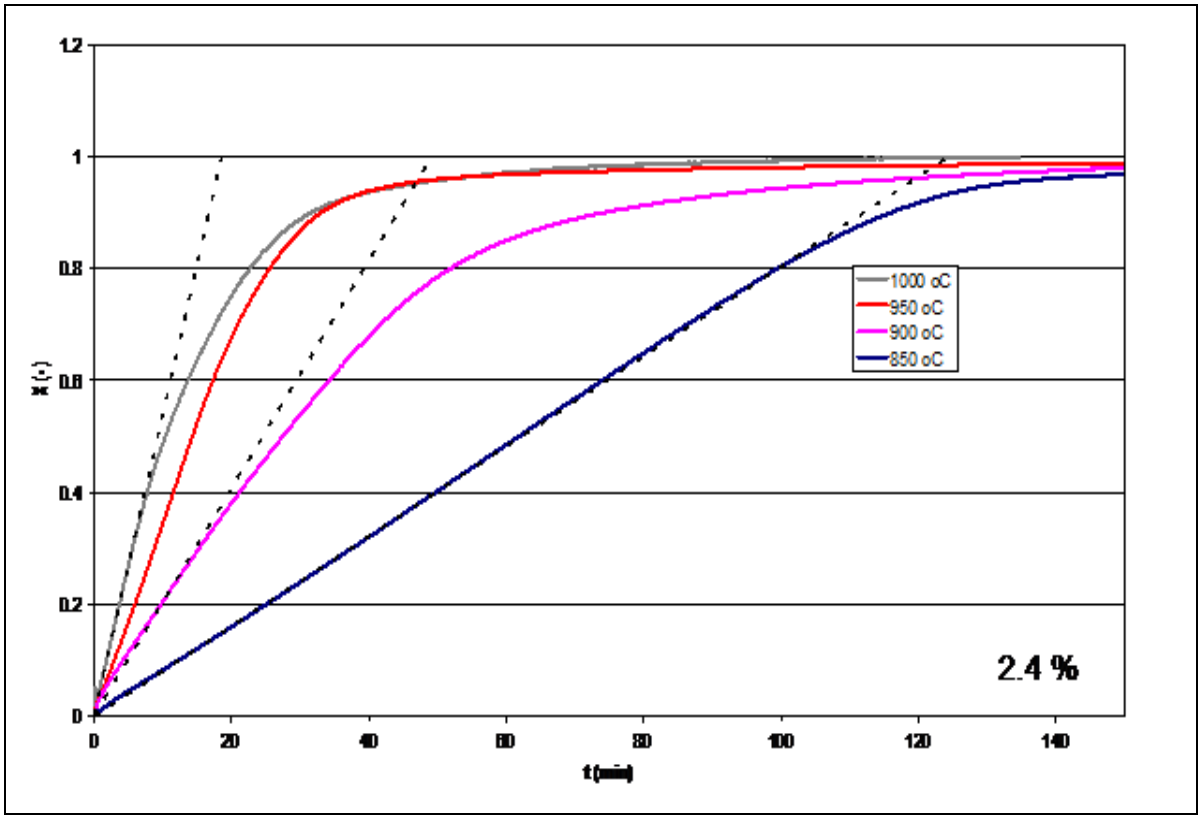

Figure 3.37(a). A graphical representation of the reduction of $BaSO_4$ with 2.4% CO as a function of time and temperature.

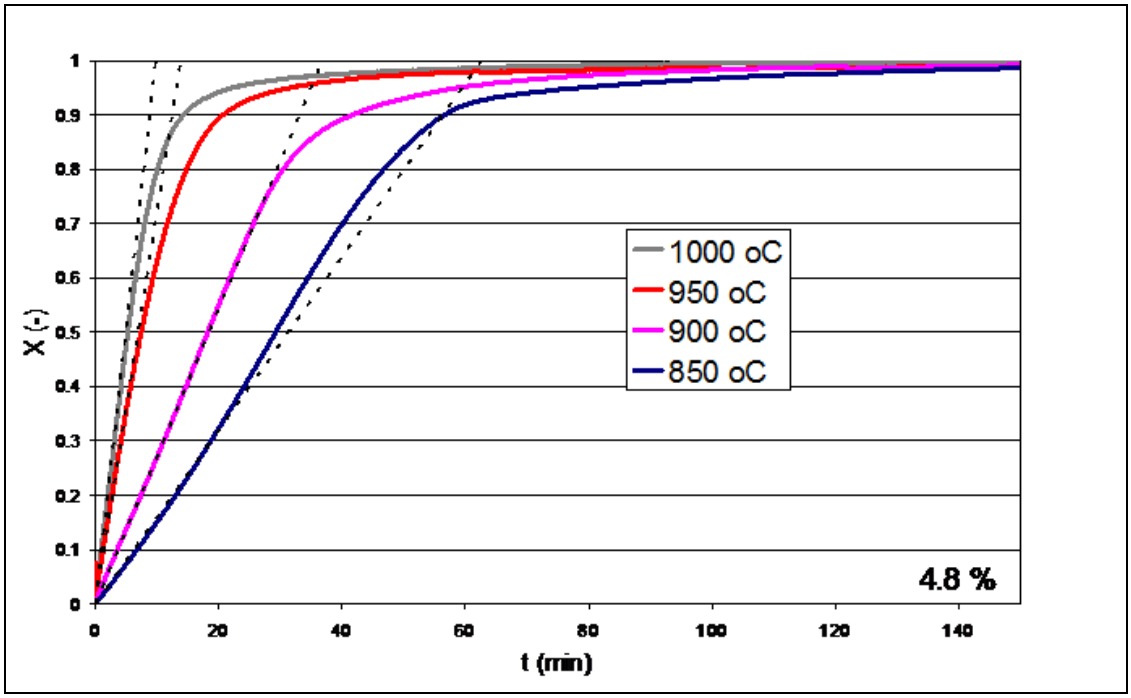

Figure 3.37(b). A graphical representation of the reduction of $BaSO_4$ with 4.8% CO as a function of time and temperature.

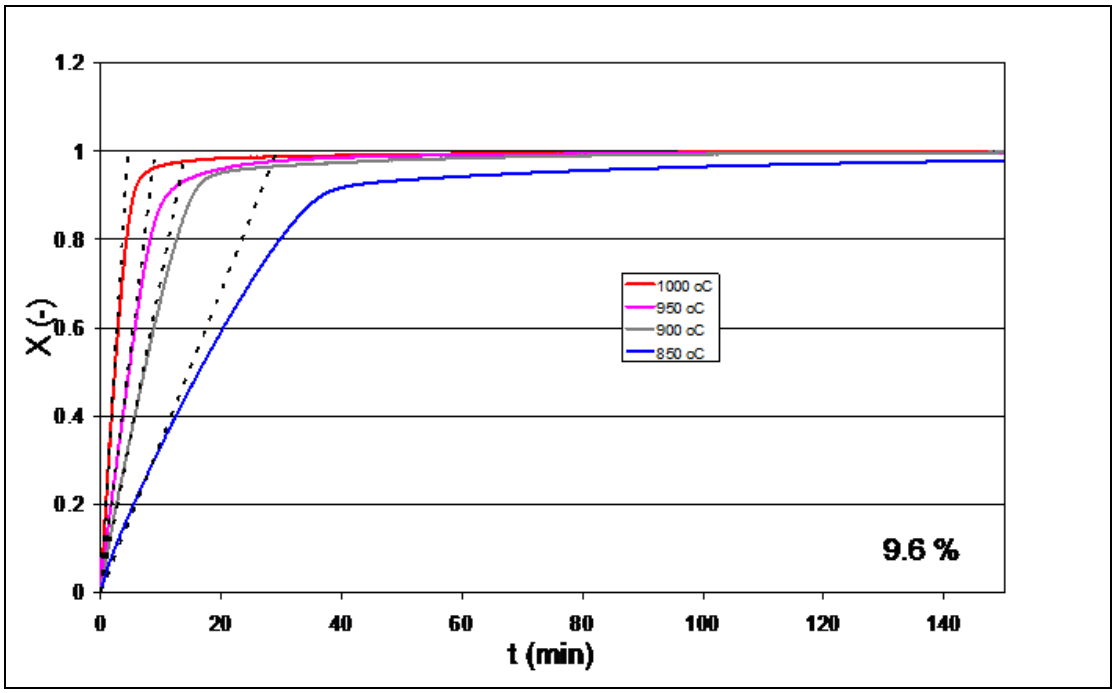

Figure 3.37(c). A graphical representation of the reduction of $BaSO_4$ with 9.6% CO as a function of time and temperature.

From the three figures (above), the conversion-rate increased with temperature, and by comparing the three figures, it was again concluded that the conversion-rate increased with the CO partial pressure. It was also concluded that the conversion increased initially linearly, and subsequently flattened abruptly at higher conversion, especially when high reaction rates were observed. As a measure of the reactivity, the initial slope was used, and the dotted curves are fitted lines, representing the initial reaction rate (r_0). They are given for all experiments in Table 3.3.

Table 3.3. Determined r_0 values (s^{-1}) for all isothermal experiments

P_{CO} (Pa)	**8400**	**4200**	**2100**
T (^{0}C)			
850	0.000568	0.000266	0.000134
900	0.001184	0.000453	0.000339
950	0.001841	0.001204	0.000562
1000	0.003690	0.001701	0.000896

3.41. Proposed reaction kinetic equation.

The proposed reaction kinetic equation was based on the Arrhenius Equation, which accounts for the effect of temperature, in combination with a power rate-law, which accounts for the effect of the partial pressure of CO, according to:

$$r_0 = k_0 e^{\left(\frac{-E_{act}}{RT}\right)} P_{CO}^{m} \qquad (79)$$

The activation energy was found by plotting ln(r_0) as a function of (1/T) for the different CO fractions and given in Figure 3.38

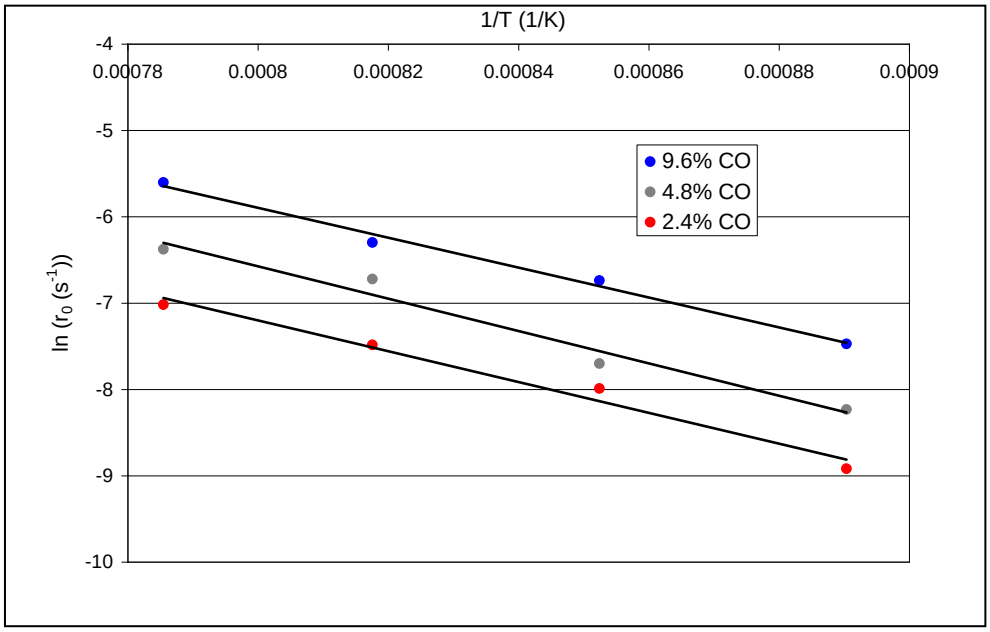

Figure 3.38. Arrhenius plot of the reduction of $BaSO_4$, for different CO fractions.

From the slopes of the plots in Figure 3.38, activation energies of 148, 156 and 144 kJ/mol were obtained for the 2.4, 4.8 and 9.6 %CO values, respectively. From these values an activation energy of 149 (±10) kJ/mol was determined**.** To obtain the kinetic dependency of the partial pressure of CO (m), a plot of $\ln(r_0)$ as a function of $\ln(P_{CO})$ was drawn for different temperatures. The results are given in Figure 3.39:

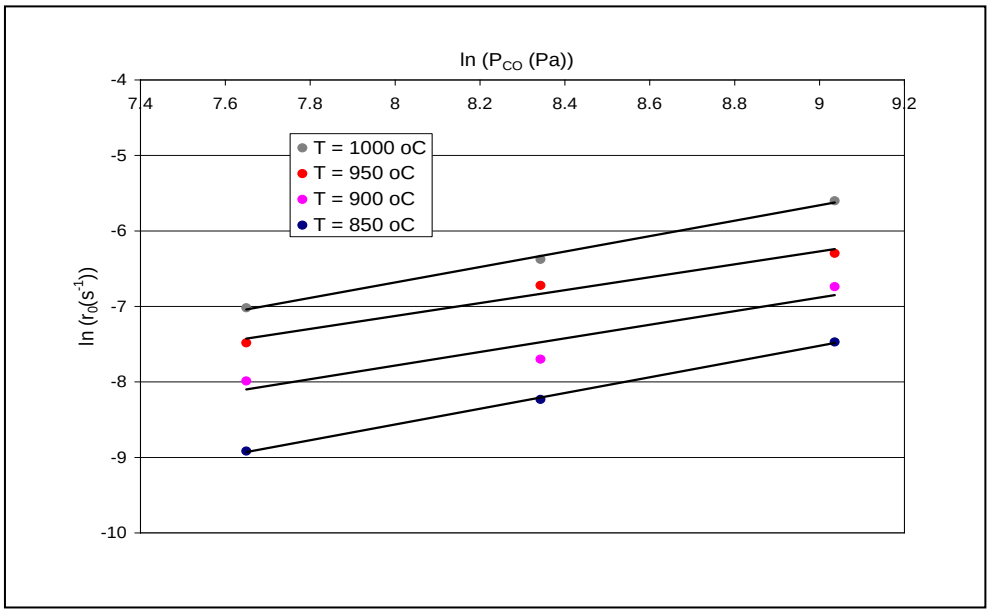

Figure 3.39 The graphs of $\ln(r_0)$ as a function of $\ln(P_{CO})$, for different temperatures.

From the slopes of the graphs in Figure 3.39, the values of m were obtained directly and found to be 0.99, 0.90, 0.86 and 1.02 for 850, 900, 950 and 1000 ^{o}C respectively. From these values, an average value of 0.94 (± 0.12) was obtained, which suggested that the reduction of $BaSO_4$ with CO is a first order reaction in CO. A value for k_0 was regressed, based on the proposed values of E_{act} and m and was found to be 0.57 (±0.10). All errors were obtained from a 95% confidentiality interval. The overall rate equation for the reduction of $BaSO_4$ with CO in the temperature range of 850 – 1000 ^{o}C, 2.4 – 9.6% CO, is given as:

$$r_0 = 0.57 \cdot e^{\frac{-149000}{RT}} \cdot P_{CO} \qquad (80)$$

The experimental r_0 data (Table 3.3) were compared with the modelled data as calculated using the proposed rate-equation, above. A parity plot was used as given in Figure 3.40.

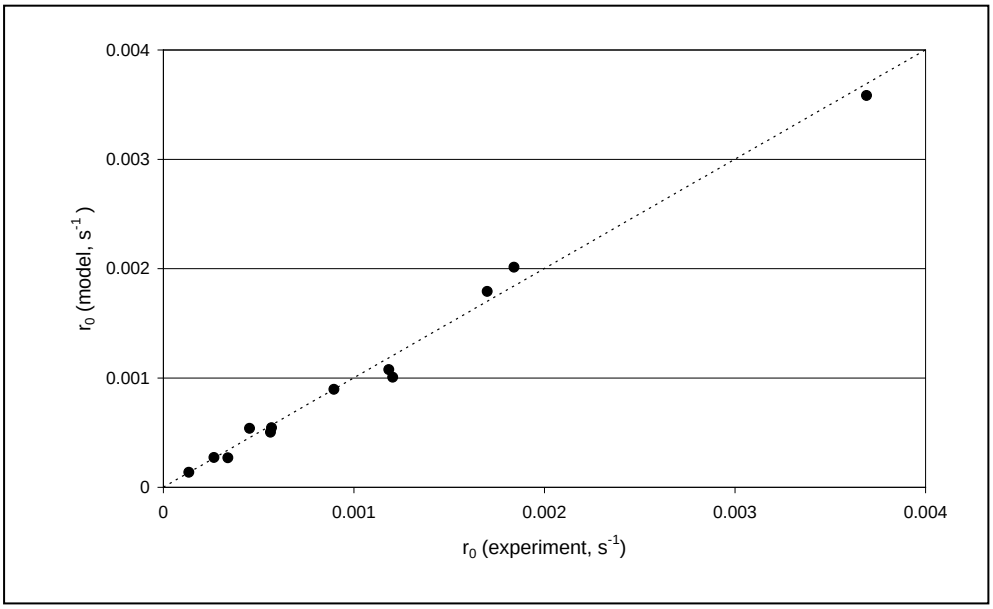

Figure 3.40. The graph of parity of the experimental and the modelled data.

From Figure 3.40 it can be seen that the proposed rate equation gave an accurate quantification of the initial reaction rate.

3.5. H_2S stripping confirmation studies.

The success of the H_2S stripping during a batch study was indicated by the reduction in the sulphide concentration in solution, as the reaction progressed. Figure 3.41 depicts a graphical representation of the preliminary results, showing a decrease in the sulphide concentration. The initial sulphide concentration (as BaS) in the stripping vessel was 330 mmol/L. From this graph, 77% sulphide (330 – 75 mmol/L) was stripped from the BaS solution in 90 min, when excess CO_2 was passed.

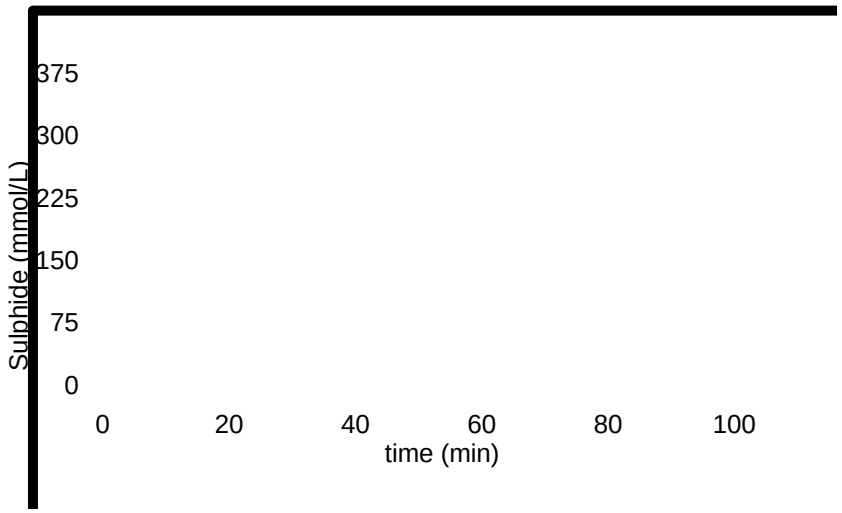

Figure 3.41. The graphical representation of the decrease in sulphide concentration, as a result of H_2S stripping from the BaS solution with CO_2, as a function of time.

Previous studies, where Na_2S was used as a source of sulphide, revealed that up to 95% sulphide stripping could be achieved (Maree *et al.,* 2004). The reason for the lower stripping efficiency (77%) in the current study was attributed to the instability of BaS in solution, being easily oxidized to $BaSO_4$ when exposed to air. The main limiting factor in the study carried out by Maree *et al.* (2004), was found to be the CO_2 flow-rate and the Na_2S concentration. Hence excess CO_2 was used in this study.

In the current research, a study to evaluate the relationship between the CO_2 flow-rate and the BaS concentration was undertaken. Initially, an excess CO_2 (molar load

ratio of CO_2/S^{2-} = 7.96) was fed into a BaS solution of a low concentration (75 mmol/L) at a flow-rate of 6.6 mmol/min over a period of 90 minutes. The results from this experiment yielded 80% H_2S stripping efficiency, as 60 mmol of the original 75 mmol sulphide was stripped from the BaS solution. A maximum H_2S stripping efficiency, from the BaS solution, indicated by the flattening of the stripped sulphide curve, is shown in Figure 3.42.

Even though efficient H_2S stripping was achieved, under these conditions, not all the stripped H_2S was absorbed into the zinc acetate solution, as shown by the curve of the sulphur that formed (Figure 3.42). The reason for this was that the residence time was too short to allow for complete absorption of H_2S into the zinc acetate, due to the high flow-rate of CO_2 through the system. Therefore, a disproportionality was found in mass balance between the sulphide stripped and the sulphur formed, as 60 mmol of sulphide was stripped whilst only 30 mmol of sulphur was formed, after 90 minutes.

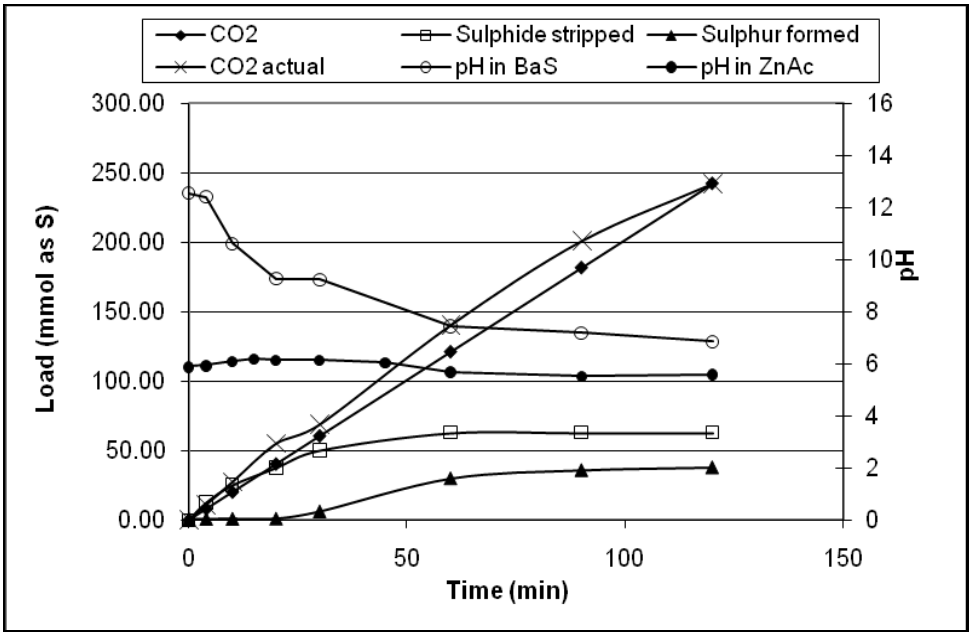

Figure 3.42. The graphical representation, showing the change in different parameters during H_2S stripping, from a BaS solution, for a molar load ratio of CO_2/S^{2-} = 7.96, as a function of time.

Figure 3.43 indicated that, when the CO_2 flow-rate was lowered from 6.6 - 2.3 mmol/min and the sulphide concentration was increased to 150 mmol/L, such that the CO_2/S^{2-} molar ratio was 2.8, the same H_2S stripping efficiency from the BaS solution was obtained, with improved H_2S absorption into the zinc acetate solution. The ratio H_2S-stripped/H_2S-absorbed = 1 after 45 minutes as indicated by the overlap between the curve of sulphide stripped and sulphur formed. However, excess CO_2 load was still needed to attain these results.

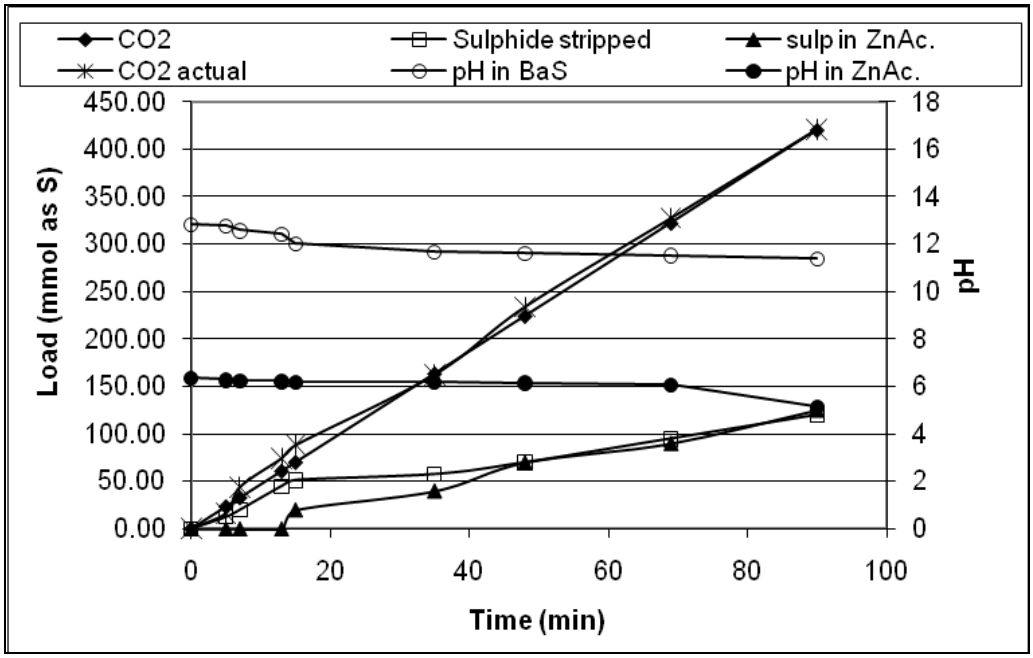

Figure 3.43. The graphical representation of the relationship between various parameters during H_2S stripping, for a molar ratio of CO_2/S^{-2} = 2.8, as functions of time.

The H_2S stripping efficiency remained virtually the same, when the CO_2 flow-rate was adjusted to 4.7 mmol/min and the initial BaS concentration increased to 325 mmol/L (CO_2/S^{2-} = 1.29). For these conditions, the actual CO_2 flow required for optimum sulphide stripping was equal to the theoretical/planned flow (Figure 3.44). These results suggested that BaS concentrations higher than the stoichiometric amounts were needed in order to ensure minimum CO_2 consumption while keeping the stripping efficiency at maximum levels.

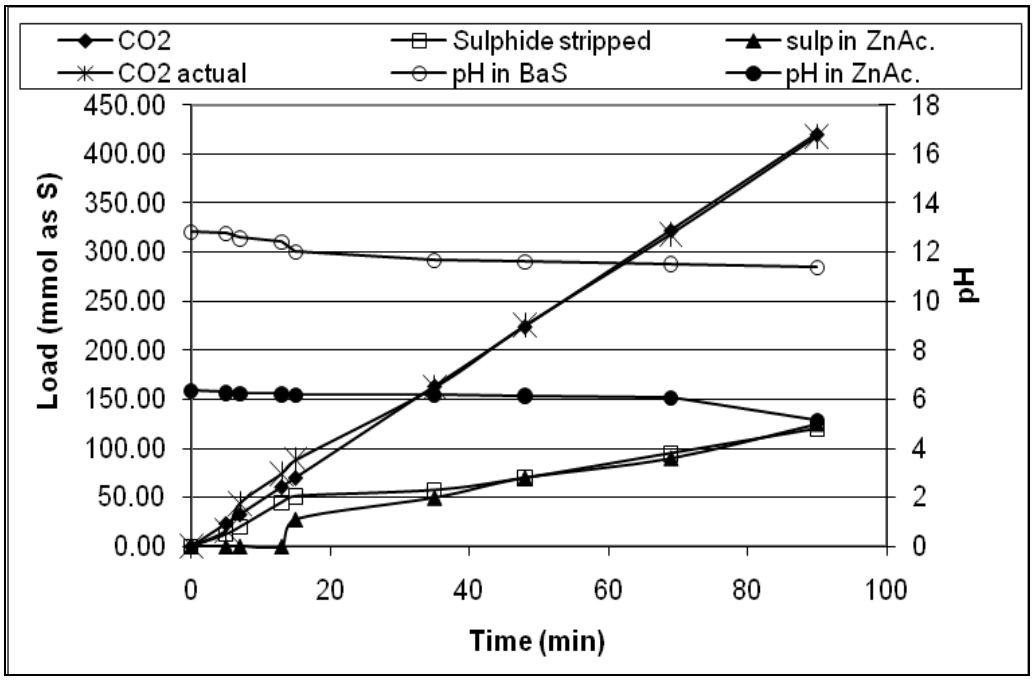

Figure 3.44. The graphical representation of the relationship between various parameters, during H_2S stripping, for CO_2/S^{2-} = 1.29, as functions of time.

The results also revealed the role of pH in dictating the mass balance of this process. A closer look at the relationship between the pH range and stripping efficiency showed that the molar ratio between CO_2 fed and sulphide stripped was almost equal to 1 only at a pH > 12. A drop in pH shifted the ratio to higher values i.e. $CO_2/H_2S \geq 2$, hence excess CO_2 was needed to produce the same amount of H_2S. This implied that H_2S stripping must be operated at pH > 12, with BaS concentrations higher than the stoichiometric amounts, to ensure minimum CO_2 consumption.

It was important that all the stripped H_2S be absorbed into the zinc acetate solution in preparation for sulphur production. Whilst all experiments have shown that there is, ultimately, efficient absorption of H_2S into a zinc acetate solution, no sulphide was detected in the zinc acetate solution at pH > 12, despite appreciable sulphide removal in the stripping reactor. The appearance of sulphide in the zinc acetate solution as the pH dropped to < 6, led to the conclusion that this was attributable to the formation of equilibrium complexes, as has been mentioned previously.

CHAPTER 4

CONCLUSIONS AND CLOSING REMARKS

Water treatment

In the present investigation, it was shown that a stoichiometric amount of sulphate can be removed from AMD by dosing the molar equivalent of barium carbonate. An increase in the sulphate removal rate, with an increase in the dosed barium carbonate concentration, indicated the dependence of the sulphate removal rate on the barium carbonate concentration.

The solubility of barium carbonate was shown to be one of the important factors that affect the efficiency of barium carbonate in removing sulphate from sulphate-rich water. Barium carbonate was found to be more effective in removing sulphate that is associated with the Ca^{2+} ion, as the presence of this ion enhances the solubility of barium carbonate in water due to the ion-exchange effect, which results in precipitation of calcium carbonate. In contrast, the effectiveness of barium carbonate in removing sulphate is affected when waste water with very high alkalinity (measured in mg/L $CaCO_3$) is treated with barium carbonate, as the high alkalinity decreases the barium carbonate solubility. Alkalinity levels ≥ 200 mg/L $CaCO_3$ were found to have a significant negative impact on the effectiveness of barium carbonate in removing sulphate.

The presence of magnesium in the treated water was found to not directly influence the effectiveness of barium carbonate in removing sulphate. It was the inability of Ba^{2+} -ion to remove the sulphate associated with the Mg^{2+} -ion that affected the stoichiometric removal of sulphate by barium carbonate, from sulphate-rich water. Therefore, sulphate can only be removed to the level equivalent to the magnesium concentrations in the water, provided the magnesium is associated with sulphate. If sulphate needs to be removed to a level below that of sulphate that is associated

with magnesium, then pre-treatment of the water with lime, for magnesium removal, was found to be necessary.

Controlled precipitation

Addition of coagulants to enhance the settling rate of the amorphous barium sulphate, during solids separation from treated water, can be avoided by controlling the precipitation process to yield particles with improved settling rates. The results have shown that precipitation of barium sulphate from the reaction between Ba^{2+} and SO_4^{2-} from treated water can be controlled by optimizing a number of parameters involved in the precipitation process. An in-line dosing system has elucidated important information on the precipitation of barium sulphate that can be used during the designing of a suitable precipitation reactor for the treatment of sulphate rich water with barium.

It was concluded from the current studies that, crystals within the size range 10 – 100 µm can be obtained by using an in-line dosing system. Particle growth occurs in all particle size ranges as was indicated by the shift of the CSD towards larger size ranges. The particle growth rate (G) was seen to be dependent on the size of the particles, with the growth rate being higher for a larger particle size range. New crystals were formed by secondary nucleation

The particle average growth-rate (G_{av}) can be enhanced by lowering the Ba^{2+}-concentration, which in turn lowers the super-saturation level of the solution thus discouraging nucleation. Increasing the number of feed points into the precipitator enhances crystal growth rate due to overlapping precipitation plumes which lead to rapid interaction between nuclei. This led to the conclusion that a multiple $Ba(NO_3)_2$ solution dosing system produces larger particles with improved settling properties when compared to a single $Ba(NO_3)_2$ solution dosing system. A multiple dosing system ensures that, while the $Ba(NO_3)_2$ solution concentration is lowered in favour of the average particle growth rate, as discussed,above, the sulphate removal rate is not negatively affected by ensuring that sufficient Ba^{2+} ions are still available for interaction with SO_4^{2-} ions in solution.

Mixing was found to play a very important role in controlling the precipitation of barium sulphate. Increased turbulence as a result of an increased Reynolds number led to improved mixing, enhancing interaction between nuclei. The resultant effect of this improved mixing was increased average growth rate. However, excessively high turbulence led to attrition and a reversed growth due to crystal breakage.

As a general conclusion, these studies have demonstrated that by changing the reactant concentration, the number of feeding points into the precipitator, and the stirrer speed, the extent of the feeding zone and the level of supersaturation in this zone are affected, as well as the size of the precipitated particles. This information is crucial when designing a precipitation reactor that will yield particles with good settling properties.

Barium sulphate reduction

The current studies have confirmed literature reports and have yielded new information on the reduction of barium sulphate, in the presence $CaCO_3$, using solid carbon as reducing agent.

The current studies have shown, from the product of the reduction of an equimolar $CaCO_3$ + $BaSO_4$ mixture, that the reduction of barium sulphate is to some extent affected by the presence of $CaCO_3$. The CaS product from the concomitant reduction of $CaCO_3$ responsible for about 40% of the measured sulphide content of the product mixture. Thus the presence of $CaCO_3$ in $BaSO_4$ affects the reduction of $BaSO_4$ but does not affect the total sulphide yield of the reaction. Therefore, the presence of $CaCO_3$ in $BaSO_4$ from the treatment of sulphate-rich water does not pose any problem to the integrated barium carbonate process, as CaS is also stripped to H_2S in the H_2S stripping stage of this process.

The tube furnace offered a better reducing environment for the reduction of barium sulphate when compared to the muffle furnace. The results of the studies on the effect of sample mass on BaS yield, in the muffle furnace, showed the importance of the furnace dimensions and avoidance of oxygen in the system, on the effective reduction of barium sulphate. It was found that the reduction rate of $BaSO_4$ is

dependent on the partial pressure of CO and temperature, and that the reaction is first order with average activation energy, E_a = 149 (±10) kJ/mol.

H_2S stripping

H_2S was successfully stripped from a BaS solution by passing CO_2 through the stripping vessel. The challenge associated with this process was to attained stoichiometric balance between the CO_2 flow and the amount of stripped H_2S. The pH of the BaS solution played a significant role in the effective stripping of H_2S. The balance between the CO_2 dosed into the stripping vessel and the amount of stripped H_2S could only be attained when the pH of the BaS solution was above 12. The stripped sulphide only gets absorbed into the Zn-acetate solution under acidic conditions.

Closing remarks

A pilot-scale plant using the integrated barium carbonate process was operated at Harmony Mine in Randfontein from March - June 2008. The results from this trial were highly promising. The information from the investigations, described in this thesis, have assisted in the optimization of the process on pilot-scale and will aid future improvement of the technology. Furthermore, the implementation of the integrated barium carbonate process for sulphate and metal removal from acid mine drainage has been approved for full-scale implementation with economic feasibility as outlined here below.

Economic Feasibility

Table 4.2 shows the running cost, estimated capital cost and value of by-products. The total running cost of treating the water amounted to R1.28/m³ (US$1.00 = ZAR7.00) of treated water, compared to the value of R2.78/m³ for the products (water and sulphur). The capital redemption cost was estimated at R1.08/m³. Sludge disposal cost would be negligible as sludge production only amounts to be 929 kg/h.

Table 4.1. The running cost, estimated capital cost and value of by-products.

Parameter	Unit	Value
Lime		
Lime dosage (100% $CaCO_3$)	mg/L	1448
$CaCO_3$ intake (Purity = 87%, 5% losses)	kg/h	727
Lime usage (87% $CaCO_3$)	kg/h	1456
$Ca(OH)_2$ recovered (as $CaCO_3$)	kg/h	562
$CaCO_3$ recovered	kg/h	167
$BaSO_4$		
$BaSO_4$ sludge (100%)	kg/h	3641
$BaSO_4$ losses (5%)	kg/h	182
Coal		
Coal for CaO	kg/kg $CaCO_3$	0.27
Coal usage for CaO	kg coal/h	393
Heat of Formation	MJ/kg $BaSO_4$	2.03
Coal Energy value	MJ/kg coal	28
Coal for Energy (80% utilization efficiency)	kg/kg $BaSO_4$	0.09
Coal for $BaSO_4$-reduction	kg/kg $BaSO_4$	0.22
Coal usage for BaS	kg/kg $BaSO_4$	0.31
Coal usage for BaS	kg coal/h	1190
Coal usage for CaO + BaS	kg coal/h	1583
Chemical prices		
$BaSO_4$ Price	R/t	1650
$CaCO_3$ Price	R/t	220
Coal Price	R/t	180
Running cost		
$CaCO_3$ cost	R/m^3	0.19
$BaSO_4$ cost	R/m^3	0.36
Coal cost	R/m^3	0.34
KOH & Citric acid	R/m^3	0.03
Operators, Electricity, Maintenance, etc	R/m^3	0.36
Total Running cost	R/m^3	1.28
Capital cost		
Capital	R	-50000000
Capital redemption cost (10%/year, 120 months)	R/m^3	R 1.08
Value of products		
Sulphur	kg/h	500.00
Price	R/t	450.00
Sulphur value (5% losses)	R/m^3	0.26
Water value	R/m^3	2.50
Value of products	R/m^3	2.76

Note: U.S. $1.00 = ZAR7.00, July 2009

BIBLIOGRAPHY

Adlem, C.J.L., Maree J.P. & du Plessis, P., (1991), Treatment of sulphate-rich mining effluents with the barium hydroxide process and recovery of valuable by-products, Proceedings of the 14th International Mine Water Ass. Congress, Rustenburg, SA, p211 – 222.

APHA, (1997), Standard Methods for the Examination of Water and Wastewater, 17th Edit, American Public Health Association, New York, p4 – 197.

Akhmetov, T.G., (1974), Khimiya i tchnologiya soedineniya, bariya, Khmia, Moscow.

Aubé, B., (1999), Innovative Modification to High Density Sludge Process, Proceedings of the Sudbury '99, Mining and Environment II, Sudbury Ontario, Canada, May, p32.

Aubé, B. & Zinc J., (2003), Lime treatment of acid mine Drainage in Canada, Proceedings of the Brazil Seminar on Mine on Mine Rehabilitation, Florianó polis, Brazil, p8 – 9.

Aubé, B., (2004), A pilot study of High Density Sludge Production in Acid Mine Drainage treatment, Masters Thesis submitted to Universitié de Montréal - Ėcole polytechnique.

Baldyga, J. & Orciuch, W., (2001), Barium sulphate precipitation in a pipe – an experimental study and CFD modelling, Chemical Engineering Science, 56 (7), p2435 – 2444.

Baldyga, J., Makowski Ł. & Orciuch, W., (2007), Double-feed semibatch precipitation effects of mixing, Transition Institute of Chemical Engineers, 85 (A5), p745 – 752

Bamforth, A.W., (1965), Industrial Crystallization, London, Leonard-Hill, p128 -155.

Bosman, D.J., Clayton, J.A., Maree, J.P., & Adlem, C.J.L., (1990), Removal of sulphate from Mine Water with barium sulphide, Proceedings of the Lisboa 90th International symposium on Acid Water in pyritic environments 16 -19 September, Lisbon, Potrugal.

Barnes, H.L. & Romberger, S.B., (1968), Chemical Aspects of Mine Drainage, J. WPCF. p371 – 384.

Brown, M.E & Galway, A.K., (2006), Kinetic background to thermal analysis and Calorimetry,p1 - 38.

(CMRO), (1998), Chamber of Mines Research Organization, New desalination programme on streams, October, R & D News.CM.

Chien, L., Robertson, H., & Gerrard, J.W., (1968), Infantile gastroenteritis due to water with high sulfate content, Journal of Canadian Medical Association, 99, p102 – 104.

Cooper, E.L. & Wagner, C.C. (1973), The effects of acid mine drainage on fish populations. In: Fish and Food Organisms in Acid Mine Waters of Pennsylvania, Environmental Protection Agency Report No. EPA-R3-73-032, p114.

Criado, J.M., Gonzalez, F. & Moralez, J., (1975), Application of programmed temperature decomposition; the study of solid decomsposition reactions taking place through the prout and Tompkins mechanism, Thermochimica Acta., 12(4), p337–342.

Criado, J.M. & Moralez, J., (1976), Defects of thermogravimetric analysis of discerning between first order reactions and those taking place through Avrami-Erofeev's mechanism, Thermochimica Acta., 16(3), p382 – 387.

Criado, J.M. & Moralez, J., (1980), On the evaluation of the kinetics parameters from thermogravimetric curves, Thermochimica Acta., 41(1), p125 –127.

Daniels, J.I., (1988), Evaluation of Military Field-Water Quality: Health Criteria and Recommendations Chemicals and Properties of Military Concern Associated with Natural and Anthropogenic Sources, AD UCRL-21008, 1(4).

Davies, C.W., (1962), Ion association, Butterworths, London, p65 - 83.

du Preez, (1994), L.A. & Maree, J.P., Pilot-scale bilogical sulphate and nitrate removal utilizing producer gas as energy source, Proceedings of the 7th Internaltional Symposium on Anaerobic Digestion, p190 – 204

DWAF, (1996), South African water quality guidelines, 7, Aquatic ecosystems, Pretoria.

DWAF BPGs, (2008), Department of Water Affairs and Forestry, RSA, Best Practice Guilines - A5: Water Management for Surface Mine, p(iv)-(v).

DWAF BPGs, (2008), Department of Water Affairs and Forestry, RSA, Best Practice Guilines– G3: Water Monitoring System, p4.

DWAF BPGs, (2006), Department of Water Affairs and Forestry, RSA, Best Practice Guilines – H3: Water Reuse and Reclamation, p1 - 4.

Faulkner, B.B., (1996), Acid Mine Drainage treatment recommendations, West Virginia Mining and Reclamation Association, Charleston, WV, p112 - 126.

Fichett, D., & Tarbell J., (1990), Effect of mixing on the precipitation of barium sulphate in an MSMPR reactor, AlChE Journal, 36, p511.

Garn, P.D, (1965), Thermoanalytical methods of investigation, Academic Press, New York.

Garner, W.E., (1955), Chemistry of the solid state, Chapter 7, Butterworth, London, p72 - 93.

Geldenhuys, A.J., Maree J.P., de Beer M., & Hlabela P., (2003), An integrated limestone/lime processes for partial sulphate removal, Journal of South African Institute of Mining and Metallurgy, p345 – 354.

Givan, A.L., (2001), Flow cytometry: first principles, 2nd ed., John Wiley & Sons, Inc., New York.

Grayson, M., (1979), Barium compounds - Kirk-Othmer Encyclopaedia of Chemical Technology, 3rd ed., Johnn Wiley & Sons, p464 – 479.

Gunn D.J & Murthy M.S., (1972), Kinetics and Mechanisms of precipitation, Chemical Engineering Science, 27 (6), p 1293 – 1313.

Gryka, G.E., (1992), System for recovering sulfur from gases, especially natural gas, PIPco Inc.

Heynike, J.J.C., (1981), The economic effect of the mineral content present in the Vaal River Water on the community of PWVS complex, Report of the Water Research Commission, Pretoria, p121 – 126.

Heynike, J.J.C., (1987), Salination of Vaal River: economic effects (desk study), Report of the Water Research Commission, Pretoria, p113.

Hlabela, P., Maree J. & Bruinsma D., (2007), Barium carbonate process for sulphate and metal removal form mine water, Mine Water and Environment, 26 (1), p14–22.

Hostomskỳ, J. & Jones, A.G., (1991), Calcium carbonate crystallization kinetics, agglomeration and from during continuous precipitation from solution, Journal of Physics D: Applied Physics, 24, p165 – 170.

(INAP), (2006), International Network for Acid Prevention: available on http//www.who.int.

Jaworski, Z. & Nienow, A.W., (2003), CFD modelling of continous precipitation of barium sulphate in a stirred tank, Chemical Engineering Journal, 91(1-2), p167–174.

Jones, A., Rigopoulos, S. & Zauner, R., (2005), Crystallization and precipitation engineering, Computers and Chemical Engineering, 29, p1159 –1166.

Judat, B. & Kind, M., (2004), Morphology and internal structure of barium sulphate – derivation of a new growth mechanism, Journal of Colloidal Interface Science., 269, p341.

Kramer, H.J.M., (2003), Crystallisation: Control of Crystallizers and Dynamic Behaviour, In: Encyclopedia for Separation Science level II/crystallization(Academic Press), p950 - 961.

Kucher, M., Babic, D. & Kind M., (2005), Precipitation of barium sulphate: Experimental investigation about the influence of supersaturation and free lattice ion ratio on particle formation, Chemical Engineering and Processing: precipitation of barium sulphate.

Kun L.E., (1972), A report on the reduction of the sulphate content of acid mine drainage by precipitation with barium carbonate, Internal report, Anglo American Research Laboratories, Project D/3/W/1.

Kershaw M.G.,(1995), Modernisation of the leaching circuit at Pasminco metals—EZ, Hydrometallurgy, 39 (1-3), p129 -145.

Kuusik, R., Saikkonen, P. & Niinistö, L., (1985), Thermal decomposition of calcium sulphate in carbon monoxide, Journal of Thermal Analysis, 30, p187-193.

Loewenthal, R.E., Wierhers, H.N.S., & Marais, G.V.R., (1976), Softening and stabilization of municipal waters, Ann Arbor Science, p244 – 247.

Loewenthal, R.E., Wierhers H.N.S., & Marais G.V.R., (1986), Softening and stabilization of municipal waters, Water Research Commission Report, p3.17 – 3.24.

Marchisio, D.L., Barresi, A.A., Garbero, M., Vanni M. & Baldi, G., (2002). Study of aggregation in barium sulphate precipitation, Proceedings of the 15th International Symposium on Industrial Crystallization 15 – 18 September, Sorrento, Italy.

Maree, J.P., (1988), Sulphate removal from industrial effluents, PhD Thesis submitted to the University of Orange Free State, Bloemfontein.

Maree J.P., Bosman, D.J., & Jenkins, G.R., (1989), Chemical removal of sulphate, calcium and heavy metals from mining and power station effluents, Proceedings of the 1st Biennial Conference of the Water Institute of Southern Africa.

Maree, J.P., Leibowitz, A. & Dods, D., (1990), Sulphate wastes, Proceedings. Rustenburg Symposium, South Africa.

Maree, J.P. & Clayton J.A., (1992), United State Patent, Patent No. 5156746.

Maree, J.P. & du Plessis., (1993), Neutralization of acid mine water with calcium carbonate, Proc. IAWQ Conf. on Pre-treatment of Industrial Wastewaters, Athens, p399 – 411.

Maree J.P., (1994), Neutralization of acidic effluents with limestone, Water Reasearch Commision Report. No. 355/1/94.

Maree, J.P. & du Plessis P., (1994), Neutralization of acid mine water with calcium carbonate, Water Science Technology, 29(9), p285 – 296.

Maree, J.P., van Tonder, G.J., Millard P. & Erasmus C., (1996a), Pilot scale neutralization of underground mine water sewage, Water Science Technology, 34(10), p141–149.

Maree, J.P., van Tonder, G.J., Millard P. & Erasmus C., (1996b), Underground neutralization of mine water with limestone, Water Sewage and Effluents, 16(3), p21–24.

Maree, J.P., Hlabela P., Geldenhuys, A., Nengovhela R., Mbhele N., & Nevhulaudzi T., (2004), Treatment of mine water for sulphate and metal removal using Barium sulphide, Mine Water and Environment, p195 – 203.

Mckenzie, R.C, (1969), Talanta, 16, p1227.

Mead, J.S., (2005), Determination of economic impact of changing water quality standards for sulphate coal mines, Final Technical Report, ICCI Project Number: 03-1/US-4.

Mersmann, A., (1990), Nucleation in crystallization process, Journal of Crystal Growth, 102, p841.

Mersmann, A., (2009). Crystallization technology, Chemical Engineering Journal, 138, p498 – 509.

Mersmann, A., (2001), Crystallization Technology Handbook, 2nd ed, Marcel Dekker, New York, p341 - 382.

Moore, E.W., (1990), Physiological Effects of the Consumption of Saline Drinking Water, in A Progress Report to the 16th Meeting of Subcommittee on Water Supply of the Committee on Sanitary Engineering and Environment. (National Academy of Sciences, Washington, DC). Federal Register. 143 (55) p30382 - 30383

Mudder, J., (1995), [letter] (Personnal Communication), Pretoria.

Myerson, A.S., (1993), Handbook of Industrial Crystallization, Butterworth-Heinemann, Boston, MA, London, p345 - 368.

Murthy M.S., (1994), Theory of crystal growth in phase transformation: precipitation of barium sulphate, Chemical Engineering Science, 49 (13), p2389 – 2393.

NAS, (1977), National Academy of Sciences, Drinking Water and Health, p425 - 428.

Nengovhela, R. N., Strydom, C. A., Maree, J.P., Oosthuizen, S. & Theron, D.J., (2007). Recovery of sulphur and calcium carbonate from waste gypsum, Water S.A., 33 (5), p741 – 748.

Nielsen, A.E. and Söhnel O., (1971), Journal of Crystal Growth, 11, p233

NIPOHIM, (1979), Technologiya Soedineniya Bariya i Strontsiya, A Collection of papers of, Kahrkov.

NWA, (1998), National Water Act 36 of 1998

NWA GN 704, (1998), National Water Act 36 of 1998, Government Notice 704

Öncül, A.A., Niermann, B., Sunmacher, K. & Thévenin D., (2008), CFD modelling of $BaSO_4$ precipitation inside microemulsion droplets in a semi-batch reactor, Chemical Engineering Journal, 138, p498 – 509.

Osuchowski, (1992), R., Advanced treatment of acid mine water, Technology SA, p9 - 11.

Pelovski Y. & Taniguchi M., (1981), Barium reduction with carbon, Proceedings of the 17th Annual Conf. of the Society of Calorimetry and Thermal Analysis, Shizuoka University, p70.

Pelovski, Y., Gruncharov, Iv. & Dombalov I., (1987), Barium reducition by carbon in the presence of additives, Journal of Thermal Analysis, 32, p1743 – 1745.

Pelovski Y. & Taniguchi, M., (1988), Barium sulphate reduction with carbon, J. Therm.Anal., 33, p603 - 608.

Peterson, N.L., (1990), Sulfates in drinking water. Off. Bull. N.D. Water Sewage Works. 18 (10/11)11. (1951). (Cited in: Federal Register, 143 (55), p30382 - 30383.

Randolph, A.D., & Larson, M.A., (1988), Theory of Particulate Processes, 2nd ed., New York, Academic Press.

Ray, W.G., (1990), Process for recovery of sulphur values from a gas stream, US patent 5,057,298.

Rhodes, M., (1988), Introduction to Particle Technology, 1st ed., Chichester, Wiley.

Rochelle, G.T. & King, C.J.; (1979), Process alternatives for stack gas desulfurization with H_2S regeneration to produce sulfur. AIChE Symposium series, 188 (75), p48 – 61.

Rochelle, G.T. & Gibson, M.M. (1982), Thermal degradation of sodium citrate solutions containing SO_2 and thiosulfate, Industrial Engineering and Chemistry, 21, p569 - 574.

Skousen, J., Ploitan K., Hilton T. & Meck A., (1990), Acid Mine Drainage, treatment Systems,Chemicals and Costs, Green Lands, 20(4), p31 - 37.

Skousen, J., Lilly, R. & Hilton, T., Special chemicals for treating acid mine drainage, Green Lands, (1993), p34 – 41.

Skousen, J. & Ziemkiewicz, (1995), Acid Mine Drainage Control and treatment, National Research Centre for coal and energy, National Mine Land Reclamation Centre, West Virginia University, Morgantown, West Virginia, p43.

Skousen, J., Ziemkiewicz, P. & Simmons, J., (2002), Long-term Performance of Passive Acid Mine Drainage Treatment Systems, Technical Report.

Söhnel, O., and Garside, J., (1992), Precipitation; basic principles and industrial applications, Butterworth Henneman, Oxford.

Smit, C.C., (1993), East Rand Regional Services Council, Personnal Communication.

(WQA), (2005), Technical application bulletin, Water Quality Association.

Thomas, B.A., (1970), Planning of gold mines to minimize pollution problem at closure, Convention Proc. Water for Future, p1 - 6.

Trusler, G.E, Edwards R.I, Brouckaert C.J & Buckley C.A., (1988), The chemical removal of sulphates, Proc, 5th National Meeting of the S.A. Institution of Chemical Engineers, Pretoria, W3-0 – W3-11.

Ulrich J. and Strege C., (2002), Industrial crystallization: Some fields of problems, Proc. Eurostar-Science Organization Conference.

USEPA, (1990), National Primary and Secondary Drinking Water Regulations; Synthetic Organic Chemicals and Inorganic Chemicals. Federal Register, 143 (55), p30370.

van der Leeden, (1991), The role of polyelectrolytes in barium sulphate precipitation, PhD Thesis submitted to Delft University of Technology.

van Leeuwen, (1998), Precipitation and mixing, Ph.D Thesis submitted to Delft University of Technology.

van Leeuwen, M.L.J., Bruinsma O.S.L. & van Rosmalen, (1998), Three-zone approach for precipitation of barium sulphate, J. Crystal Growth, 166, p1004 – 1008.

van Rosmalen, G.D., Kramer, H.J.M., & Bruinsma, O.S.L., (2000), Industrial Crystallisation in: 1st Summer School on Advanced SeparationTechnology, Astro Villa, p7 - 12.

Vasan, S., (1975), The citrex process for SO_2 removal, Chem. Engineering. Pro. 71, p61 - 65.

Volman, R., (1984), The use of barium sulphide to remove sulphate from industrial effluents, MSc Thesis (Chem.Eng.) submitted to University of Stellenbosch.

Wei, H., (1997), Application of computational fluid dynamics techniques to the modelling of precipitationprocesses, PhD Thesis submitted to UMIST, UK.

Wei, H.Y. & Garside, J., (1997), Application of CFD modelling to precipitation systems, Transition Institute of Chemical Engineers, 75, p219 – 227.

Wei, H. & Garside, J., (1999), CFD-simulation of precipitation in stirred tanks, Proceedings of the Institute of Chem Engineer, Jubilee Research Event, Nottingham, UK, p517 – 520.

Wells, A.E., (1917), An investigation of industrial and engineering chemistry, J. Ind. and Eng. Chem., 9(9), p872 – 873.

WHO, (1984a), World Health Organization Guidelines for Drinking Water Quality. Health Criteria and Other Supporting Information, Vol 2.

Wilmoth, R.C.,(1974), Limestome and limestone-lime neutralization of acid mine drainage, National Research Centre, EPA, Cincinnati, Report No. EPA-670/2-74-051.

Wilsnach, I.T., (1980), Cost estimate for barium sulphate reduction, Int. Report, Div of Water Technology, CSIR, Project 620/2616/5.

ANNEXURES

Appendix A – A list of publications

1. Hlabela P., Maree J. and Bruinsma D., (2007), Barium carbonate process for sulphate and metal removal form mine water, Mine Water and Environment, 26 (1), p14–22.

2. PS. Hlabela, HWJP. Neomagus, FB. Waanders and OSL. Bruinsma, Thermal reduction of barium sulphate with carbon monoxide – thermogravimetric study, submitted to Thermochimica Acta., April 2009.

3. P Hlabela, OSL Bruinsma and FB Waanders, Controlled precipitation of $BaSO_4$, - 'submitted to Chemical Engineering Science*,* May *2009*.

4. J.P. Maree, P. Hlabela, R. Nengovhela, A.J. Geldenhuys, N. Mbhele, T. Nevhulauzi and F.B. Waanders, (2004), Treatment of Mine Water for sulphate and metal removal using barium sulphide, Mine Water and the Environment, p195 – 203.

5. Geldenhuys, A.J., Maree J.P., de Beer M., and Hlabela P., (2003), An integrated limestone/lime processes for partial sulphate removal*.* Journal of South African Institute of Mining and Metallurgy, p345 – 354.

6. J.P. Maree, M.J. Hagger, G. Strobos, P. Hlabela, H. Cronje, A. Van Nikerk, A. Wurster, R. nengovhela and F.B. Waanders, (2004), Design Criteria for Limestone Neutralization at a nickel Mine, Mine Water and Environment, p152 – 156.

7. Maree J.P., Theron D., Hlabela P.S., Nengovhela R.N., (2005), Sulphur from smelter gases and sulphate – rich effluents. Journal of South African Insitut. of Mining and Metallurgy. (105), p1 – 4.